UNIVERSITY OF CALIFORNIA,
IRVINE

Solvent Extraction and Complexation Studies of Actinyl Cations by Multidentate Schiff Base Ligands for Nuclear Fuel Cycle Applications

DISSERTATION

submitted in partial satisfaction of the requirements
for the degree of

DOCTOR OF PHILOSOPHY

in Chemical and Biochemical Engineering

by

Christian Guerrero Bustillos

Dissertation Committee:
Professor Mikael Nilsson, Chair
Professor A. J. Shaka
Professor Elizabeth Read

2018

DEDICATION

To Maria, Guerrero, Steven, Tracy, and the rest of my family
for their unconditional
love and support

TABLE OF CONTENTS

LIST OF FIGURES

LIST OF TABLES

ACKNOWLEDGEMENTS

I would like to express the deepest gratitude and appreciation to my advisor and committee chair, Professor Mikael Nilsson. Thank you for your support, time, encouragement, patience, and for allowing me to join your research group and introducing me to the field of nuclear science.

I would like to thank my committee members Professor Elizabeth Read and Professor A.J. Shaka as well as Professor Hung Nguyen and Professor William J. Evans for serving on my advancement committee.

I would like to thank Professor Cory Hawkins for his assistance and mentorship during the early years of my graduate studies.

I would also like to thank Iain May, Roy Copping, Sean D. Reilly, and Brian L. Scott from the Los Alamos National Laboratory for their expertise and mentorship.

I would like to thank the UC Irvine Reactor Facility and Dr. George Miller and Jonathan Wallick for their assistance throughout the years.

A very special thanks to the members of the Nilsson Research Group, past and present, who have made my graduate studies an enjoyable experience.

I thank the University of California UCOP Grant ID# 12-LF-237291, the Los Alamos National Laboratory Seaborg Institute for Summer Research Fellowships, the UC Irvine Nuclear Graduate Fellowship (NRC-HQ-84-14-G-0041) and the Estate of Richard Harburger for the William R. Harburger Memorial Dissertation Fellowship.

CURRICULUM VITAE

Christian Guerrero Bustillos

2010	NSF-REU Summer Research Fellow California State University, Los Angeles
2011-12	NIH Maximizing Access to Research Careers (MARC) Fellow University of California, Los Angeles
2012	B.S. in Chemistry University of California, Los Angeles
2012	P.P.G. Aerospace Sylmar, California
2012-18	Graduate Student Researcher University of California, Irvine
2014-15	Glenn T. Seaborg Summer Research Fellow Los Alamos National Laboratory
2015	M.S. in Chemical and Biochemical Engineering University of California, Irvine
2016	Teaching Assistant University of California, Irvine
2015-17	U.S. Nuclear Regulatory Commission (NRC) Graduate Student Fellowship University of California, Irvine
2018	William R. Harburger Memorial Dissertation Fellowship University of California, Irvine

FIELD OF STUDY

Solvent Extraction, Spent Nuclear Fuel, Actinide Chemistry

PUBLICATIONS

C. G. Bustillos, M. Nilsson, "Kinetic and Thermodynamic Features of Uranyl(VI) Extraction by Tetradentate Schiff Base Ligands". Manuscript in preparation for submission to the Journal of Solvent Extraction and Ion Exchange.

C. G. Bustillos, J. M. Swarts, M. Nilsson, "Hydrolytic, Radiolytic and Post Radiolytic Extraction Studies of N_2O_2 Donor Schiff Base Ligands". Manuscript in preparation for submission to the Journal of Solvent Extraction and Ion Exchange.

C. G. Bustillos, M. Nilsson, "Extraction Behavior of Actinyl(VI) Cations by Tetradentate Schiff Base Ligands". Manuscript in preparation for submission to the Journal of Solvent Extraction and Ion Exchange.

C. G. Bustillos, C. A. Hawkins, R. Copping, B. L. Scott, I. May, M. Nilsson, "Aqueous Soluble Pentadentate N_3O_2 Schiff Base Complexation of Actinyl Cations and the Effect on An/Ln Separation". Manuscript in preparation for submission to Dalton Transactions.

C. G. Bustillos, R. Copping, B. L. Scott, I. May, M. Nilsson, "Complexation of High Valency Mid-Actinides by a Lipophilic Schiff Base Ligand. Synthesis and Structural Characterization". Manuscript in preparation for submission to Inorganic Chemistry.

C. G. Bustillos, M. Nilsson, Complexation and Solvent Extraction of High Valency Actinides by Hard/Soft Donor Schiff Base Ligands, Annual Transactions of the American Nuclear Society, **2016**, Vol. 114, p. 125

C. A. Hawkins, C. G. Bustillos, R. Copping, I. May, M. Nilsson, Water-soluble Schiff base-actinyl complexes and their effect on the solvent extraction of *f*-element, *Dalton Trans.*, **2016**, 45, 15415

C. A. Hawkins, C. G. Bustillos, R. Copping, I. May, M. Nilsson, Investigations of Hydrophilic Schiff Base Ligands for the Separation of Actinyl and Lanthanide Cations. In, *Proceedings from 13 IEMPT* (pp. 305-313) **2015**. OECD/NEA 13th Information Exchange Meeting on Actinide and Fission Product Partitioning and Transmutation. Seoul, South Korea.

C. A. Hawkins, C. G. Bustillos, R. Copping, I. May, M. Nilsson, Investigations of water-soluble Schiff base ligands for the separation of actinyl and non-actinyl cations. In, P*roceedings from the International Solvent Extraction Conference* (pp. 172-177) International Solvent Extraction Conference **2014**. Wurzburg, Germany.

C. A. Hawkins, C. G. Bustillos, R. Copping, B. L. Scott, I. May, M. Nilsson, Challenging Conventional f-Element Separation Chemistry - Reversing Uranyl(VI)/Lanthanide(III) Solvent Extraction Selectivity, *Chem. Commun.*, **2014**, 50, 8670-8673

ABSTRACT OF THE DISSERTATION

Solvent Extraction and Complexation Studies of Actinyl Cations by Multidentate Schiff Base Ligands for Nuclear Fuel Cycle Applications

By

Christian Guerrero Bustillos

Doctor of Philosophy in Chemical and Biochemical Engineering

University of California, Irvine, 2018

Professor Mikael Nilsson, Chair

Continued research into advanced separations technology for the reprocessing of spent nuclear fuel (SNF) is imperative for a sustainable, zero CO_2 emission future. More specifically, increased knowledge in the area of actinide coordination and extraction chemistry can prove beneficial in driving interest towards novel separation processes and strengthening public opinion towards nuclear power. Numerous extraction systems have been developed for the separation of various components present in spent nuclear fuel (SNF). Most notably, the PUREX process (Plutonium Uranium Reduction Extraction) has been used commercially for decades focusing on the extraction and recovery of uranium and plutonium from other components such as neptunium, americium, and other highly radiotoxic elements. The successful separation of these mid-actinides (U, Np, Pu, Am) from other elements is imperative for drastically lowering the long-term radiotoxicity of SNF. The solution chemistry of the mid-actinides permits a wide range of oxidation states (+III, +IV, +V, +VI) where the +V and +VI oxidation states exist in a linear dioxo actinyl cation AnO_2^{n+} $(O=An=O)^{n+}$, offering the possibility of co-separation of all 4 actinide cations. The actinyl moiety permits ligand

coordination in the equatorial plane of the metal ion center, affording a geometry for unique bonding characteristics. Multidentate Schiff base ligands can be prepared with synthetic ease and have rather planar structures that chelate around the equatorial plane of actinyl ions through their nitrogen and oxygen donor groups. This distinct coordination environment may facilitate the selective solvent extraction or aqueous retention of pentavalent and hexavalent actinides.

This work examines the potential use of functionalized multidentate Schiff base ligands for the selective group extraction, or retention, of the actinyl cations in a biphasic liquid-liquid separation process. Solvent extraction studies provided details into the equilibrium, stoichiometry, selectivity, kinetic and thermodynamic parameters of the separation process while complexation chemistry experiments elucidated detail of the actinyl-ligand coordination environment. Solvent extraction studies indicate that the group separation of the mid-actinides is possible although redox stability poses a challenge.

1. INTRODUCTION

With an expected global human population of 9.8 billion people by the year 2050, increasing global energy demand and consumption will need to be addressed.[1] Although nuclear energy currently makes up 11% of electricity produced worldwide, nuclear reactors could be a suitable source for the needed energy expansion.[2] Nuclear reactors provide an attractive options for significant base load power generation with low carbon emissions and minimal contributions to air pollution, desirable features when aiming to curb anthropogenic climate change.[3,4] Nuclear reactors create energy through the splitting of heavy fissile atoms. Commercial light water reactors often use fuel comprised of enriched uranium where ^{235}U is the target nuclei and undergoes fission by a thermal neutron capture.[5] The uranium nucleus absorbs the thermal neutron resulting in an unstable nucleus that splits into two lighter nuclei, known as fission products (FP), with the release of, on average, 2.5 neutrons and 200 MeV of energy. The fission products are usually unstable and undergo radioactive decay in order to achieve stability. Although the uranium nuclei can undergo a fission event, an incident neutron may also be captured by the uranium nuclei to form a heavier isotope without undergoing fission. The resulting heavier nuclide can also capture an incident neutron to form another heavier nuclei in a process known as successive neutron capture, or undergo radioactive decay. The combination of these processes in commercial nuclear reactor fuel leads to the production and presence of the middle actinides elements neptunium, plutonium, americium and curium. The elements neptunium, americium, and curium are readily referred to as the minor actinides (MA), as they are present in relatively low quantities.[6] Although present in relatively small amounts, the presence of the long-lived transuranic minor actinide elements are major contributors to the long-

term radiotoxicity of the spent nuclear fuel (SNF) and present a monumental challenge in the management of spent fuel.

SNF is highly radioactive, with components remaining radioactive for up to hundreds of thousands of years, and must be treated in a manner that is socially, environmentally, and economically friendly and viable.[7] SNF is typically comprised of 95.6% uranium and 0.9% plutonium while the remaining 3.5% consists of the minor actinides (neptunium, americium, curium) and other fission products (FP).[8] Once the SNF has been removed from the reactor, there are effectively two options which can be pursued. One method is direct disposal, or the "once-through" option, where the fuel is used once and, following several years of interim storage, is stored in a final repository deep underground. The alternative method for managing SNF is reprocessing or partitioning, where uranium and plutonium can be separated from other elements in the used fuel. The recovered material can be recycled into new fuel containing only uranium, or both uranium and plutonium as a mixed-oxide (MOX) fuel. The MOX fuel can then be used as fuel commercial thermal reactors. The remaining waste is composed of the minor actinides (Np, Am, Cm) and numerous fission and corrosion products. Once U and Pu are removed, the highly radiotoxic minor actinides are still present in the waste and would require long-term storage. The successful removal of the MA from SNF can allow for the conversion of the MA into short lived products utilizing fast neutron reactors in a process called transmutation, the conversion of a nuclide into another nuclide through nuclear reactions.[9] Additionally, the MA may be combined with uranium and plutonium for use as advanced MOX fuel in fast reactors.[10] Removal of the long-lived minor actinides from bulk waste will greatly reduce the radiotoxicity of SNF down to the level of natural uranium ore in a shorter time frame than if only direct disposal is practiced.[7] The additional advantages of reprocessing is that the final waste

volume of the bulk SNF to be stored is reduced, along with conservation efforts as uranium is preserved. The reduction of the radiotoxicity of SNF is an essential step toward increasing the public acceptance of nuclear energy as a component for a low emission energy future.

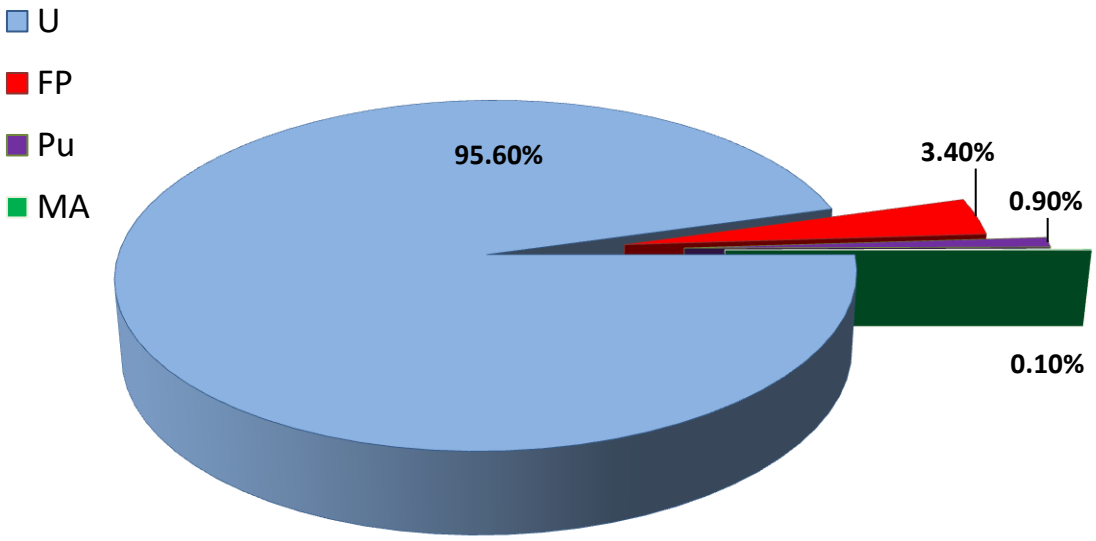

Figure 1.1. Typical Composition of SNF after 10 years of cooling.[7]

Detrimental to the would-be transmutation process is the presence of numerous elements other than the minor actinides present in the SNF. Many of these elements have large neutron absorption cross section, meaning they readily absorb incident thermal neutrons, and these elements will interfere with the transmutation process as they will absorb neutrons intended for the transmutation of the desired elements, in this case the minor actinides.[11] Absorption of neutrons by undesired elements can also lead to the build-up of additional unwanted long-lived radiotoxic nuclides. Because of the aforementioned consequences, it is highly desirable to completely separate the minor actinides from fission products, in particular the lanthanides.

Complete separation from the lanthanides is necessary due to the high neutron capture cross section of some of the lanthanides. Similar behavior of the 4f and mid-5f elements in solution due to their similar ionic radii, oxidation state and chemical properties has posed a great challenge in the development of separation process between these two group of elements.[12,13] Improved separation processes can improve the overall efficiency, economy, and selectivity.

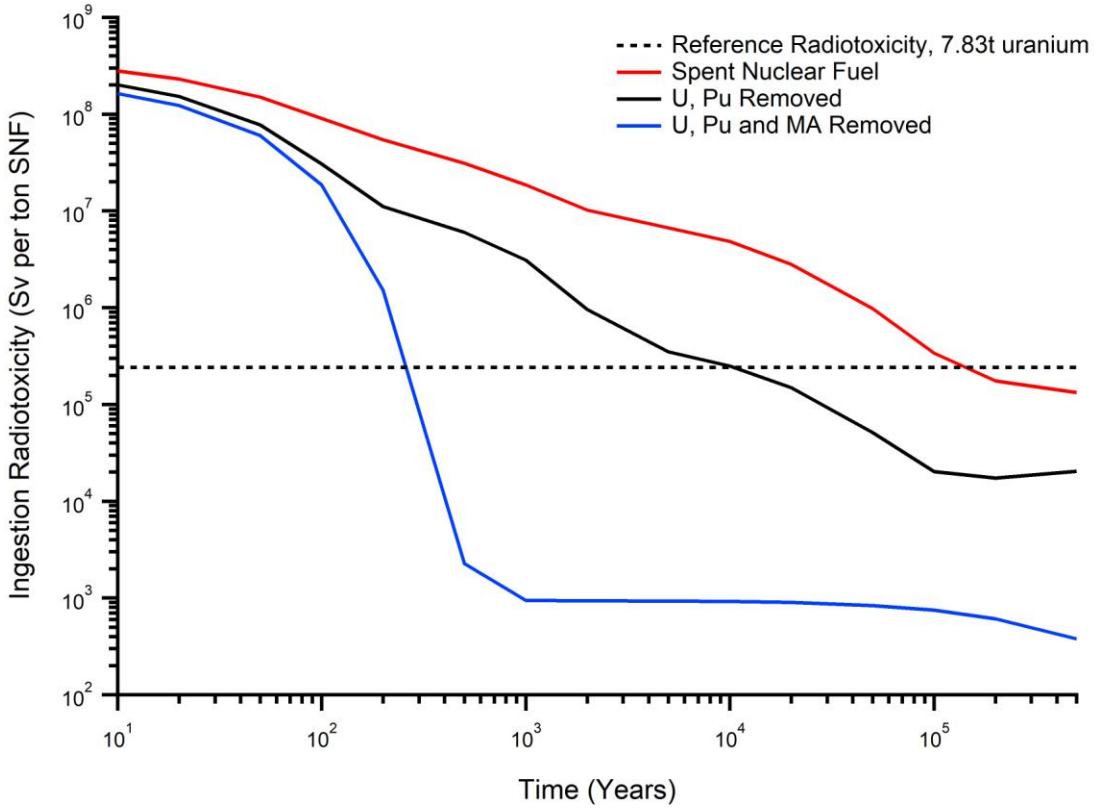

Figure 1.2. Effect of partitioning on the ingestion radiotoxicity of Spent Nuclear Fuel.[14]

Commercial reprocessing of SNF has been practiced for decades in a few countries outside of the United States through the PUREX Process (Plutonium Uranium Reduction Extraction) where uranium and plutonium are recovered from SNF and can be utilized for further fuel fabrication.[15,16] No processes to separate the remaining highly radiotoxic minor actinides from other portions of SNF have been developed on a similar scale. Currently employed and

proposed reprocessing methods rely on biphasic solvent extraction to selectively separate SNF components.[17] Solvent extraction facilitates the transport of a desired solute, such as metal ions, between two immiscible organic and aqueous phases utilizing an extraction agent in the organic phase. The relative differences in chemical affinity of each solute to lipophilic complexing agents in the organic phase compared to those in the aqueous phase drives the separation process. Lipophilic extraction agents form a hydrophobic complex with the solute to make it soluble in the organic phase. Advanced separation methods for the minor actinides utilizing solvent extraction have been thoroughly investigated and, in some cases, demonstrated on actual spent nuclear fuel.[18,19,20] Many of these processes involve treatment of the SNF after uranium, plutonium, and some neptunium, has been removed from the SNF through an improved PUREX process. Typically, americium and curium, and the lanthanides, are extracted from the PUREX raffinate followed by separation of actinides from the lanthanides. Contemporary efforts are aimed at a process which can replace PUREX by simultaneously removing all actinides (uranium, neptunium, plutonium, americium and possibly curium) from SNF.[21] This type of process has the potential to simplify reprocessing of SNF, minimize waste generated from waste streams, and offer greater proliferation resistance with the elimination of a sole plutonium stream. The collected bulk mid-actinides can then undergo transmutation, or be used as fast neutron fission targets, while the fission and corrosive products, with now much lower long-term radiotoxicity, can be stored in a geological waste depository for a much shorter period of time. This type of process can play a pivotal role in closing the nuclear fuel cycle and help in the increasing public acceptance of nuclear power.

The design of ligands which can achieve this type of bulk separation will play a pivotal role. Proposed extractants in a organic phase, or ligands in the aqueous phase acting as hold

back reagents, must have functionalized groups which can provide selectivity for actinides over lanthanides by taking advantage of the subtle differences in chemical properties. A good level of selectivity must be displayed by the ligands for actinides over the lanthanides in order to achieve a separation process with minimal number of steps, yet form a complex where the metals can be stripped and recovered. The extracting ligand and the complex formed during the extraction process must exhibit high solubility in the organic diluent in order to minimize precipitation and the formation of a third phase, which will disrupt the efficiency of the equipment used. The ligand must also demonstrate resistance towards hydrolysis and radiolysis, eliminating the possibility of degradation products interfering with the separation process, and must be able to perform in an aqueous medium of low pH, since SNF is usually dissolved in nitric acid solutions. In order for such processes to be commercially viable and operated in a large scale, the synthesis of the extracting agent should be practical and cost-effective.

The aim of this work is to develop a biphasic liquid-liquid extraction process where the mid-actinides (U, Np, Pu, Am) are selectively extracted into the organic phase by an organic soluble ligand, or are retained in the aqueous phase through the utilization of an aqueous soluble complexant. We wish to accomplish these goals by utilizing functionalized multidentate Schiff base ligands containing nitrogen and oxygen donor atoms. The dissertation is outlined below as follows:

1. Chapter 2 will provide more theoretical background relevant to the material that will be covered in the thesis.
2. Chapter 3 presents an overview of the experimental technique used throughout the dissertation.

3. Chapter 4 will cover results obtained from this work, which will include complexation chemistry, solvent extraction, and hydrolytic and radiolytic degradation studies.

Conclusions regarding the ability of functionalized multidentate Schiff base ligands to be used for fuel cycle applications will be made.

2. Background

2.1. Liquid-Liquid Extraction Theory

Liquid-liquid extraction can be described as the separation of a solute between two immiscible liquids. The immiscible liquids usually consist of an organic and an aqueous phase. The organic phase could contain one or several extractants which participate and facilitate the extraction. A more complex system can consist of the extractant in the organic phase and the addition of a holdback reagent in the aqueous phase. Solvent extraction is the technique which is utilized for the reprocessing of SNF but it can also be practiced on a small, laboratory scale. The two immiscible phases are contacted (shaken vigorously) followed by separation of the phases by centrifugation. A sample is then taken from each phase in order to measure the separation, or distribution, of the solute in each phase. When a metal (M) is distributed between the phases during an extraction process, the distribution between the two phases can be expressed as the distribution ratio D:

$$D_M = \frac{[M]_{tot,org}}{[M]_{tot,aq}} = \frac{\text{Total concentraction of M in the organic phase}}{\text{Total concentration of M in the aqueous phase}} \qquad \text{(eq. 1)}$$

The work presented consists of radioactive metals which were extracted. The distribution ratio D_M is then calculated by measuring the activity in each phase using radioanalytical techniques. The specific radioactivity in each phase is proportional to the concentration of the radioactive metal, therefore:

$$D_M = \frac{[M]_{tot,org}}{[M]_{tot,aq}} \propto \frac{\text{Radioactivity in the organic phase}}{\text{Radioactivity in the aqueous phase}} = \frac{S_{org}}{S_{aq}} \qquad \text{(eq. 2)}$$

The separation factor (SF) describes the extent of separation of two different solutes that were present in the same extraction system. The ratio of the distribution ratios between M_1 and M_2 provide the SF. A larger SF is obtained when $D_{M_1} \gg D_{M_2}$.

$$SF_{M_1/M_2} = \frac{D_{M_1}}{D_{M_2}} \quad \text{(eq. 3)}$$

There are multiple extraction mechanisms that can describe the extraction of a cationic metal ion, M^{n+}, from the aqueous phase. The type of extraction mechanism will depend on the molecular properties of the extracting agent as well as the complexing properties between the extractant and metal of interest. The mechanisms through which a solute is distributed in the two phases during solvent extraction can be categorized into the following classes: A (MX_n), B (MA_z), C (ML_zB_b), D (Q^+L^-) and E.[17] These classes are summarized in Table 1.1.

Table 2.1. Description of Different Solvent Extraction Classes

Class	Description	Example
A	Extraction of simple inorganic molecules	$MX_N = GeCl_4$
B	Neutral complexes between a metal ion and a lipophilic organic acid	$MA_Z = Th(RCOO)_4$
C	Neutral complexes between a metal ion and a ligand. The complexes are unsaturated and can accept uncharged organic molecules are solvating agents	$ML_ZB_b = (UO_2)(NO_3)_2(TBP)_2$
D	Ion pair extraction. An anion or a cation exchange mechanism takes place	$Q^+L^- = R_3N^+Cl^-$
E	Other extractions	Crown ether

The metal can not be extracted as a charged species and must be neutralized in the aqueous phase by anions. The neutral complex is transferred into the organic phase by binding of an adduct. The adduct can replace water molecules still bound to the complex, therefore increasing the hydrophobicity of the complex. Solvent extraction studies carried out with Schiff base ligands are a result of the class B extraction mechanism.

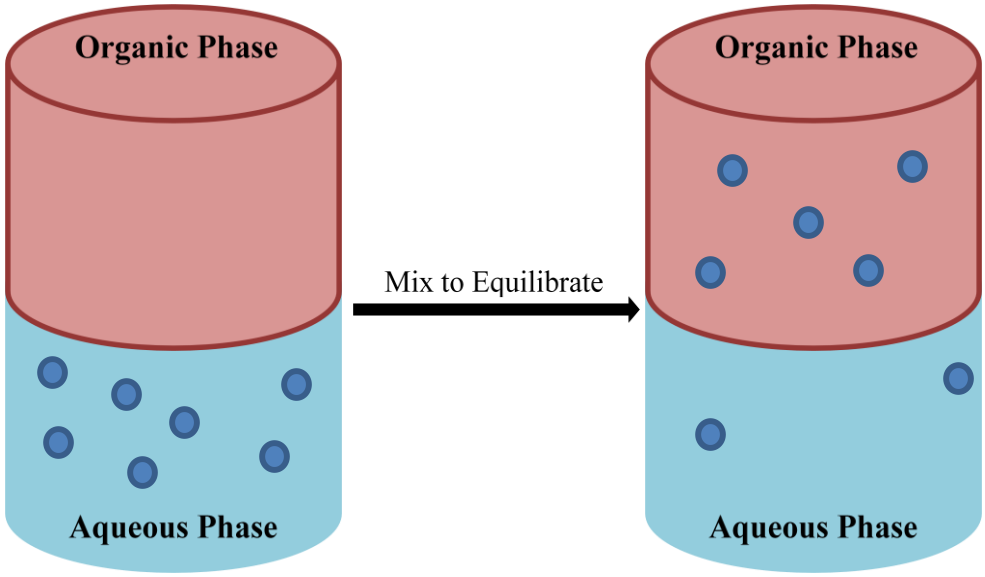

Figure 2.1. Idealized depiction of solvent extraction.

2.1.1. Slope Analysis Method

Solvent extraction is a versatile technique which can yield quantitative information regarding the extraction process. In order to determine In order to determine the number of ligand molecules bound to the metal ion during an extraction process the slope analysis method can be applied.[22,23] Here there distribution ratio D is measured while changing one component in a system, such as the free ligand concentration with all other variables held constant. Consider the following general reaction of the extraction, where M is the metal and B is the extracting ligand and L is a charge neutralizing agent:

$$ML_{z_{aq}} + bB_{org} \leftrightharpoons ML_zB_{b_{org}} \quad \text{(eq. 4)}$$

The distribution ratio of the equation can then be written as follows:

$$D_M = \frac{[ML_zB_b]}{[ML_z]} \quad \text{(eq. 5)}$$

And the equilibrium constant can be written as:

$$K'_{ex} = \frac{[ML_zB_b]}{[ML_z][B]^b} \quad \text{(eq. 6)}$$

By assuming constant ionic strength and neglecting concentration variations in the organic phase, the following substitution can be made

$$D_M = K'_{ex}[B]^b \quad \text{(eq. 6)}$$

which can then be written in its linear form

$$\log D_M = \log K'_{ex} + b\log[B] \quad \text{(eq. 7)}$$

Therefore the average number of ligand molecules which are bound to a metal during solvent extraction is given by the slope of the logD vs log[B] plot. Since it is an average, the slope can be an integer or a number between two integers.

2.2. Complexation Chemistry

A solvent extraction process is facilitated by the chemical and structural features of the complexant and metal ion. Metal ions present in aqueous solutions are surrounded by water molecules coordinating by the oxygen atom. The number of coordinating water molecules can

vary depending on the size of the metal, ranging from 2 water molecules coordinating to alkali metals to 9 water molecules coordinating to trivalent lanthanides.[12a] Complexation of a ligand to a metal ion occurs when coordinated water molecules are replaced by functional, coordinating groups on the ligand. The rate at which this exchange takes place can affect the kinetics of the complexation reaction therefore affecting the solvent extraction process.

The Hard-Soft Acid-Base (HSAB) concept is a qualitative approach for explaining the reaction mechanisms and stability of compounds.[24] The concept assigns the terms "hard", smaller atomic radii and high oxidation state, and "soft", larger atomic radii and lower oxidation states, to Lewis acids (electron pair accepting) and Lewis base (electron pair donating). The principle states that hard Lewis acids prefer to form complexes with hard Lewis bases and soft Lewis acids prefer to form complexes with soft Lewis bases. The interaction between hard Lewis acids and hard Lewis bases are usually ionic in character whereas the interactions between soft Lewis acids and soft Lewis bases are more covalent.[25] The lanthanide and actinide elements are considered hard Lewis acids but the HSAB concept is not sufficient enough in explaining complexation behavior of the f elements. The f elements display a variance in ionic character, some exhibiting covalent characteristics. However, the covalent features are larger for trivalent actinides than they are for trivalent lanthanides.[26,27]

A ligand which binds to a metal through two or more coordinating atoms on the ligand is referred to as a chelate. Chelating ligands often form more stable complexes compared to monodentate ligands. More water molecules coordinated to the metal are replaced per ligand for chelating ligands than during monodentate ligand complexation, leading to an increase in the degrees of freedom in the system. The increase in the degrees of freedom in the system increase the entropy of the system rendering a more stable complex.[25]

2.3. Actinides and Lanthanides

The actinide and lanthanide elements differ from the main group elements and transition metals because of the presence of partially filled f orbitals. The f-orbitals corresponding to the lanthanides are strongly shielded from its surroundings by p and d orbitals and therefore do not participate directly in bonding.[12a] The lanthanides predominantly posses trivalent (+III) oxidation state in solution.

The principal difference between the actinides and lanthanides (4f and 5f orbitals) is that the 4f orbitals are buried towards the nucleus and are therefore more 'core-like'. Although the lanthanides primarily exist in the +III valent state, the actinides on the other hand can exist in a range of oxidation states.[28] The energy separation between the 5f, 6d, 7s and 7p orbitals is small enough that multiple valence states can be attained. The valence electrons in the early part of the actinide series (Ac-Pa) are in high energy and are easily lost. In regards to the mid-actinides (U - Am), the 5f and 6d orbitals are close in energy and electrons are able to "switch" between 6d and 5f orbitals. The availability and ability to interchange leads to a wide range of oxidation states (+III, +IV, +V, +VI, +VII) that are accessible for the mid-actinides. As the 5f orbitals gradually fill up, there is an inversion in orbital energy as the 5f orbitals become lower in energy than the 6d orbitals and the energy gap between the two orbitals widen. For the later part of the actinides (Cm - Lr) the energy gap between the 5f and 6d orbitals is large enough that the wider range of oxidation states is unavailable and instead exhibit trivalent (+III) oxidation states similar to the lanthanides.

Table 2.2. Oxidation States of the Actinide Elements

Element	Oxidation States					
Ac		3				
Th		3	4			
Pa		2	4	5		
U		3	4	5	6	
Np		3	4	5	6	7
Pu		3	4	5	6	7
Am		3	4	5	6	
Cm		3	4			
Bk		3	4			
Cf	2	3	4			
Es	2	3				
Fm	2	3				
Md	2	3				
No	2	3				
Lr		3				

Due to their electropositive nature, the actinides can readily lose their outer electrons and form cations in their range of oxidation states in aqueous solutions. The behavior and solution chemistry of a given actinides is strictly dependent on the oxidation states of that cation. The high oxidation state (+V, +VI) of the mid-actinides (U, Np, Pu, Am) are sufficiently electropositive that in aqueous solutions they can strip oxygen atoms from water resulting in the formation of a linear dioxo cation species AnO_2^{n+} (n=1, 2). This species is often referred to as an actinyl cation $(O=An=O)^{n+}$.[29] Although a wide range oxidation states are available for the mid-actinides, their stability is strongly pH dependent and certain species are more favorable in certain conditions than others. The differences between the redox potentials for the actinide elements means that for a given set of conditions, the actinides can exist in different oxidation states. U(III) easily oxidizes to U(IV), while U(V) readily disporportionates to U(IV) and U(VI). Neptunium is the most stable in its oxidation state of +V, while +VI can slowly reduce to +V.[30] Due to reduction potentials being similar in value, oxidation states in the range of +III to +VI can

exist simultaneously for plutonium.[31] However, in general Pu(IV), Pu(V), and Pu(VI) are favored in acidic, near neutral and slightly basic conditions.[31] Although the most common oxidation state of americium is the +III species, the +V and +VI species are accessible by the addition of strong oxidants.[32]

2.3. 4f and 5f Element Chemistry in Separation Processess

The linear dioxo actinyl cation O=An=O is a structural feature is unique to the mid actinides and provides stark chemical differences from the rest of the actinides series and the lanthanide elements. The linear actinyl moiety of the mid actinides affords unique binding characteristics for complexation and extracting compounds can take advantage of the steric demands of the moiety in a separation process. The differences in oxidation state stability of the actinides are exploited and provide a means for partitioning in separation processes.[33] In the PUREX process, SNF is dissolved in nitric acid and is contacted with an organic phase containing tri-n-butyl phosphate (TBP). Uranium (+VI) and plutonium (+IV) are extracted as TBP/nitrate complexes, according to mechanism class C in table 1, while neptunium (+V) and americium (+III), as well as other fission and corrosion products are not extracted to any appreciable extent.[34] Extraction of uranium(VI) and plutonium(IV) into the organic phase is achieved by charge neutralization by nitrate groups and the increase in hydrophobicity caused by complexed TBP molecules. Further separation between U and Pu is achieved when plutonium is reduced to the +III oxidation state where it is no longer extractable by TBP. In another separation process named UREX (URanium EXraxtion), neptunium and plutonium are held back in the aqueous phase through the complexation of the +IV species with hydroxamic acids, forming hydrophilic complexes.[35]

The exploitation of the trivalent oxidation state is observed in the TALSPEAK process. In the TALSPEAK process (Trivalent Actinide Lanthanide Separation by Phosphorous Extractants and Aqueous Komplexant) trivalent lanthanide elements are extracted into the organic phase by an organophosphorous extractant, HDEHP, while the trivalent actinides are held back in the aqueous phase by a hydrophilic complexant DTPA (diethylenetriamine pentaacetic acid).[36,18] Due to similar behavior in solution, extracting agents which contain only oxygen donating groups unable to efficiently separate actinides(III) from lanthanides(III).[37] However, preferential complexation of actinides(III) over lanthanides(III) was demonstrated in the early 1980's by nitrogen donating ligands ushering interest in nitrogen donating ligands for the separation of trivalent f-elements.[38,39,40] It is believed greater covalent interactions between the 5f actinides and nitrogen donating groups on DTPA provides the selectivity for trivalent actinides.

The complete extraction of neptunium in the PUREX process is made difficult because of the disproportionation of the +V cation to the +IV and +VI species.[30] Although the +IV and +VI species are extracted by TBP, the +V species remains inextractable due to weak complexes formed by the species due to the low charge density of the neptunyl(V) cation.[30] Complete redox control and stability of neptunium in an extraction process is important for its complete recovery. Uranium chemistry research has mainly focused on uranium(VI) because its chemical stability. However, recent efforts have opened the door to synthetic, spectroscopic and structural chemistry with uranium(V), which tends to disproportionate (to +IV/+VI) or rapidly oxidize to +VI in solution.[41,42,43] Similar efforts have also been achieved in the stabilization of Np(V/VI)[44], Pu(VI)[45] and Am(VI)[32]. Considering that only these 4 mid actinides form the unique linear

dioxo species, guaranteeing different chemical properties from the rest of the actinides and lanthanides, an actinyl separation process utilizing this phenomenon can be proposed.

2.4. Schiff Base Ligands

Numerous ligand systems have been developed that demonstrate complexation, selectivity and extraction for uranyl(VI).[46] Since U(VI) is the most stable oxidation state in aqueous solution, this is a simple task compared to the complexation and/or stabilization of the other actinyl cations (+V, +VI) for neptunium, plutonium and americium. As previously noted, to warrant any sort of separation process potential, the complexing ligand must be stable in, or in contact with, acidic solutions. A class of ligand, so called Schiff bases, which possess both nitrogen and oxygen groups which participate in complexation, was recently used to complex and stabilize uranyl(VI)[41,42,47]. These ligands provide multi-dentate coordination to the equatorial plane, therefore inhibiting the disproportionation mechanism, and this behavior might be extended to the rest of the actinyl cations. With U, Np, Pu and Am stabilized in their actinyl(V/VI) complexes, the rest of the f elements will be present in their +III oxidation states. The separation of these elements must be with the complete exclusion of all other elements, therefore they should be selectively extracted into the organic phase or retained in the aqueous phase in a biphasic separation system. For aqueous phase group actinide retention, Schiff base ligands can be functionalized with hydrophilic groups. Aliphatic and aromatic groups can be added in order to achieve greater solubility in the lipophilic phase. The oxygen groups on the ligands provide an overall charge of 2- which will form neutral complexes with actinyl(VI) cations. For this class of ligands, the hard trivalent lanthanides will not readily complex with the softer nitrogen donors on the Schiff base ligands. The actinyl cations, while still considered

hard, have a slightly softer character and may complex with the softer nitrogen donors, inducing separation from the lanthanides.

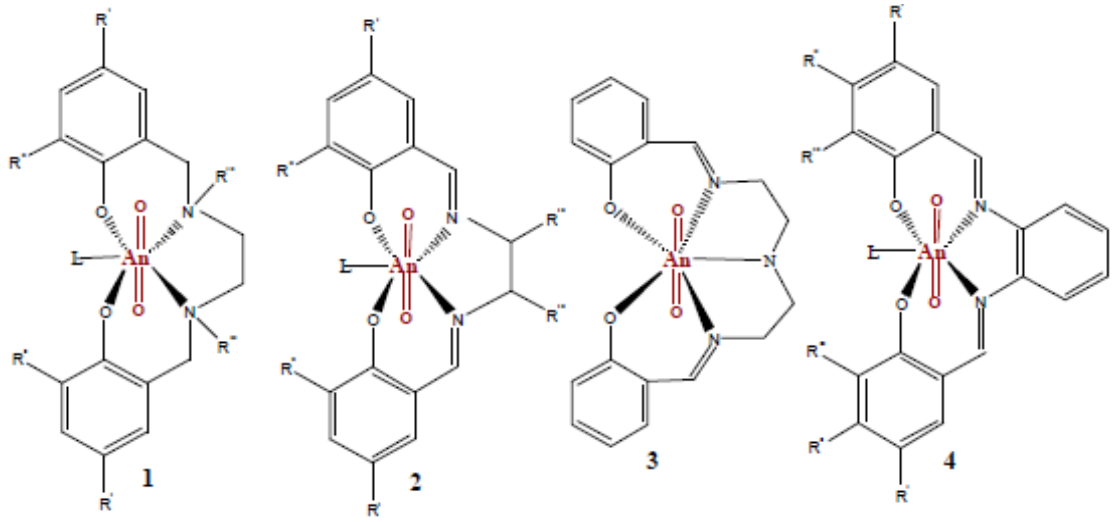

Figure 2.2. Coordination of actinyl cations by select Schiff base ligands. The linear dioxo cations are chelated about the equatorial plane.[48]

Schiff base ligands have been primarily used in transition metal chemistry and catalysis.[49,50,51] Use of Schiff base ligands in solvent extraction studies has largely been limited to transition d elements and the uranyl(VI) cation.[52,53,54] In addition, solvent extraction studies have been carried out in chlorinated and hydrochloric media, conditions impractical for the reprocessing of SNF.[54,55] At the commencement of this work, actinide complexation studies utilizing water-soluble Schiff base ligands had not been performed. We therefore proposed this to be a suitable starting point for our studies.

2.5. Radiolysis

Since reprocessing conditions are incredibly radioactive, it is important to incorporate radiolytic studies in order to understand how the radiation will affect the solutions, extraction and separation process. Radiolysis is the dissociation, or breakdown, of chemical species or

bonds due to ionizing radiation. Ionizing radiation refers to energy which can ionize chemical molecules and is comprised of charged particles, alpha and beta particles, and photons (gamma rays). Absorbed dose is the physical quantity used to express absorbed ionizing radiation and is represented by the unit Gray (Gy), where 1 Gy is 1 J/kg. Radiolysis can occur in solid, gaseous and liquid phases, and our studies are strictly limited to organic solutions. Products resulting from the direct radiolysis of organic solutions can include solvated electrons, radical species, hydrogen radicals, and other ionic species.[56] Solvated electrons and hydrogen radicals are primarily of the upmost importance due to their overall reducing chemistry.[57,58] The primary products can then undergo additional reactions to form secondary products through the decomposition of molecules to other molecular, ionic, and radical species, or through the recombination of multiple species. As organic diluent solutions generally possess more atoms per molecule than aqueous solutions, a diverse array of degradation products can be expected. Functional groups present in the organic molecules will largely affect the composition of the radiolytic products.[57] In compounds containing polar functional groups, a rupturing of the bond in the α-position to the functional group tends to predominate.[59] The presence of unsaturated bonds and aromatic groups also increase the overall radiolytic stability of compounds.[60,61,62] Noted trends can aid in identifying the possible chemical structure of radiolytic products.

3. Experimental Procedures

3.1. Origin and Purity of Chemicals

The following is a list of chemicals purchased from commercial suppliers and, unless stated, were used without further purification.

General

Acetic acid, EMD Chemicals, GR ACS, 99.7%

Benzene, ACS Reagent, 99.0%

Aniline, Sigma Aldrich, ACS Reagent, 99.5%

(3,5,)-di-t-butyl salicylaldehyde, Sigma Aldrich, 99%

Ethanol, Rossville Gold Shield Alcohol

Ethylenediamine, Sigma Aldrich

Ethylenetriamine, Sigma Aldrich, Reagent Plus, 99%

Di-ethyl-hexyl phosphoric acid (HDEHP), Sigma Aldrich, 97%

Methanol, Rossville Gold Shield Alcohol

Nitric acid, Macron Fine Chemicals, ACS

1-Octanol, Acros Chemicals, 99%

1,2-Phenylenediamine, Alfa Aesar, 98%

Potassium Hydroxide, Fisher Scientific, Certified ACS

Potassium Nitrate, Fisher Scientific, Certified ACS

Salicylaldehyde, Sigma Aldrich, Reagent Grade, 98%

Sodium Bicarbonate, Macron Fine Chemicals, ACS

Sodium Bismuthate, Chemsavers, ACS, 93%

Sulfuric acid, Fisher Scientific, Certified ACS Plus

Toluene, Fisher Scientific, Certified ACS

3.2. Synthesis of Schiff Base Ligands

Schiff base ligands can be prepared and functionalized with the addition of hydrophobic or hydrophilic groups to the starting materials as described below.[51] The ligands were then used after a single purification step. Purity was confirmed by ESI-MS, ^{1}H-NMR and FT-IR.

3.2.1. Synthesis of Organic Soluble Ligands

Lipophilic Schiff base ligands can be readily synthesized by the condensation of salicylaldehyde and a half equivalent of a selected diamine in EtOH in a round bottom flask. The reaction mixture was stirred and heated under reflux for 2-6 h. The solution was allowed to cool to room temperature and then cooled in an ice bath for 1 h. Yellow solids were collected by vacuum filtration and washed with cold EtOH. The figure below summarizes the synthesis of organic soluble ligands (Figure 3.1).

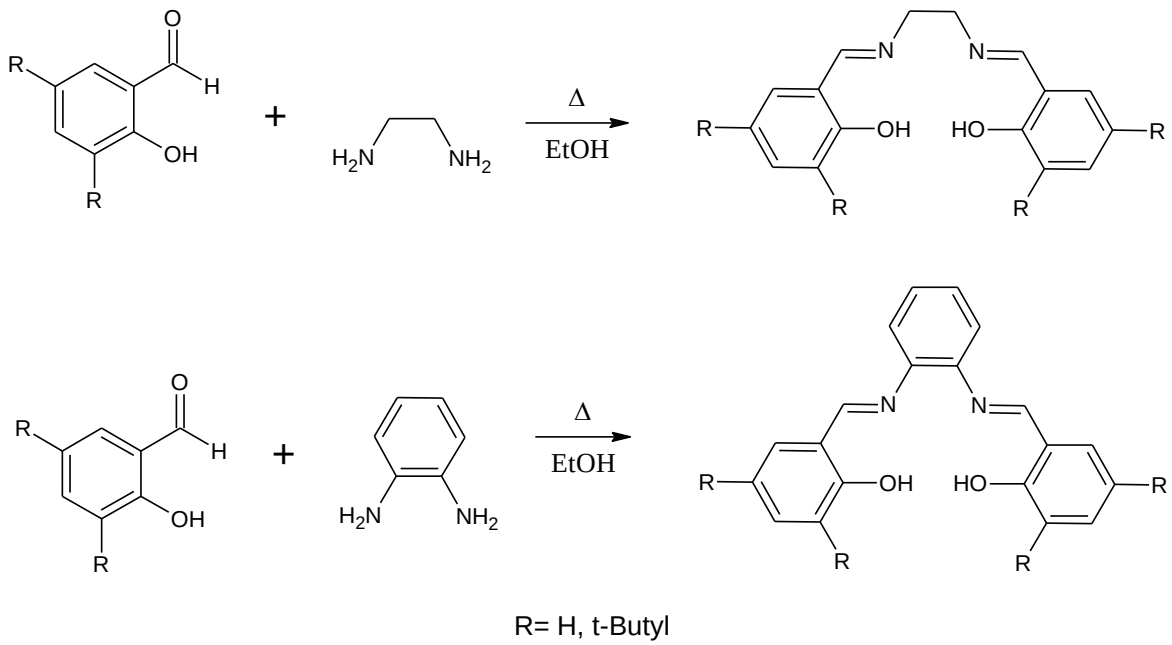

Figure 3.1. Scheme for the synthetic route for tetradentate organic soluble N_2O_2 donor ligands.

Results presented in this thesis will consist of 4 organic soluble ligands (Figure 3.2): N,N'-Bis(salicylidene)-1,2-ethylenediamine, N,N'-Bis(salicylidene)-1,2-phenylenediamine, N,N'-Bis(3,5-di-tert-butylsalicylidene)-1,2-ethylenediamine, and N,N'-Bis(3,5-di-tert-butylsalicylidene)-1,2-ethylenediamine. Ligands will be referred to as Salen, Salophen, di-t-butyl Salen, and di-t-butyl Salophen, respectively.

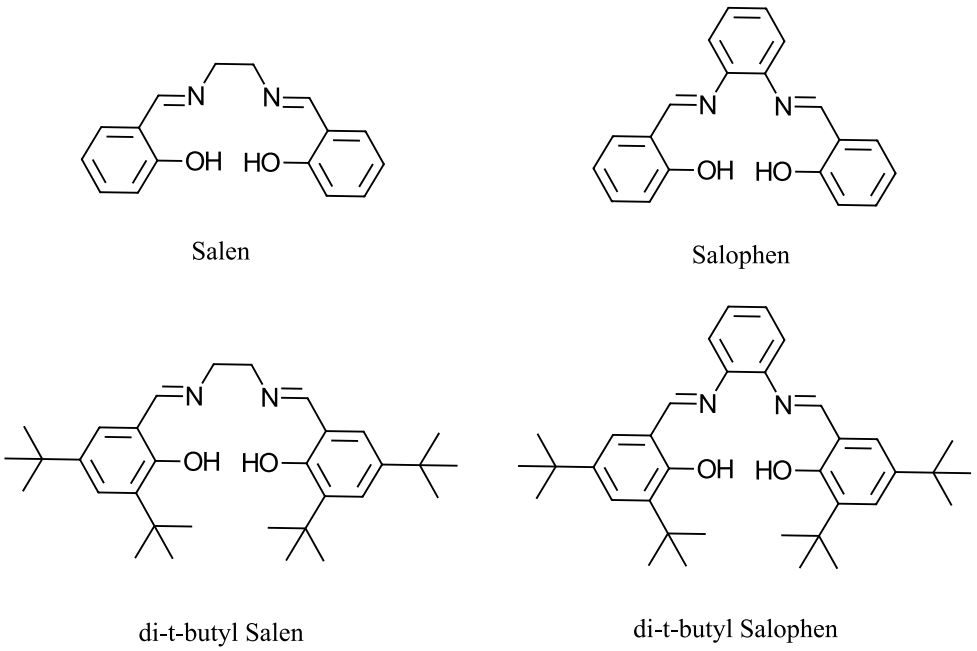

Figure 3.2. Chemical structural representation of ligands used in this work.

Salen (400 MHz, CD_2Cl_2) δ: 13.18 (s, 2H, OH), 8.39 (s, 2H, HC=N), 7.28 (m, 4H, bz, J=10.8 Hz), 6.89 (m, 4H, bz, J=10.24 Hz) and 3.93 (s, 4H, CH_2) ppm. (m/z)= 268 (M+H).

Salophen (500 MHz, DMSO) δ: 12.93 (s, 2H, OH), 8.93 (s, 2H, HC=N), 6.96 -7.68 (m, 12H, bz) ppm. (m/z)= 315 (M+H).

di-t-butyl Salen (400 MHz, CD_2Cl_2) δ: 13.71 (s, 2H, OH), 8.32 (s, 2H, HC=N), 7.30 (s, 2H, bz), 7.01 (s, 2H, bz), and 3.34 (s, 4H, CH_2) and 1-2.1 (m, 18H, CH_3) ppm. (m/z)= 492 (M+H).

di-t-butyl Salophen (400 MHz, CD_2Cl_2) δ: 13.60 (s, 2H, OH), 8.71 (s, 2H, HC=N), 6.7-7.5 (m, 12H, bz) and 1-1.4 (m, 18H, CH_3) ppm. (m/z)= 540 (M+H).

3.2.2. Synthesis of Water Soluble Ligands

Results presented will consist of complexation studies performed with the water soluble tetradentate N,N'-bis(5-sulfanato-salicylidene)-ethylenediamine disodium salt and pentadentate

N,N'-Bis(5-sulfonato-salicylidene)-ethylenetriamine disodium salt. From here on the tetradentate ligand will be referred to as H_2Salen-SO_3 and the pentadentate ligand will be referred to as H_2Saldien-SO_3.

3.2.2.1. Synthesis of N,N'-bis(5-sulfanato-salicylidene)-ethylenediamine disodium salt (Salen-SO_3)

A solution of aniline (4.38 g, 0.047 mol) in 45 mL of EtOH was added to a stirring solution of salicylaldehyde (5.75 g, 0.047 mol) in 45 mL EtOH and was allowed to stir for an additional 3 h. A yellow precipitated product was collected and washed with cold EtOH. The yellow product (1) (4.78 g, 0.0242 mol) was then suspended in concentrated sulfuric acid (13 mL, 0.244 mol) and refluxed for 2 h at 95 ˚C and was then allowed to cool to room temperature. The orange solution was then poured into an Erlenmeyer flask containing an ice/water mixture and stirred vigorously. The temperature was increased in order to dissolve the precipitated solids back into solution. The solution was then cooled to room temperature and the precipitated yellow solids were collected by vacuum filtration and washed with cold ethanol and acetone. The yellow solids (2) (6.28 g, 0.0276 mol) were dissolved in a solution of sodium carbonate (4.21 g, 0.0397 mol) in 69 mL of water and maintained at 150 ˚C for 2 h. After cooling to room temperature, the pH of the solution was decreased to pH=5.00 with acetic acid. The 5-sulfonato-salicylaldehyde salt (3) was collected after crystallization in an ice/water bath and the pale yellow solids were washed with cold EtOH. The sulfonated salicylaldehyde (0.5 g, 2.23 mmol) was then added to a solution of ethylenediamine (0.0671 g, 1.11 mmol) in 10 mL EtOH and refluxed for 2 h. The yellow solids (4) (0.500 g, 0.105 mol) were collected by vacuum filtration and washed with cold ethanol.

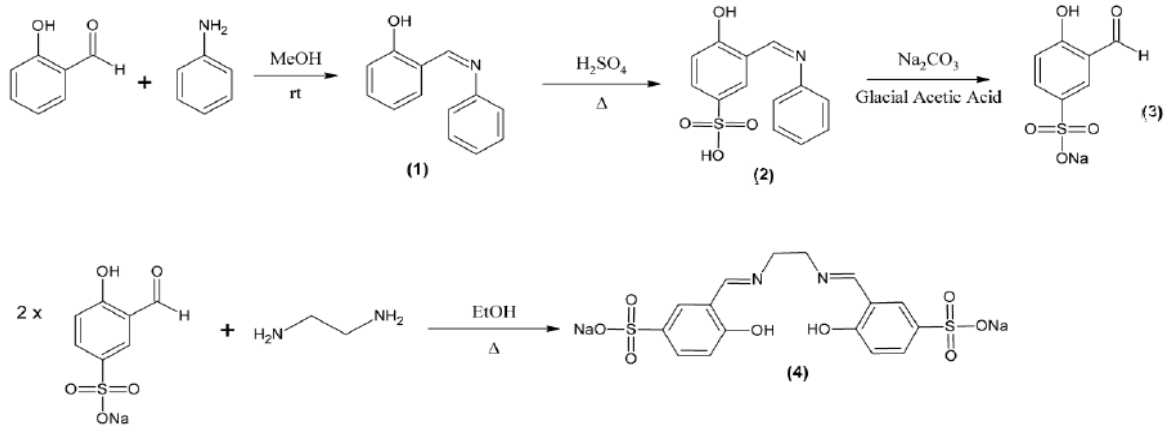

Figure 3.3. Synthesis of tetradentate water-soluble Salen-SO_3.

3.2.2.2. Synthesis of N,N'-bis(salicylidene-5-sulfanato)-triaminoethane disodium salt (Saldien-SO_3)

Synthesis of Saldien-SO_3 was carried out with exact conditions as Salen-SO_3 but diethylenetriamine was used instead of ethylenediamine (Figure 3.4).

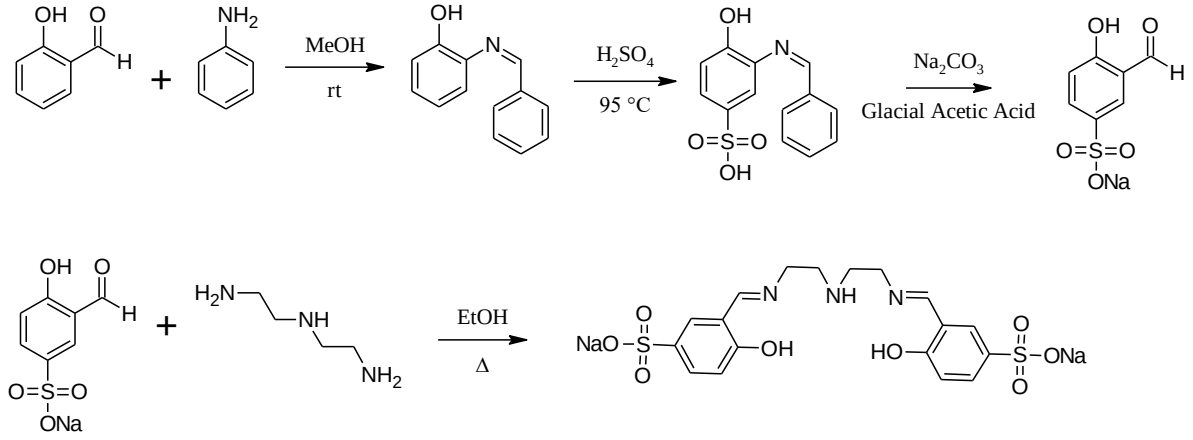

Figure 3.4. Synthesis of pentadentate water-soluble N_3O_2 donor Saldien-SO_3.

3.3. Synthesis of Ligand-Actinyl Complexes

Synthetic details of the preparation of the actinyl stock solutions and complexation studies performed will be described in this section. Preparation of actinyl stock solutions and complexation reactions were monitored by a Cary 6000i UV-Vis-nIR Spectrophotometer. In figures below, the spectra of the pure stock solutions are over laid with the spectra of their complexation reaction for comparison.

3.3.1. Preparation of Actinyl Solutions

3.3.1.1. Preparation of U(VI)

Aqueous solutions of uranyl nitrate in H_2O were evaporated to dryness with heat and allowed to cool to room temperature. The resultant yellow uranyl nitrate hydrate solids were then used for complexation studies.

3.3.1.2. Preparation of Np(VI)

A previously prepared stock solution of NpO_2^{2+} was evaporated to near dryness resulting in grey/green/brown solids. The solids were then re-dissolved in 0.5 mL of 1 M HNO_3 and 0.5 mL H_2O to produce a green/blue solution, indicating the presence of NpO_2^{2+} as the dominant species. Ozone was bubbled through the solution which quickly turned brownish in color. A 0.1 M solution of NaOH was then added dropwise to the brown solution which produced brown precipitates. The solution was centrifuged several times and the brown solids were collected. The supernatant was removed and the residual brown solids were washed twice with 2 mL of H_2O. The brown solids were dissolved in 1 mL of 1 M HNO_3 to yield a NpO_2^{2+} solution of a concentration of 0.210 M (49.8 mg/mL). The absorption spectrum of a 10 uL assay of this

solution in 1 mL 2 M $HClO_4$ was recorded in a 2 mm path length cell which indicated the presence of NpO_2^{2+}. This Np(VI) stock solution was used for complexation experiments.

3.3.1.3. Preparation of Pu(VI)

A stock solution of PuO_2^{2+} was prepared by oxidation of a plutonium solution with ozone as described previously[63]. A mixture of plutonium from a plutonium residues pot was added dropwise to a stirring solution of 15 mL of 10 M NaOH in an Erlenmeyer flask giving a hazy green/yellow solution. The resulting suspension was centrifuged in batches in 50 mL PPCO Oak Ridge tubes, yielding green Pu^{4+} hydroxides and a colorless supernatant. The supernatant was removed and 7 mL of H_2O was added to the remaining green solids in the PPCO Oak Ridge tube and the tube was vortexed for a more thorough washing. The suspension was centrifuged, the colorless supernatant discarded, and the H_2O wash step repeated. The resulting green solid was suspended in 2 mL of 0.1 M NaOH, vortexed and transferred to a 20 mL glass vial. Ozone was bubbled through the resultant suspension with stirring for 24 h in order to fully oxidize Pu to $Pu^{VI}O_2^{2+}$, producing dark brown solids. The solution was stirred as 70 uL of 4 M HNO_3 was added and the dark brown solution turned cloudy. Ozone was bubbled through the suspension for an additional 2 h in order to oxidize the remaining Pu^{4+} to $Pu^{VI}O_2^{2+}$. The hydroxide concentration was raised to *ca.* 1 M NaOH with the addition of 340 μL of 10 M NaOH and ozone was bubbled through the solution for an additional 2 h. The pH of the solution was then lowered to 0.6 with the addition of 350 μL of 12 M HNO_3 resulting in an orange pink solution with some haziness. The orange pink solution was then added to a glass vial containing 0.470 mL of 1 M $(NH_4)_2CO_3$ with stirring, yielding a greenish solution at first but eventually turning a red color as more of the plutonium solution was added. The suspension was allowed to settle,

giving a nearly colorless/slightly yellow supernatant at a measured pH of 5.5. The suspension was transferred to an Oak Ridge tube and centrifuged. The slightly yellow supernatant was removed, and the remaining light brown solids were washed with H_2O twice. The washed solids were then suspended in 500 μL of 4 M HNO_3 in the Oak Ridge tube to yield a hazy orange brown solution which was then filtered into a small glass vial. The clear orange brown solution was analyzed by UV-Vis-nIR spectrometry in a 1 cm path length cell in 1 M $HClO_4$ confirming the presence of PuO_2^{2+} with a sharp peak at 830 nm yielding a 0.176 M solution (ε_{830}=555 $\frac{1}{\text{M cm}}$). The PuO_2^{2+} solution was then transferred to a 5 mL pyrex volumetric flask with the neck wrapped in aluminum foil and heated on a stir plate to near dryness. The residual light brown solution was diluted with 200 μL of 0.2 M HNO_3 and transferred to a glass scintillation vial. 5 μL of this solution was analyzed by UV-vis-nIR spectrometry in 800 μL 1 M $HClO_4$ in a 1 cm path length cell. A sharp peak at 830 nm suggested a pure PuO_2^{2+} solution at a concentration of 0.270 M with no characteristic Pu^{4+} bands at 469 nm or Pu^{3+} bands at 600 nm. This Pu(VI) stock solution was used for complexation experiments.

3.3.1.4. Preparation of Pu(V)

A combined mixture of 790 μL H_2O, 4 μL of 0.2 M HNO_3 and 2 μL of a 1.796 M H_2O_2, a reductant for Pu(VI), solution was stirred while 5 μL of a 1.16 M Pu(VI) solution in 1000 μL of water was added. The pH was measured as 1.18 and was raised to 4.15 with the addition of 75 μL of 0.1 M NaOH and 45 μL of 1 M NaOH. The solution was allowed to stir overnight. The solution was transferred to a small Oak Ridge tube, centrifuged and the supernatant was collected. The supernatant was analyzed by UV-Vis-nIR spectrometry which showed a prominent peak at 570 nm corresponding to a 6.0 mM Pu(V) solution.

3.3.2. Synthesis of Organic Soluble Ligand-Actinyl Complexes

Coordination chemistry experiments were conducted with U(VI), Np(VI) and Pu(VI). Actinyl stock solutions were evaporated to dryness with heat and allowed to cool to room temperature. The resultant solids were then stirred in 1 mL CH_3CN and yellow t-butyl salen suspended in 1 mL CH_3CN was added with continuous stirring, producing dark colored solutions. The reactions were diluted with the additional CH_3CN. The reactions were stirred for 3 hours affecting the precipitation of dark colored solids. The solutions were centrifuged and filtered through a glass wool column in a glass pasteur pipette. The supernatant was collected and stored in a freezer, producing diffraction quality crystals after several weeks. The crystalline solids were then analyzed by X-Ray diffraction. Structural data collected from X-Ray crystallography can give us a detailed look into the coordination environment of the ligand-metal complex. The supernatant from the reactions were analyzed spectroscopically. This will be discussed in the Results chapter.

3.3.3. Synthesis of Water Soluble Ligand-Actinyl Complexes

Coordination chemistry experiments were conducted with U(VI), Np(V), Np(VI), Pu(VI) and Pu(V). Aqueous solutions of the actinyl cations were evaporated to dryness with heat and allowed to cool to room temperature. The resultant solids were then stirred in 1 mL H_2O and yellow H_2Salen-SO_3 dissolved in 1 mL H_2O was added with continuous stirring. The reactions were diluted with the addition of 1 mL H_2O, centrifuged, and filtered through a glass wool column in a glass pasteur pipette. The supernatant was collected, diluted with the addition of an equal volume of EtOH and stored in a freezer. Crystalline solids suitable for X-Ray diffraction

were only collected for the $[(Salen\text{-}SO_3)(UO_2)(H_2O)]^{2-}$ and $[(Saldien\text{-}SO_3)(UO_2)]^{2-}$complex. The supernatant from the reactions were analyzed spectroscopically. This will be discussed in the Results chapter.

3.4. Solvent Extraction Studies

3.4.1. Materials

Aqueous solutions were prepared using deionized water obtained with a resistivity of at least 18 MΩ cm^{-1}, using a MilliQ laboratory purification system (Millipore, Bedford, MA), and degassed by sparging with nitrogen gas. For the solvent extraction experiments, a $UO_2(NO_3)_2$ working stock solution was prepared from a commercial ICP standard solution of depleted (0.2% ^{235}U) uranyl nitrate (1000 ppm, Inorganic Ventures, Christiansburg, VA, USA). Potassium nitrate was used as the background electrolyte to maintain a constant ionic strength of 0.1 M of solutions. Plutonium-239,Neptunium-237, and Amerecium-243 were obtained from Idaho National Laboratory. The Pu(IV) was stored in 8 M while solutions of Np(V) had been prepared from a more concentrated stock and stored in 0.5 M HNO_3. Working solutions of Pu(VI) and Np(VI) used for solvent extraction studies were prepared from these stock solutions by dilution and oxidation state adjustment.

3.4.2. Uranium Extraction Studies

Extraction studies were carried out using an aqueous phase containing 0.001 M uranyl(VI) in 0.1 M KNO_3 with an adjusted pH (initial pH, pH_i) of 3.00. The organic extractant phase was prepared by dissolving weighed amounts of extractant in a diluent mixture composed of 1-octanol/toluene (7:3 v/v). The organic phase was pre-equilibrated with 0.1 M KNO_3

without any metal present. An equal volume (500 µL) aliquot of each organic and aqueous solution was placed in a 2 mL glass vial with a screw cap and was shaken vigorously on a vortex shaker for a predetermined amount of time. The details of each experiment will be described below. The organic and aqueous phases were then separated by centrifugation and an aliquot of 100 µL of each phase was placed and sealed into a 1.4 mL neutron activation analysis (NAA) polytube followed by secondary containment in an 8 mL NAA polytube. The samples were irradiated at the UC Irvine Mark I TRIGA Reactor for 1 hour at a power level of 250 kW at an estimated neutron flux of $8x10^{11}$ n cm^{-2} s^{-1}. The ^{239}U product ($t_{1/2}$=23 min) was allowed to decay and the subsequent ^{239}Np ($t_{1/2}$=2.3 days) decay gamma rays were counted using a Canberra High Purity Germanium (HPGe) detector operated with Genie^{TM} 2000 (v. 3.2.1) gamma acquisition and analysis software. The count rates were normalized to the reactor shutdown time and the distribution ratios were determined from the gamma count rates from the organic phase to the aqueous phase (using the gamma peak at 109.7 keV for ^{239}Np). All experiments were done in triplicate and the error bars for distribution ratios (D) in the figures are based on the standard deviations in these triplicates.

Initial extraction experiments were carried out in toluene. When it was noted that the ligand-metal complex would precipitate from solution, extraction studies were carried out in order to identify an optimized diluent mixture that results in greater metal extraction and total mass recovery. All subsequent extractions consisted of the selected diluent mixture, 7:3 1-octanol.toluene (v/v). Initial extraction experiments were then carried out to investigate the time needed to reach extraction equilibrium for each ligand. Organic solutions of (Salen, di-t-butyl Salen and di-t-butyl Salophen) at a concentration of 0.025 M and Salophen at a concentration of 0.012 M were contacted with 0.001 M UO_2^{2+} in 0.1 M KNO_3 for a varied amount of time. Time

taken to reach extraction equilibrium was the time of contact used for each ligand in the following extraction studies. In order to estimate the average number of ligand molecules bound to each actinyl metal ion, extraction experiments with varying concentration of the ligand in the organic solution were carried out. Organic solutions of Salen (0.001 - 0.025 M) were contacted for 10 min, solutions of di-t-butyl Salen and di-t-butyl Salophen (0.001 - 0.025 M) were contacted for 2 h and solutions of Salophen (0.001 - 0.012 M) were contacted for 1 h. Contact times were determined based on results from the kinetic extraction experiments described above. Extraction experiments to investigate the pH dependence of the system were also carried out. Organic solutions of the ligands were contacted with 0.001 M UO_2^{2+} in 0.1 M KNO_3 at varying initial pH. The pH_{eq} of the aqueous phases were recorded immediately after the organic and aqueous phases were separated. A semi-micro refillable electrode (Beckman-Coulter) was calibrated with the mV of standard buffer solutions (Fisher Scientific- pH 4, 7, 10).

3.4.3. Plutonium Extraction Studies

An aliquot (300 μL) of Pu(IV) in 8 M HNO_3 was added to 1 mL of 0.5 M HNO_3 and heated to near dryness. An additional 1 mL of 0.5 M HNO_3 was added to the residue and the process was repeated several times. This treatment is reported to oxidize Pu(IV) to Pu(VI) after several hours.[31, 64] The solution was then diluted in 3 mL of 0.1 M KNO_3 and the pH was increased to 3.00. Equal volumes of an organic solution of di-t-butyl Salen (0.025 M) were contacted with aqueous solutions containing Pu(VI). After extraction, an aliquot (50 μL) of the aqueous samples were electroplated onto stainless steel planchets from a dilute sulfuric acid electrolyte as described by Phoenix Scientific Sales for analysis by alpha spectroscopy.[65] Since the electrodeposition of organic solutions can lead to inconsistent results[66] the distribution ratio

for Pu was determined from the activity in the aqueous phase only. Sample of the aqueous phases before contact were collected and the estimated activity in the organic phase was based on the difference in the aqueous phase before and after contact. The ^{239}Pu alpha decays were counted using a Canberra Alpha Analyst operated with Alpha Acquisition and analysis software. The distribution ratio was determined from the count rates in the aqueous phases based on the alpha peak at 5,157 keV. All experiments were done in duplicate and the error bars for distribution ratios (D) in the figures are based on the standard deviations in these duplicates.

3.4.3.1. Plutonium Continuous Extraction Studies

An aliquot of a freshly made Pu(VI) solution was diluted in 0.1 M KNO_3 to a total volume of 5 mL and, in separate experiments, water-soluble Schiff base ligands (Salen-SO_3 and Saldien-SO_3) (0.010 M) were added to the aqueous solution. Ammonium acetate and ammonium nitrate was then added in a mixture that resulted in a pH of 5.5. An organic solution of equal volume (5 mL) consisting of 0.010 M HDEHP in toluene was slowly layered over the aqueous phase. The two phases were vigorously mixed and aliquots from the organic and aqueous phase were samples at various time points. Aqueous aliquots were analyzed by alpha spectroscopy. The same experiment was repeated but with no water-soluble Schiff base present in the aqueous phase in order to measure the plutonium partitioning by 0.010 M HDEHP only.

3.4.4. Neptunium Extraction Studies

An aliquot (60 μL) of a previously made Np(V) working stock solution was diluted in 1 mL of 4 M HNO_3 and heated to near dryness. An additional 1 mL of 4 M HNO_3 was added the residue and the process was repeated several times. This treatment is reported to oxidize Np(V)

to Np(VI). The solution was then diluted in 3 mL of 0.1 M KNO_3 and the pH was increased to 3.00. Equal volumes of an organic solutions of di-t-butyl Salen (0.025 M) were contacted with aqueous solutions containing Np(VI). After extraction, an aliquot (50 μL) of the aqueous samples were electroplated onto stainless steel planchets as described above for the Pu analysis. The ^{237}Np alpha activity in each sample was determined from the count rates in the aqueous phases at 4,790 keV. All experiments were done in duplicate and the error bars for distribution ratios (D) in the figures are based on the standard deviations in these duplicates.

3.4.5. Americium Continuous Extraction Studies

An aliquot of an Americium-243 stock solution was diluted 0.1 M HNO_3 and underwent oxidative treatment by excess sodium bismuthate for 12 h. This process is known to oxidize Am(III) to Am(V).[67,32] The solution was then filtered to remove residual particulates and the collected solution was diluted in 0.1 M KNO_3. Ammonium acetate and ammonium nitrate were added in a ratio that resulted in a pH of 5.5. Salen-SO_3 (0.010 M) was added to the aqueous solution and an organic solution of equal volume (5 mL) consisting of 0.010 M HDEHP in toluene was slowly layered over the aqueous phase. The two phases were vigorously mixed and aliquots from the organic and aqueous phase were samples at various time points. Aliquots of organic and aqueous phases were analyzed by gamma ray spectroscopy and distribution ratios were calculated from count rates at 80 keV. The same experiment was repeated but with no water-soluble Schiff base present in the aqueous phase in order to measure the americium partitioning by 0.010 M HDEHP only.

3.5. Hydrolytic Studies

A 0.025 M solution of di-t-butyl Salen in a diluent mixture of 70% (1-octanol/toluene) was contacted with an aqueous phase consisting of 0.1 M KNO_3 at different pH levels for a varied amount of time up to 24 hours on a vortex shaker. The two phases were then separated by centrifugation and the organic phase was collected and analyzed by absorption and ESI-mass spectrometry.

3.6. Low LET Radiolytic Studies

Solutions were irradiated in a Cs-137 gamma irradiator at a dose rate to water of 2 kGy/h. The dose rate of the source was determined by Fricke dosimetry.[68] Organic solutions (10 mL) of 0.025 M di-t-butyl Salen, 0.025 M Salen and 0.012 M di-t-butyl Salophen 70% (1-octanol/toluene) in a glass vial were placed in the gamma irradiator cell and aliquots of 500 μL were removed from each solution periodically. Organic solutions were analyzed by absorption spectroscopy and ESI-MS. Absorption spectra were collected on an Olis-upgraded Cary 14 UV-vis-NIR dual-beam spectrometer using a cm 1 cm path length cell and ESI-MS spectra were collected on a ESI LC-TOF Premier Micromass LCT 3 in flow injection analysis mode operating Waters MassLynx V 4.0.

4. Results

4.1. Structural Characterization of Ligand-Actinyl Complexes

4.1.1. (AnO_2)(di-t-butyl Salen)(CH_3CN)

Isostructural complexes between t-butyl salen and uranyl(VI), neptunyl(VI) and plutonyl(VI) were structurally characterized (Figure 4.1-4.3). The linear dioxo actinyl moities are coordinated by the two imine nitrogens and two deprotonated phenolic oxygens of the ligand with a CH_3CN molecule occupying the fifth coordination position in a distorted pentagonal bipyramidal geometry. Pentagonal bipyramidal geometry is the most common geometric arrangement for 7-coordinate actinyl complexes.[44, 69] Select bond distances and angles between the actinyl cations and the ligand are listed in Table 1. The average An-O bond distance of the linear actinyl moiety is 1.7739 Å, which falls in the range of other structurally characterized actinyl(VI) cations.[69b,70,71] The bond distances and angles between t-butyl-Salen and U(VI) and Np(VI) are similar to those in other structurally characterized tetradentate salen-actinyl(VI) structures.[72,73] The average bond length between the central actinyl moiety and the deprotonated phenolic proton (An1-O_{ligand}) are 2.22765, 2.22105, and 2.2328 Å in the U(VI), Np(VI) and Pu(VI) complexes respectively. This result is similar to isostructures between the actinyl(VI) cations and triacetate and tricarbonate complexes where there is no noticeable trend in the An-O bond lengths in the equatorial position.[71] However, there is a slight decrease in the average bond length between the central actinyl moiety and the imine nitrogens (An1-N_{ligand}) (2.54355, 2.5346 and 2.5246 Å) going across the mid-actinide series. This could be evidence a slight strengthening of complexation between the imine nitrogen and the actinyl cation going across the series. There is a decrease in the bond angle between the central actinyl moiety and the deprotonated phenolic protons about the equatorial plane (O1-An1-O2) going across the mid

actinide series (153.18(13)°, 152.834(9)° and 149.95°). In addition, there is a slight increase in bond angles between the imine-actinyl-oxygen (O-An-N) going across the series. These trends in bond angles and the bond lengths suggest that the plutonyl(VI) cation is located deeper in the N_2O_2 bonding site of the Schiff base compared to the uranyl(VI) and neptunyl(VI) cations. The bond length between the actinyl and the CH_3CN molecule occupying the fifth equatorial position are similar for the three actinyl complexes (2.5919(52), 2.5847(3) and 2.5884 Å) across the series, but longer than the An-O bond lengths of bound water molecules (2.447(9)[74]) and methanol molecules (2.4415(14)[73]) in other An(VI) structures. A longer bond length suggests weaker complexation by CH_3CN than H_2O and EtOH to the actinyl moiety.

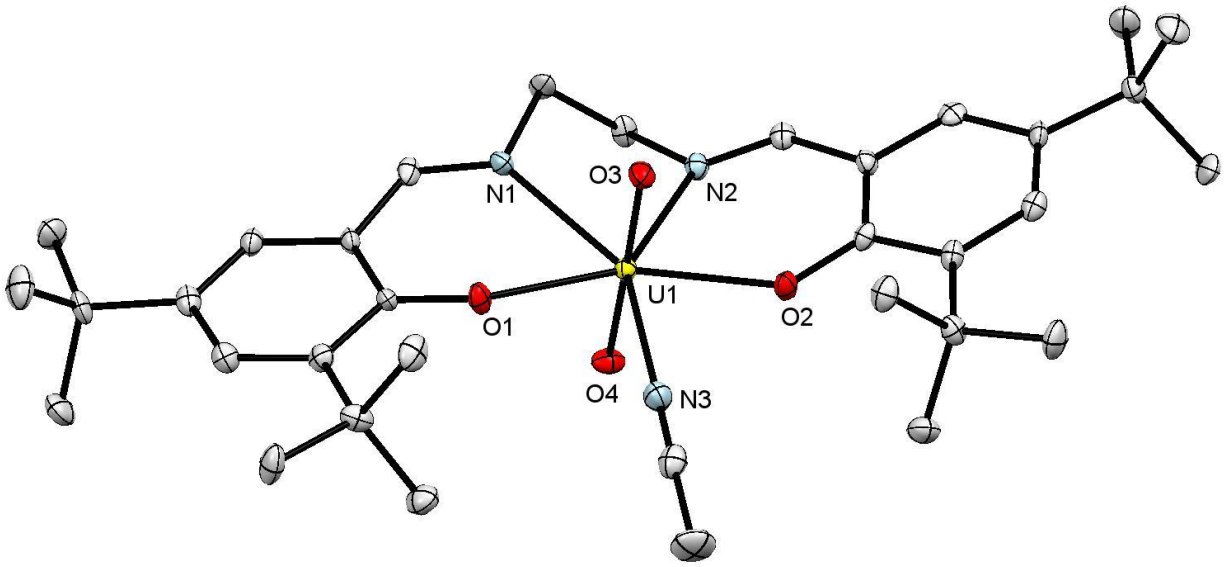

Figure 4.1. Single crystal X-ray diffraction structure of (UO_2)(N,N'-bis-(3,5-di-tert-butylsalicylidene)-1,2-ethylenediamine)(CH_3CN) complex. All hydrogen atoms have been removed for clarity. Atoms colors are C (black), N (blue, O (red) and U (yellow). Space group P $2_1/c$, a =16.5769(19), b = 7.7063(9), c = 27.118(3) Å, α = 90.00, β = 92.8260(10), γ = 90.00°, V = 3460.02(68) $Å^3$.

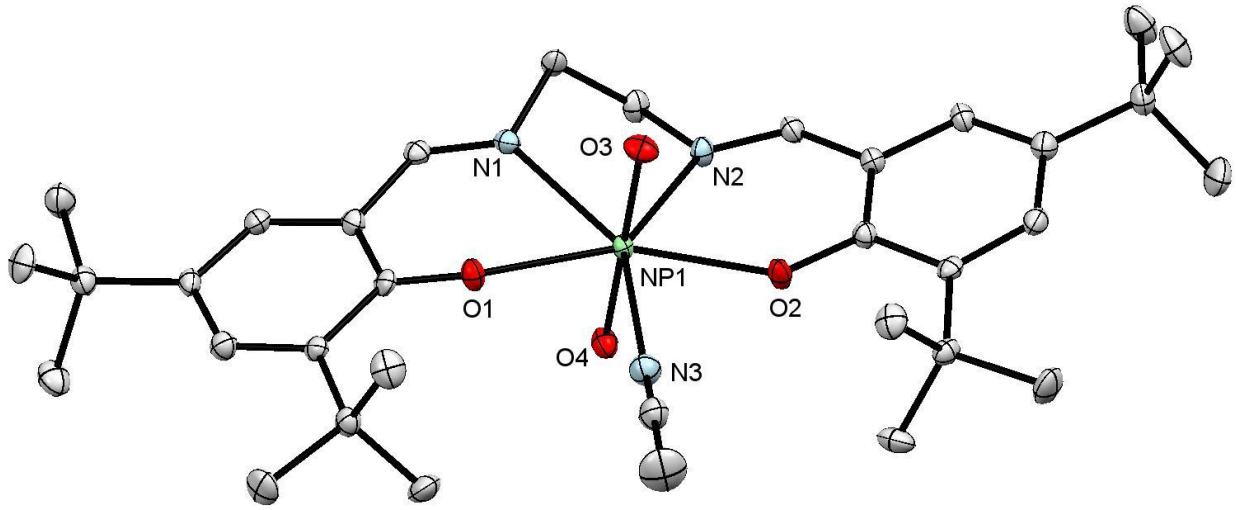

Figure 4.2. Single crystal X-Ray diffraction structure of (NpO_2)(N,N'bis-(3,5-di-tert-butyl salicylidene)-1,2-ethylenediamine)(CH_3CN) complex. All hydrogen atoms have been removed for clarity. Atoms colors are C (black), N (blue, O (red) and Np (green). Space group P $2_1/c$, a =16.5654(25), b = 7.7270(12), c = 27.1334(41) Å, α = 90.00, β = 93.069(2), γ = 90.00°, V = 3468.12(92) $Å^3$.

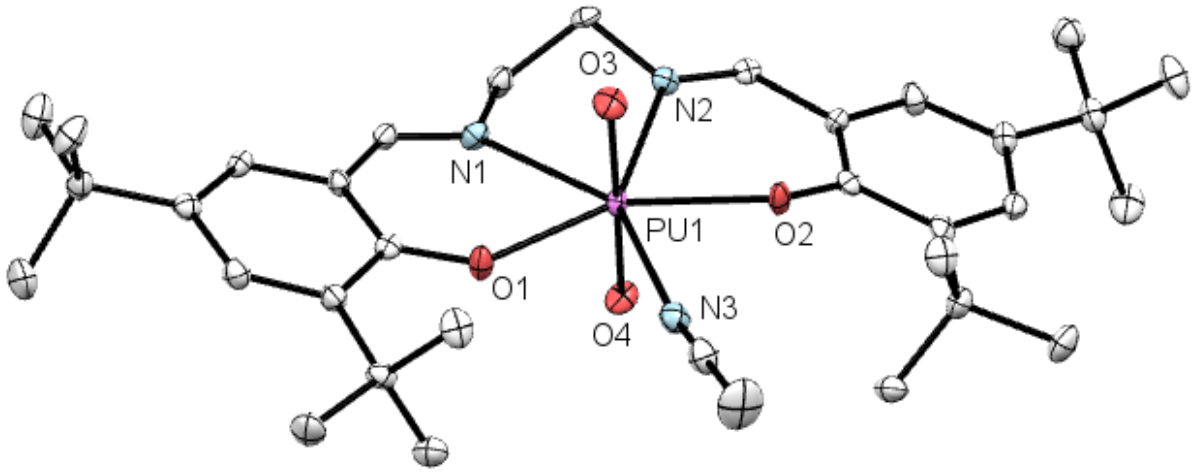

Figure 4.3. Single crystal X-Ray diffraction structure of (PuO_2)(N,N'bis-(3,5-di-tert-butyl salicylidene)-1,2-ethylenediamine)(CH_3CN) complex. All hydrogen atoms have been removed for clarity. Atoms colors are C (black), N (blue, O (red) and Pu (purple). Space group P $2_1/c$, a =16.5781(17), b = 7.7308(8), c = 27.058(3) Å, α = 90.00, β = 93.0523(16), γ = 90.00°, V = 3462.89 $Å^3$.

Table 4.1. Select bond lengths and bond angles for (UO_2)(di-t-butyl Salen)(CH_3CN), (NpO_2)(di-t-butyl Salen)(CH_3CN) and (PuO_2)(di-t butyl-Salen)(CH_3CN).

	UO_2^{2+}	NpO_2^{2+}	PuO_2^{2+}
An1-O3 (yl)	1.7774(38)	1.7719(2)	1.7686
An1-O4 (yl)	1.7761(40)	1.7689(2)	1.7805
An1-O2 (Ligand)	2.2358(34)	2.2292(3)	2.2328
An1-O1 (Ligand)	2.2195(35)	2.2129(3)	2.2506
An1-N2 (Ligand)	2.5357(46)	2.5268(3)	2.5246
An1-N1 (Ligand)	2.5514(45)	2.5424(3)	2.4846
An1-N3 (CH_3CN)	2.5919(52)	2.5847(3)	2.5884
O4-An1-O3	178.35(18)	178.290(6)	177.73
O1-An1-O2	153.18(13)	152.834(9)	149.95
N1-An1-O1	69.76(14)	70.315(5)	71.77
N2-An1-N1	66.70(14)	66.430(5)	67.1
O2-An1-N2	70.46(14)	70.487(5)	71.45

4.1.2. $[(UO_2)(Salen\text{-}SO_3)(H_2O)]^{-2}$

The linear dioxo uranyl(VI) moiety (UO_2^{2+}) is coordinated to the two imine nitrogens and two deprotonated phenolic oxygens of the salen-SO_3^- ligand with a water molecule coordinated by the oxygen atom at the fifth equatorial position.[75] The environments around the central uranium atom is a distorted pentagonal bipyramidal geometry, again, the most common geometric arrangement for 7-coordinate uranyl complexes.[69b] The distorted "stepped" conformation, observed in other previously reported hydrophobic uranyl-salen complexes[72,73], is still present suggesting that the addition of the sulfonate groups to the aromatic ring has negligible impact on the coordinating environment around the uranyl moiety or the formation of the complex. The bond lengths and angles associated with the central uranyl moiety and the

tetradentate N_2O_2-donor ligand in $[UO_2(salen\text{-}SO_3)(OH_2)]^{2-}$ are comparable to those previously reported uranyl-salen complexes.

4.1.3. $[(UO_2)(Saldien\text{-}SO_3)]^{-2}$

Single crystal X-ray diffraction revealed the linear dioxo uranium moiety UO_2^{2+} to be coordinated to three nitrogens and two deprotonated phenolic oxygens of the saldien-SO_3^{2-} ligand (Figure 4.4). The 7-coordinate uranium atom therefore has the expected distorted pentagonal pyramidal coordination environment. Comparing the structure of the aqueous soluble $[UO_2(saldien\text{-}SO_3)]^{2-}$ with the structure of the previously reported complex (UO_2)(saldien) in DMSO[42] reveals that the coordination environment around the uranium atom, bond lengths and angles, are almost identical between the different complexes (Table 1). It is evident that the addition of the sulfonate groups and the net negative 2 charge has minimal impact on the aromatic rings of the saldien and does not interfere with the complex formation, as was previously observed for the analogous tetradentate salen complex.[76] The only notable difference is the slight decrease in the equatorial O-U-O angles observed between the uranium and the phenolic oxygens for the sulfonated system vs. the non-sulfonated system (84.65(10) vs. (88.79(11)°).

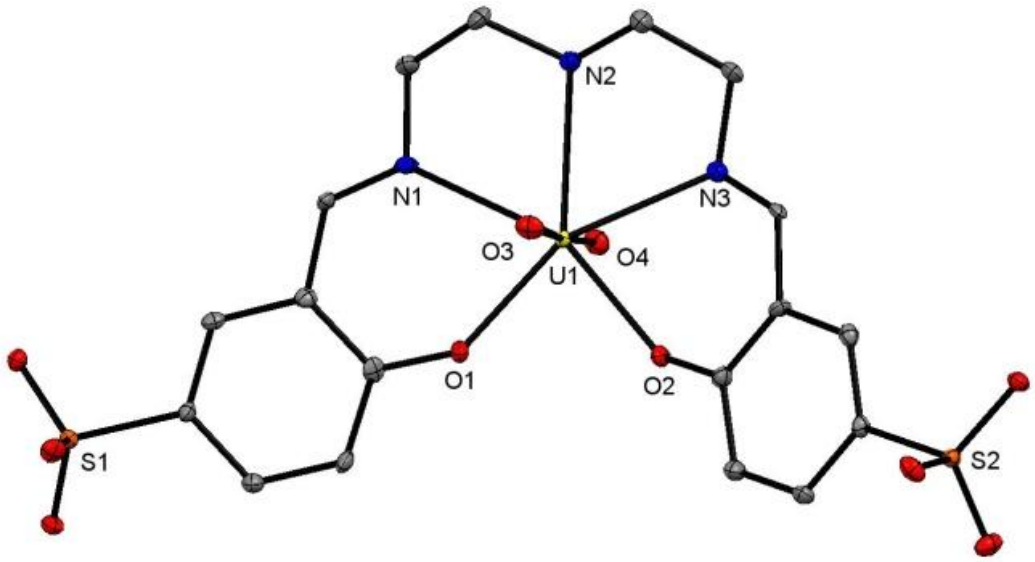

Figure 4.4. Structural representation of $[UO_2(saldien\text{-}SO_3)]^{2-}$ complex. All hydrogen atoms have been removed for clarity. Atom labelling: - uranium = yellow, nitrogen = blue, carbon = grey, sulphur = orange, oxygen = red). P 2_1, a 7.8241(9), b 10.6608(12), c 19.817(2) Å, α 90.00, β 101.3740(10), γ 90.00˚, V= 1620.50(31) $Å^3$, Z=4.

Table 4.2. Selected bond lengths and angles for $[UO_2(Saldien\text{-}SO_3)]^{2-}$ (1), (UO_2)(Saldien) in DMSO[42] (2), and $[UO_2(Salen\text{-}SO_3)(OH_2)]^{2-}$ [75] (3).

	1	2	3
U1-O3 (yl)	1.7853(24)	1.7883(33)	1.763(13)
U1-O4 (yl)	1.7826(24)	1.7899(33)	1.7700(17)
U1-O1 (Ligand)	2.2469(23)	2.2201(35)	2.2742(20)
U1-O2 (Ligand)	2.2467(24)	2.2313(33)	2.2827(18)
U1-N1 (Ligand)	2.5571(32)	2.6021(31)	2.5257(20)
U1-N2 (Ligand)	2.5741(32)	2.5810(39)	2.5661(21)
U1-N3 (Ligand)	2.5602(31)	2.5857(37)	
O4-U1-O3	176.04(18)	176.18(17)	178.74(7)
O1-U1-O2	84.65(10)	88.79(11)	
O1-U1-N1	71.16(9)	70.15(11)	69.22(7)
N3-U1-O2	71.14(9)	69.96(11)	69.15(7)
N1-U1-N2	66.86(9)	65.68(13)	
N2-U1-N3	66.90(9)	65.86(12)	

4.2. Spectroscopic Characterization of Salen-Actinyl Complexes

4.2.1. $(An^{VI}O_2)$(di-t-butyl Salen)(CH_3CN)

4.2.1.1. Absorption Spectroscopy

The absorption spectrum of the ligand and the reactions with the actinyl(VI) cations are overlaid in Figure 4.5. Although structural data was useful in determining the coordination environment between the ligand-metal complex, absorption data was invaluable in elucidating the redox stability, and confirming the oxidation states of the actinyl ions during complexation. The absorption bands for the ligand are observed around 330 nm arising from $\pi \rightarrow \pi^*$ transitions in the aromatic ring and azomethine[51] followed by an absorption band at 342 nm possibly attributed to $n \rightarrow \pi^*$ transitions in the azomethine group.[77] An appreciable amount of red shift is observed upon complexation of UO_2^{2+} by t-butyl-Salen as absorption bands appear at 342, 420 and 500 nm. These peaks are most likely a result from ligand-metal charge transfer transitions due to azomethine coordination with the actinyl cation.

The absorption spectrum of NpO_2^{2+} is primarily characterized by a band at 1223 nm likely attributed to an intra-5f transition, two transitions at 460 and 560 nm and a charge transfer transition at energies greater than 400 nm.[78] Upon complexation by the ligand, the absorption spectrum is characterized by an intense charge transfer transition (200-1300 nm) with bands in the 540-650 nm range. Although there is no blue shift by the band at 1223 nm to 1120-1140 nm, characteristic of previously studied Np(VI) complexes[79], the lack of transitions at 980 and 1000 nm, corresponding to free and complexed Np(V), suggests there was no reduction of NpO_2^{2+} to NpO_2^{+} upon complexation. In previous work from our groups[12] we have shown that an aqueous soluble Schiff-base ligand will complex NpO_2^{2+} but rapidly reduce it to NpO_2^{+}. This behavior was not observed with the lipophilic ligand used in this work. The absence of bands at 1000 nm

in the absorption spectrum of the reaction between the ligand and Np(VI) combined with structural data collected from crystalline solids in CH_3CN allowed us to confirm the +VI oxidation state for this Np complex. We therefore assign progression bands at 540-650 nm to belong to a NpO_2^{2+} complex. Similar transitions are also observed in this region for other Np(VI) complexes in $[NpO_2(CO_3)_3]^{4-}$ [80] and NpO_2Cl_2 in THF.[81] ^1H NMR spectra collected from U(VI) and Np(VI) complexes with t-butyl Salen (Figure 4.7.) further suggest the complete coordination of the actinyl cations due to missing phenolic proton signals and an overall downfield shift of proton signals arising from ligand-metal charge transfer.

The major f-f transition ($^3H_{4g}$ to $^3\Pi_{2g}$) for the PuO_2^{2+} cation in 1 M $HClO_4$ is observed at 830 nm.[82] Low energy transitions are also observed at 950 and 980 nm along with higher energy transitions at 460, 520 and 622 nm. However, the absorption spectrum for PuO_2^{2+} in CH_3CN exhibits an absorption band at 805 nm with a slight shoulder at 830 nm and multiple transitions in the 400-650 nm and 900-1100 nm range. None of the multiple transitions present in the spectra resemble sharp peaks characteristic of Pu^{3+} (600 nm), Pu^{4+} (469 nm) or PuO_2^{+} (568 nm) allowing us to confirm the presence and stabilization of PuO_2^{2+} in CH_3CN. The absorption spectrum also bears a strong resemblance to that of Pu(VI) in 15.2 M HNO_3 [74] which could be attributed to the use of nitric acid during the preparation of the Pu(VI) solution. Upon the addition of the t-butyl-Salen to the Pu(VI) solution, there is a decrease in intensity and shift to 870 nm of the band at 805 nm. A shift to a longer wavelength by the principal f-f transition would imply coordination of the actinyl cation about the equatorial plane. The red shift is consistent with previously characterized plutonyl(VI) structures.[69a,83] The transition present at 870 nm is also comparable to a plutonyl(VI)-chloride complex, also analyzed in CH_3CN,

showing a prominent band at 850 nm.[29] The absence of bands characteristic of lower valent Pu upon complexation was further confirmation of the stabilization of PuO_2^{2+} by di-t-butyl Salen.

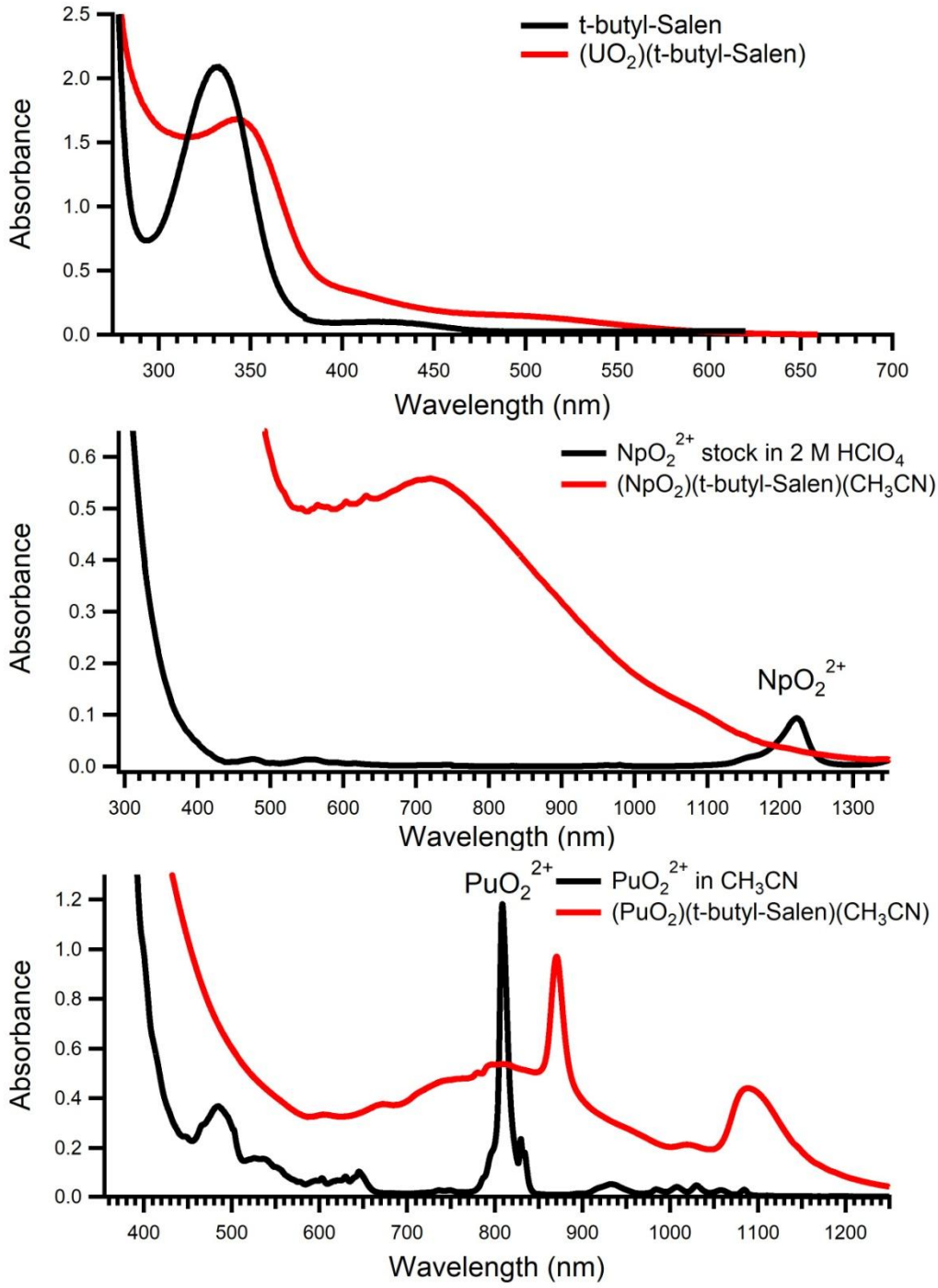

Figure 4.5. UV-Vis-nIR spectra of di-t-butyl Salen and complexes formed with U(VI) (top), Np(VI) (middle) and Pu(VI) (bottom).

4.2.1.2. NMR Spectroscopy

Figure 4.7. below show the di-t-butyl Salen molecule with each hydrogen assigned to different peaks for the purposes of the NMR spectra interpretation. The collected NMR spectra for the ligand itself, and in complex with uranyl and neptunyl are shown in Figure S2 below. The ^{1}H NMR spectra of the ligand-(UO_2) complex shows an absence of the chemical shift at 13.8 ppm, corresponding to the phenolic proton, indicating coordination through deprotonated phenolic oxygen atoms. The ^{1}H NMR spectra also depicts a significant shift in the imine HC=N proton between the free ligand (8.4 ppm) and the UO_2^{2+} complex (9.3 ppm), suggesting involvement of the lone pairs on the nitrogen and the metal center. In comparison to the free ligand ^{1}H NMR, there is an overall downfield shift of the proton signals corresponding to the diamagnetic ligand-(UO_2) complex due to the de-shielding effect of the ligand-metal charge transfer[84]. The ^{1}H NMR of the NpO_2^{2+} complex depicts the paramagnetic shift caused by the unpaired electron in NpO_2^{2+} [85,86,87]. Regardless of the paramagnetic shift, the proton signals observed in the ligand-(NpO_2) ^{1}H NMR spectra can be identified as azomethine proton at 15.21, aromatic protons at 9.45 and 7.25, ethylene protons at 2.21, CD_3CN shift at 1.99 and shifts corresponding to the tert-butyl groups at 1.34 and -0.56 ppm. Similar to the ^{1}H NMR collected of the UO_2^{2+}complex, the ^{1}H NMR of the NpO_2^{2+} complex does not show any downfield phenolic proton, further suggesting the deprotonation of the ligand during complexation.

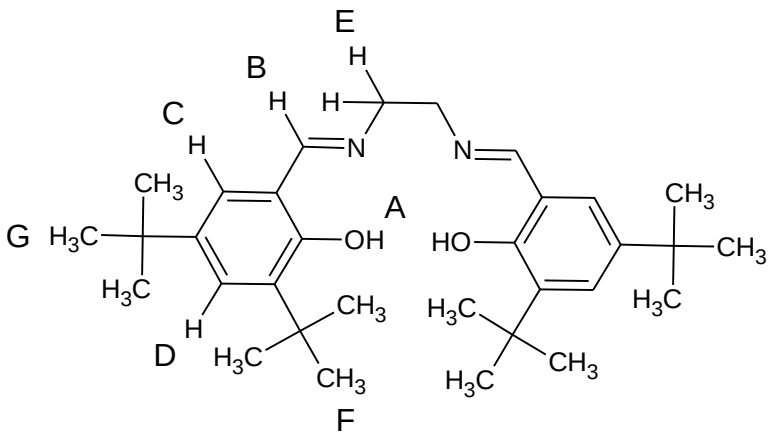

Figure 4.6. Labeled t-butyl-Salen with corresponding assigned shifts labeled in the ^{1}H NMR spectra.

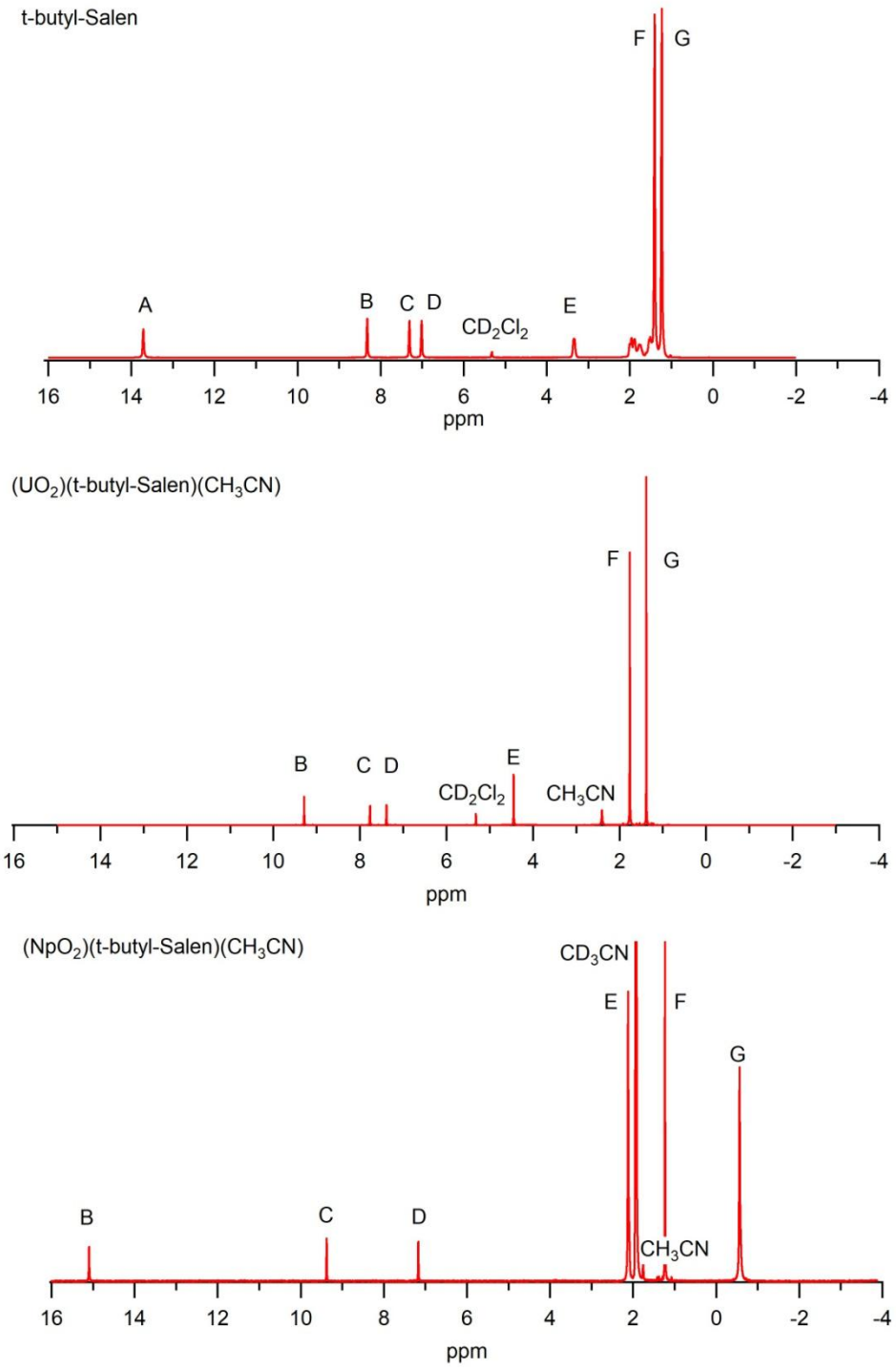

Figure 4.7. ^{1}H NMR (bottom to top) of di-t-butyl Salen in CD_2Cl_2, (UO_2)(di-t-butyl-Salen)(CH_3CN) in CD_2Cl_2 and (NpO_2)(di-t-butyl-Salen)(CH_3CN) in CD_3CN.

4.2.1.3. IR and Raman Spectroscopy

The IR and Raman spectra of the free ligand and ligand-(UO_2) complex are shown below in Figure 4. The peaks at 1630 and 1590 cm^{-1} are attributed to the combination of vibrations from C=N and aromatic C=C bonds.[88] In comparison to the IR spectra of the free ligand, there appears to be a slight shift of about 10 cm^{-1} to 1620 cm^{-1} by the stretch at 1630 cm^{-1} in the IR spectra of the ligand-metal complex, further indicating the involvement of the nitrogen atom in the coordination of the actinyl cation.[89] The most significant difference between the IR and Raman spectra of the free ligand and the ligand-(UO_2) complex is the presence of sharp, strong bands at 820 cm^{-1} in the Raman, which corresponds to the symmetric uranyl stretch[90]. The complementary symmetric uranyl stretch is observed at 840 cm^{-1} in the IR. The IR spectra of the metal complex also has a strong peak at 890 cm^{-1} which is not as prominent in the free ligand spectra. The asymmetric uranyl stretch is usually observed in 880-930 cm^{-1} for other salen-(UO_2) complexes[91] and, although there is some overlap with vibrations from C-O, C-C and C-N (from CH_3CN) bonds, we assign the stretch at 890 cm^{-1} as the asymmetric uranyl stretch.

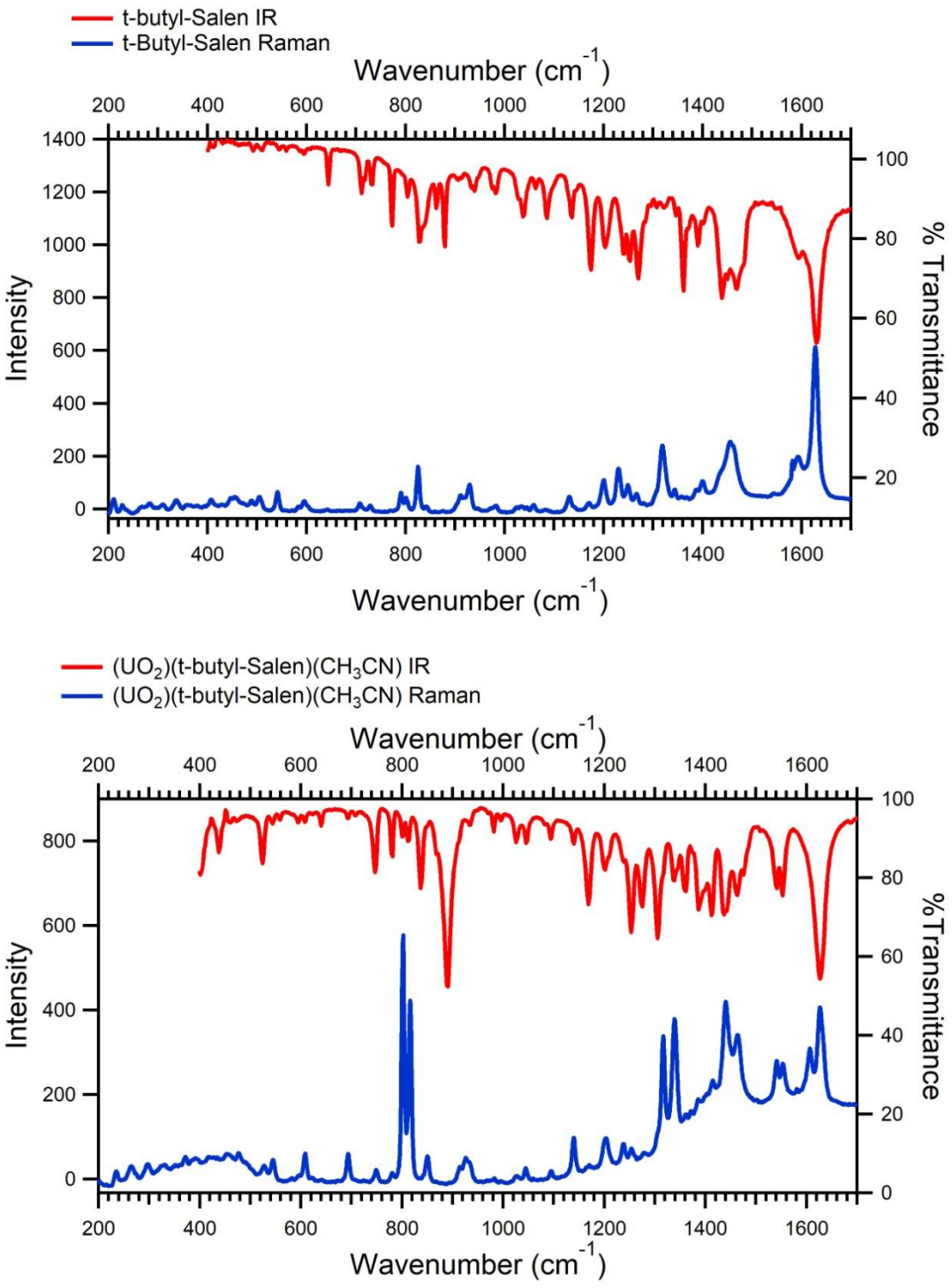

Figure 4.8. Overlay of IR and Raman spectra of free bis(3,5-di-tert-butyl) salen (top) (UO_2)(t-butyl-Salen)(CH_3CN).

4.2.2. $[(An^{V/VI}O_2)(Salen\text{-}SO_3)]^{2/3-}$

4.2.2.1. Absorption Spectroscopy

The majority of the work between Salen-SO_3 and Np(V) and Np(VI) has been previously reported in Hawkins 2014 and Hawkins 2016.[75,76] This section will focus on work carried out with plutonium.

Spectroscopic studies of the plutonyl cations with the aqueous soluble ligand were continued using stock solutions of Pu(VI) and Pu(V). An aliquot of a 0.0116 M Pu(VI) stock solution in 0.06 M HNO_3 was diluted in water and added to an equimolar solution of yellow H_2salen-SO_3 in H_2O, resulting in a pale pink color. A pH of 2.45 was recorded after 10 minutes of stirring and the solution was analyzed by UV-Vis-nIR spectrometry (Figure 4.9). The initial spectra had a prominent band at 830 nm, characteristic of free uncomplexed Pu(VI).[82] The pH was increased and the absorption spectrum was collected at each incrementing pH step ending at pH 7.30. As the pH was increased, the intensity of the band at 830 nm decreased, suggesting complexation of free Pu(VI). Similar to studies with Np(V), a pH above 7.00 was required in order to fully complex Pu(VI), evident by the absence of the 830 nm band and the presence of a red-shift band at 860 nm. We assign the peak at 860 nm to belong to the (Pu(VI))(salen-SO_3)(H_2O) complex. Structural and spectroscopic results demonstrate the stabilization and complexation of the +VI plutonyl cation by Schiff base ligands. The +VI species is complexed in CH_3CN and a high pH (> 7) was required for complexation in aqueous medium.

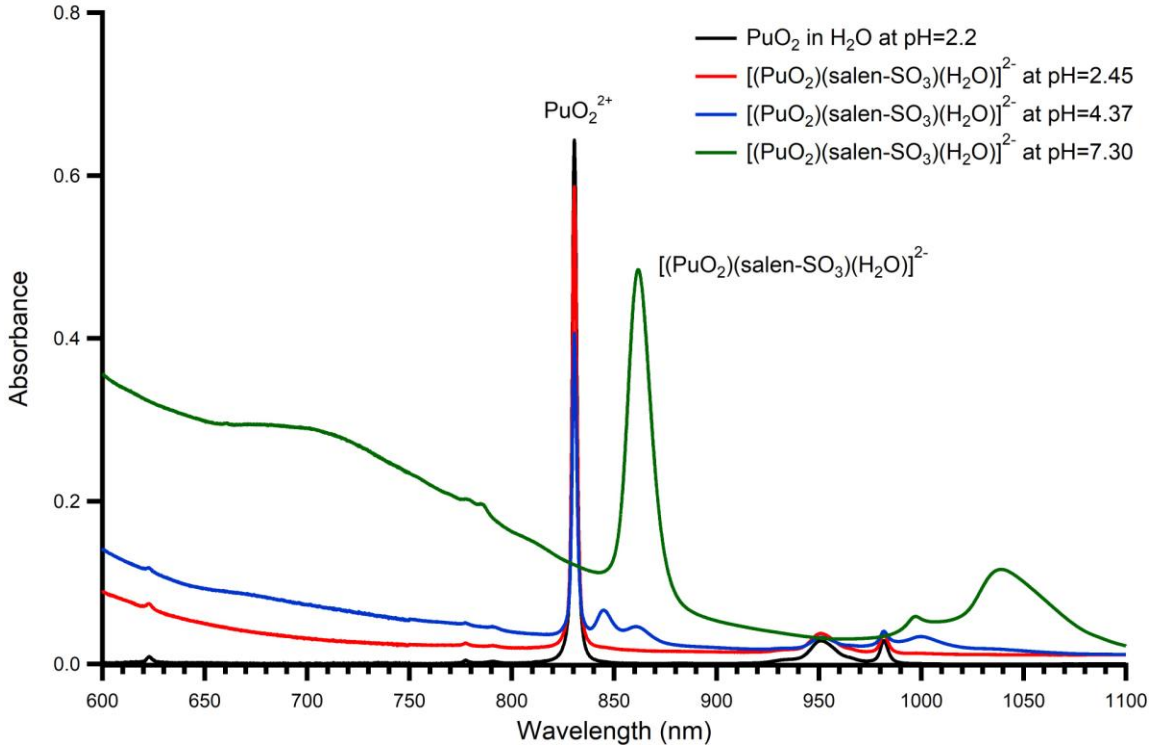

Figure 4.9. UV-Vis-nIR spectra of the reaction between Pu(VI) and H_2salen-SO_3 at increasing pH

Considering that the +V oxidation state of uranium was stabilized by a pentadentate Schiff base ligand in DMSO, spectroscopic data was collected in order to see if an aqueous soluble Schiff base ligand would stabilize the +V plutonyl species, which over time disproportionates to Pu(IV) and Pu(VI).[92] An aliquot of a 6 mM Pu(V) stock solution was carefully added to a solution of excess yellow Salen-SO_3 (2 eq) in H_2O while stirring. The solution turned a deep yellow color with a recorded pH of 6.31after the addition of Pu(VI). The UV-Vis-nIR spectra was collected 10 minutes after the start of the reaction and subsequently collected every 10 minutes (Figure 4.10). The spectral data is overlaid with an assay of the Pu(V) stock solution, which has a prominent peak at 570 nm, characteristic of Pu(V).[82] The absence of a peak at 830 nm, corresponding to Pu(VI), also confirms +V as the plutonyl species of the stock solution. However, the recorded absorption spectra bears a strong resemblance to

that of (Pu(VI))(saldien-SO3)$^{2-}$, with a band at 860 nm and a charge transfer band in the visible region.[69a, 83] The absorption band at 860 nm increases over time, attributed growth of the Pu(VI) complex. In addition, although there are no observable peaks that correspond to Pu(IV), the absorption spectra could consist of a mixture of oxidation states. Just as Salen-SO_3 has demonstrated the ability to reduce Np(VI) to Np(V)[76], it can also be reducing Pu(V) to Pu(IV) with subsequent disproportionation to Pu(VI).

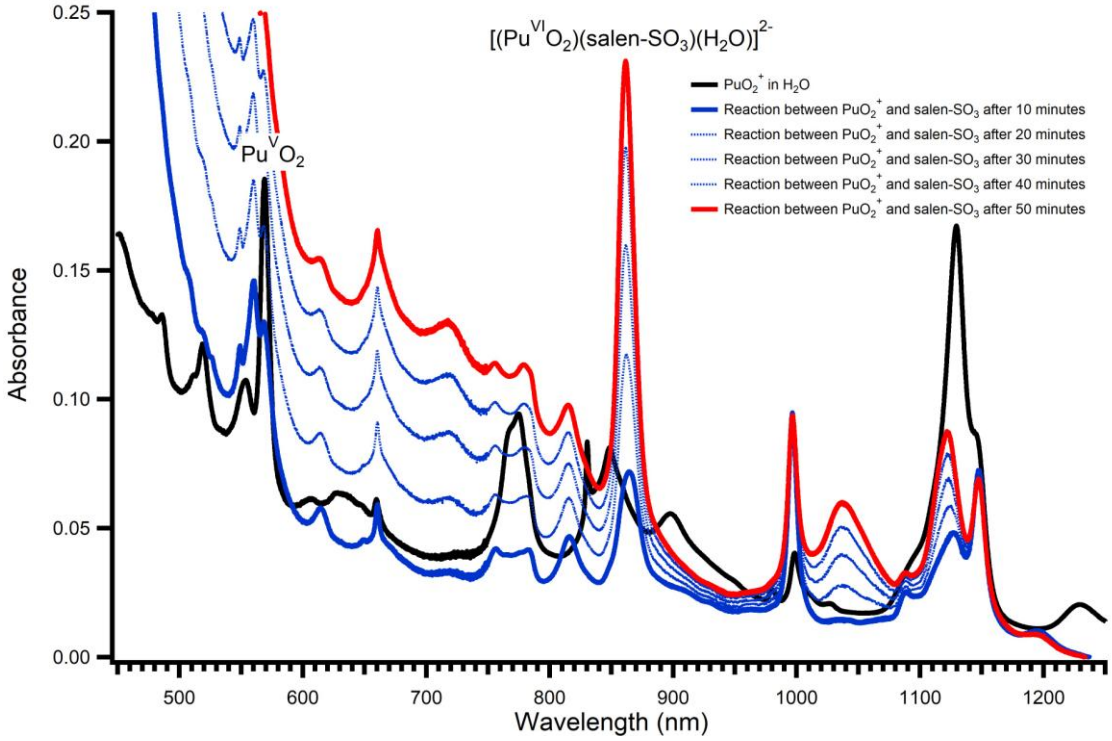

Figure 4.10. nIR/UV/Vis spectra of the reaction between Pu(V) and excess H_2salen-SO_3^- in water at pH_i=6.31 recorded over time in a 2 mm path length cell.

4.2.3. $[(An^{V/VI}O_2)(Saldien\text{-}SO_3)]^{2/3-}$

4.2.3.1. Absorption Spectroscopy

Complexation experiments were carried out with the saldien-SO_3 and neptunium(V/VI) and plutonium(V/VI) to monitor the stabilization of these transuranic actinyl cations with the pentadentate system. The +V oxidation state is the most stable redox state for Np while U(V)

readily disporportionates and Pu(V) is stable in a relatively narrow pH range. The +VI oxidation state is more stable for Np in higher acidity while the +VI oxidation state for Pu tends to be more stable at lower acidity. The complexity of the behaviour of the actinyl cations in aqueous solutions warrants studies of each redox state (+V and +VI) for Np and Pu in order to understand the behaviour the actinyl cations in conditions similar to those used in solvent extraction experiments. Results from coordination experiments should give an indication of the possible redox state and behaviour of the actinyls during biphasic solvent extraction. Previous studies with the tetradentate analogue of H_2saldien-SO_3 suggest optimal conditions for complexation at a pH above 7.[76] Thus, a pH greater than 7 was chosen to drive complexation between the aqueous soluble ligand and the metal cations. Tetrabutyl ammonium chloride ([TBA]Cl) was added to facilitate the production of crystalline material for structural characterization during Np(V) experiments.

The absorption spectrum of NpO_2^+ in dilute acid is characterized by the major f-f transition ($^3H_{4g}$ to $^3\Pi_{2g}$) at 980 nm and multiple lower energy transitions from 1000-1120 nm[30, 78,93] (Figure 4.11). Coordination about the equatorial plane of the NpO_2^+ cation results in a change in the absorption spectrum as the f-f transition is strongly affected by the coordinating ligand and the molar extinction coefficient is dependent on the symmetry of the complex.[94] Upon complexation by Saldien-SO_3 there is a shift of the band at 980 nm to 1000 nm, likely resulting from coordination with a stronger binding ligand and displacement of water molecules from the equatorial positions on the NpO_2^+ cation.[95] Overall symmetry of the complex is maintained therefore the absorption intensity is not expected to change appreciably. However, a calculated observed extinction coefficient for the band at 1000 nm of about 103.6 M^{-1} cm^{-1} is much lower than the extinction coefficient of Np(V) at 980 nm (395 M^{-1} cm^{-1}). This could

result from the spectrum being collected in water and containing (TBA)(Cl) rather than collected in 2 M $HClO_4$. The absorption spectrum is also characterized by multiple lower energy transitions at 1050-1200 nm, which appear to be red shifted from the 1000-1120 nm transitions, and a broad feature that increases in intensity with increasing energy almost across the whole spectra. The intense transition at 1000 nm is consistent with the formation of a Np(V)-Saldien-SO_3 complex and indicative of coordination of the aquo Np(V) ion through the equatorial position.[44, 76, 96] There appears to be a slight shoulder present at 980 nm in the band corresponding to the Np(V)-Saldien-SO_3 complex, attributed to uncomplexed Np(V). The complexation constant is expected to be very high under these conditions and since Saldien-SO_3 was added in equimolar amounts (1:1) to Np(V), the remaining uncomplexed Np(V) could result from hydrolysis of Saldien-SO_3.

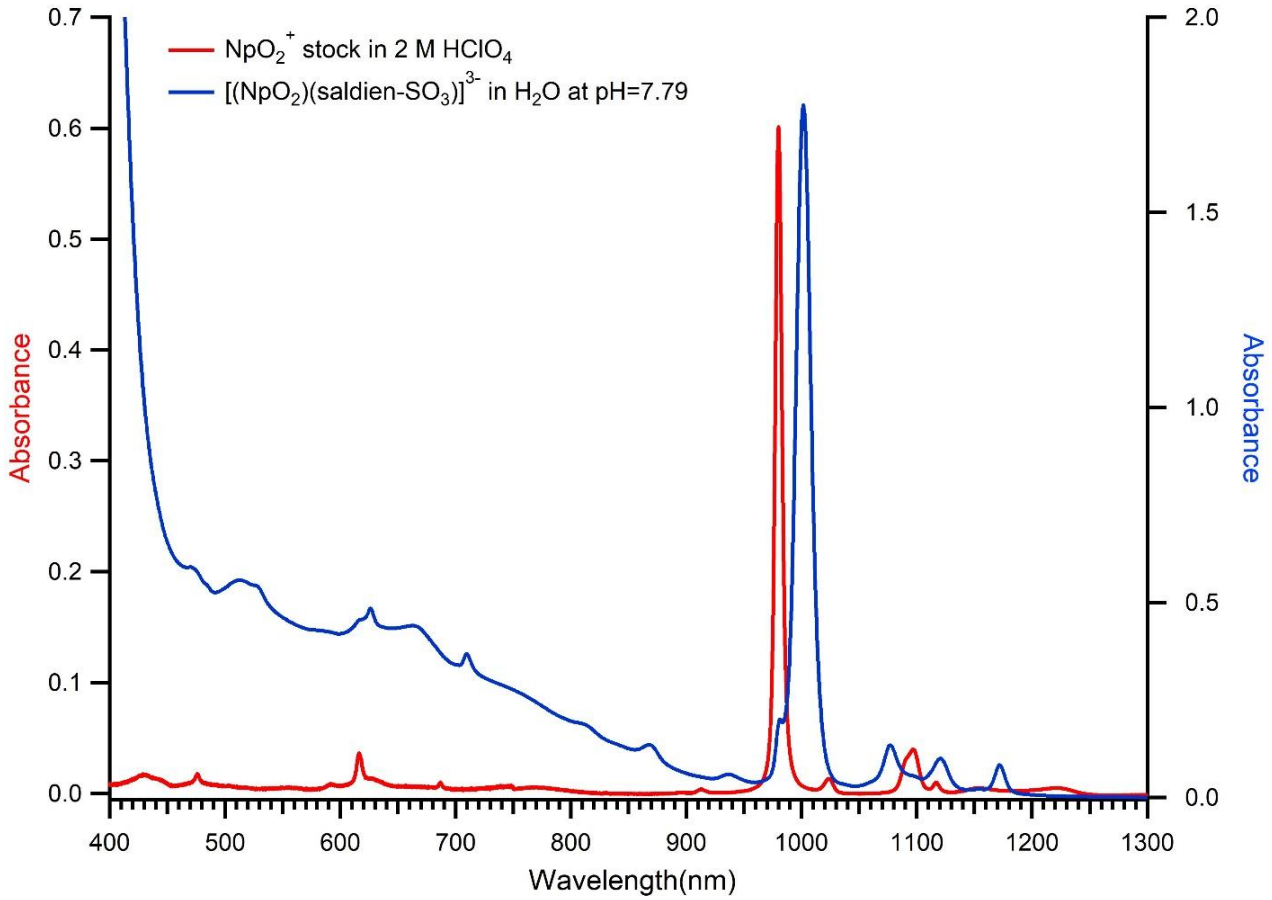

Figure 4.11. UV-Vis-nIR spectrum of a solution comprising of 1:1.5 saldien-SO_3 and NpO_2^+ in H_2O with the addition of 2 eq. of [(TBA)(Cl)] at pH 7.79, overlaid with the spectrum of NpO_2^+ recorded in a 2 mm path length cell. Absorption spectrum of NpO_2^+ only consisted of a 10 uL spike of a 0.1525 M stock solution diluted in 1 mL of 2 M $HClO_4$ and was recorded in a 1 cm path length. Concentration of NpO_2^+ in the spectrum of the reaction with saldien-SO_3 was 0.084 M.

The absorption spectrum of NpO_2^{2+} is primarily characterized by a band at 1223 nm likely attributed to an intra-5f transition.[78] However, the spectrum of the reaction between NpO_2^{2+} and saldien-SO_3 (Figure 4.12) in 1:1 H_2O/EtOH strongly resembles the spectrum of the reaction NpO_2^+ and saldien-SO_3, with a prominent sharp transition at 1000 nm, indicative of sulfonated saldien-complexed Np(V). Thus, is it likely that there is reduction of Np(VI) to Np(V). Although there is no band around 1120-1140 nm characteristic of Np(VI) complexes[79b,

[79c], the intensity of the broad transition starting at around 950 nm appears greater than observed for direct Np(V) complexation by sulfonated saldien. This initial greater intensity could result from complexes with residual Np(VI). Previous studies with the tetradentate Salen-SO_3 system and Np(VI) also indicated that reduction to Np(V) occurred.[76] Similar broad transition features were also present in the absorption spectra of that complex, which steadily decreased as a function of time (Figure S8) (We can think about including this figure, although I'm not sure if it'll be out of place or something). This decrease in intensity could be attributed to the gradual reduction of Np(VI) to Np(V). Reduction of Np(VI) could possibly be attributed to the sulfate group itself as certain conditions for the reduction of Np(VI) to Np(V) include sulfuric acid.[30] Sulfate coordination studies with neptunyl cations have also indicated the irreversible reduction of Np(VI) in high sulfate concentrations.[97] The reduction of Np(VI) could also be expedited in the high pH solution that the reaction took place in coupled with hydrolytic products (sulfonated salicylaldehyde).

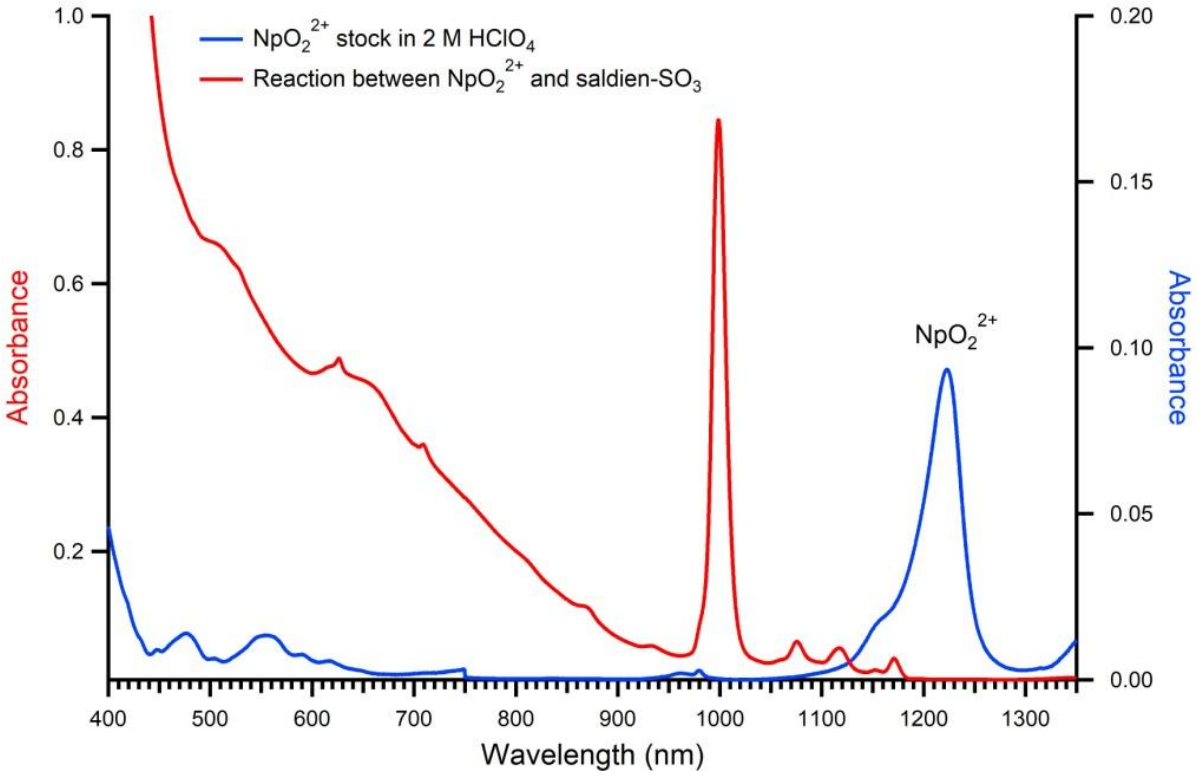

Figure 4.12. UV-Vis-nIR spectrum of the reaction between NpO_2^{2+} (0.042 mmol) and saldien-SO_3 (0.0439 mmol) in H_2O at pH=8.98 in a 2 mm path length cell. Overlay with 0.0021 M solution of the NpO_2^{2+} stock.

Although Np(VI) undergoes reduction to Np(V) upon complexation with Saldien-SO_3, this was not the case for Pu(VI). PuO_2^{2+} and NpO_2^{+} are isoelectronic and the major f-f transition ($^3H_{4g}$ to $^3\Pi_{2g}$) for the PuO_2^{2+} cation is observed at 830 nm in the absorption spectrum.[82] Low energy transitions are also observed at 950 and 980 nm. Upon the addition of Saldien-SO_3 to an aqueous acidic solution of Pu(VI), in a 2:1 molar ratio at a resultant pH of 2.2, the absorption spectrum of this sample (Figure 4.13) is dominated by the main transition at 830 nm corresponding to uncomplexed Pu(VI). As observed in complexation experiments with NpO_2^{+}, a shift to a longer wavelength by the principal f-f transition would imply coordination about the equatorial plane. When the pH is increased to 7.11, the absorption spectrum is characterized by

a charge transfer band across the 500-950 nm range and bands at 860, 990 and 1050 nm. The red shift of the band at 830 nm is consistent with other characterized Pu(VI) complexes,[69a, 83] suggesting the transition at 860 nm is for the Pu(VI)-salen-SO_3 complex.

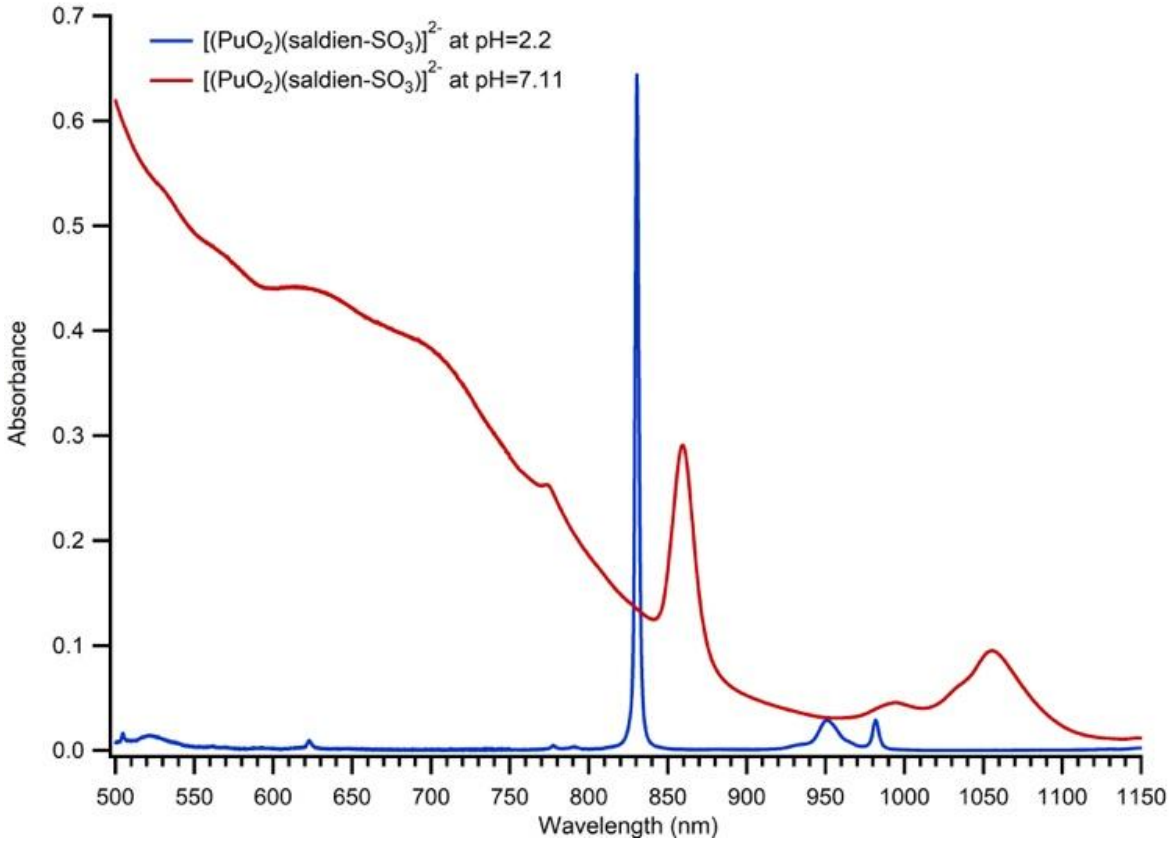

Figure 4.13. nIR/UV/Vis spectra of PuO_2(saldien-SO_3) (1.16 mmol:2.49 mmol) in H_2O in both dilute acid and near neutral pH solutions recorded in a 2 mm path length cell.

To investigate Pu(V) complexation with the pentadentate Schiff base, a solution of an aqueous solution of Pu(V) in H_2O was at a pH of 4.1 was prepared and proved to be stable, as the most prominent feature in the absorption spectrum in Figure 4.14 is a sharp transition at 570 nm.[82] The addition of Saldien-SO_3 to the Pu(V) solution, in a 1:2 molar ratio, resulted in an increase of the pH to 6.50 and the absorption spectrum bears a strong resemblance to that of

(Pu(VI))(saldien-SO3)$^{2-}$, with a band at 860 nm and a charge transfer band in the visible region.[69a, 83] As the pH was increased to 9.60 and then decreased to 6.31, there was a decrease in the intensity in both the band at 860 nm and the charge transfer band. The absorption spectrum was recorded after 4 days and a more complex spectra was collected. The band at 860 nm, as well as the charge transfer band, had disappeared, replaced by multiple bands at 550 nm and sharp transitions at 660 and 990 nm and multiple transitions across the entire spectra. There was also a change in solution colour of the complex from a brown/yellow to an orange colour, characteristic of Pu(IV). However, the transitions at 550, 660 and 990 nm are visible, although partially under the charge transfer band of Pu(VI) complex (red traces). The prominent transition at 990 nm in the 4-day spectrum does not correspond directly to any Pu(IV) transitions and the collected spectrum could be a collection of multiples oxidation states. The appearance, and then complete disappearance of the 860 nm band corresponding to complexed Pu(VI), as well as a change in colour, suggests that there was disproportionation[92, 98] of Pu(V) to Pu(VI) and Pu(IV) followed by gradual reduction to Pu(IV) and possibly Pu(III).

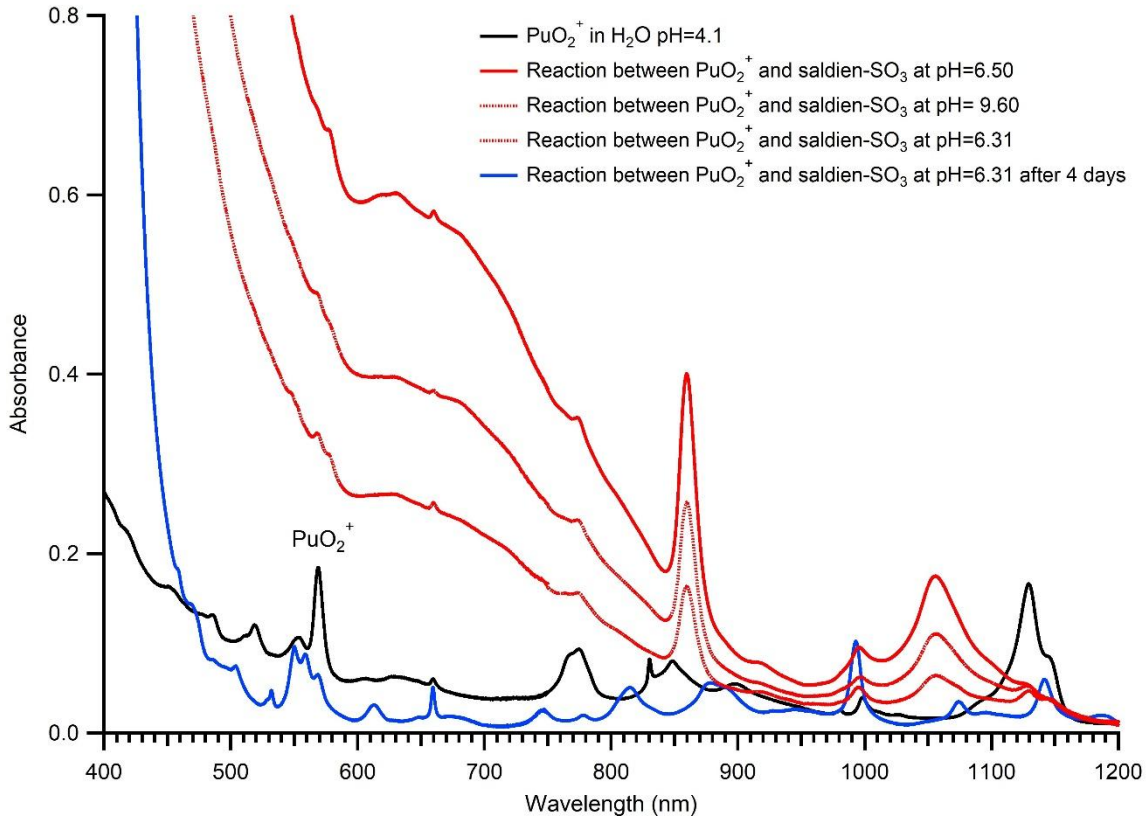

Figure 4.14. UV-Vis-nIR spectra of the reaction between PuO_2^+ (2.4 mmol) and saldien-SO_3 (4.8 mmol) at varied pH suggests complexation of Pu(VI). Spectrum collected after 4 days reveals the possible presence of Pu(IV). Spectrum was recorded in a 2 mm path length.

4.2.3.2. NMR Spectroscopy

The ^{1}H NMR spectra of the $[(UO_2)(saldien\text{-}SO_3)]^{2-}$ complex (Figure 4.16 and 4.17) reveals signals at 9.38 ppm, assigned to the azomethine (H-C=N) proton, signals at 7-8.2 ppm assigned to aryl protons (bz-H), and shifts at 3-4.6 ppm corresponding to the ethylene backbone protons (CH_2). The ^{1}H NMR spectra of the U(VI)-saldien-SO_3 complex is overall similar to that of the U(VI)-saldien complexes.[42, 99] The coupling constants (J) of the chemical signals in the 3-4.6 ppm region aid in analyzing the conformation of the sulfonated complex. The ethylene protons appear to couple each other in geminal, anti and gauche conformations. As coupling constants for anti conformation is about 10 Hz and the gauche conformation is in the 0-5 Hz, it is

possible to distinguish the different protons.[100] The signals at 3.15 ppm exhibit coupling constants of 12.3 and 3.86 Hz suggesting a gauche and anti conformation with two other protons. The slight difference in the spectra between the sulfonated salen complex and the U(VI)-salen complex in DMSO is the differing in the coupling of the backbone ethylene protons. The region (3-4.6 ppm) in Figure 4.17 appears in the (UO_2)(Saldien) in DMSO complex from 3.10-4.85 ppm. The upfield splitting at 3.4 ppm is a quadruplet of duplets while the, presumably, corresponding splitting in the saldien-SO_3 complex at 3 ppm is a triplet of doubles. This difference is likely due to coupling of the ethylene proton by the -NH proton in the DMSO complex. Although the NH proton was observed in the DMSO complex at 6.69 ppm, it was not observed in the sulfontated complex in D_2O.

The ^1H NMR spectra of the reaction between Np(VI) and saldien-SO_3 (Figure 4.18) in a 1:1 ligand metal ratio at a pH of 7.95 depicts some stark differences to that of the $[(UO_2)(\text{sadien-}SO_3)]^{2-}$ complex. There is broadening and an overall negative shift in the chemical signals, typical for paramagnetic complexes likely due to the unpaired electron in Np(VI)[85, 87], with chemical signals in the -35 to -65 ppm range. Similar broad negative shifts also appear in the ^1H NMR spectra of a tetradentate Schiff base complex with Np(V) where the signals in the negative region of the spectrum are assigned to protons on the ligand.[96] In our previous work, the ^1H NMR of a complex between an organic soluble tetradentate Schiff base ligand and Np(VI) displayed only a slight negative shift to -1 ppm. Previous studies of complexation between an aqueous soluble tetradentate Schiff base and Np(VI) indicated rapid reduction of Np(VI) to Np(V) in the presence of the ligand[75-76]. The NMR result suggests that the saldien-SO_3 is also reducing Np(VI) to Np(V). Signals in the 20-0 ppm range could be possibly attributed to degradation products from the hydrolysis of saldien-SO_3.

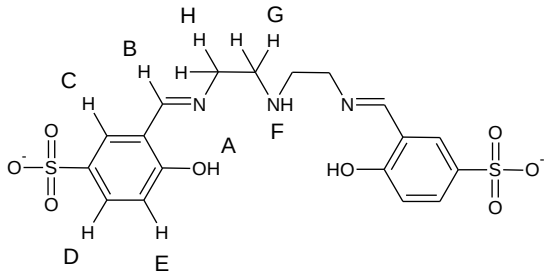

Figure 4.15. Labeled Saldien-SO_3 with corresponding assigned shifts labeled in the ^1H NMR spectra.

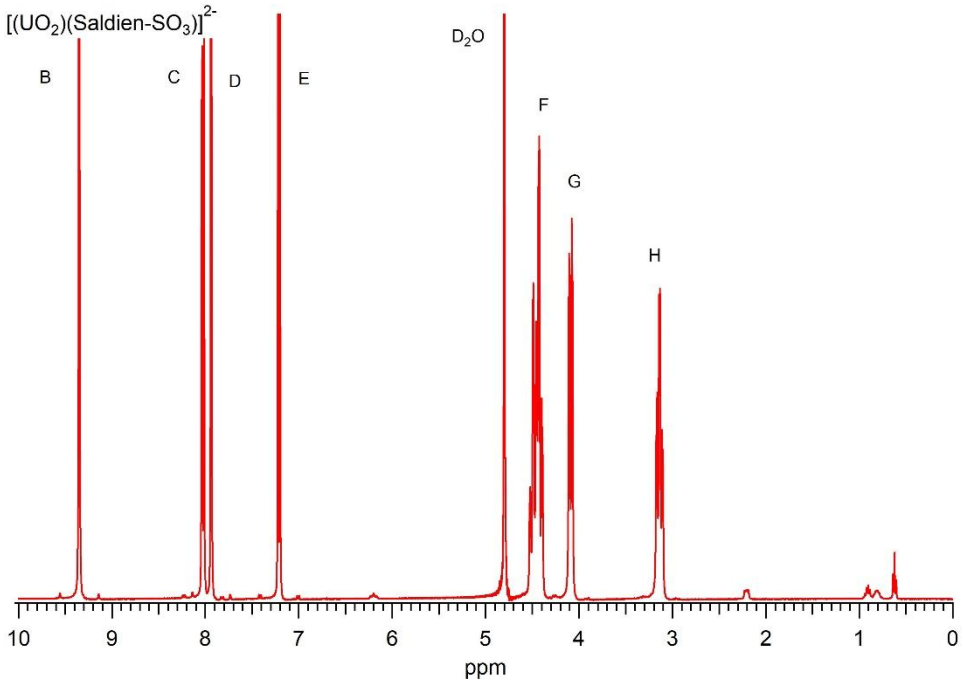

Figure 4.16. ^1H NMR spectra of $[(UO_2)(saldien\text{-}SO_3)]^{2-}$ in D_2O

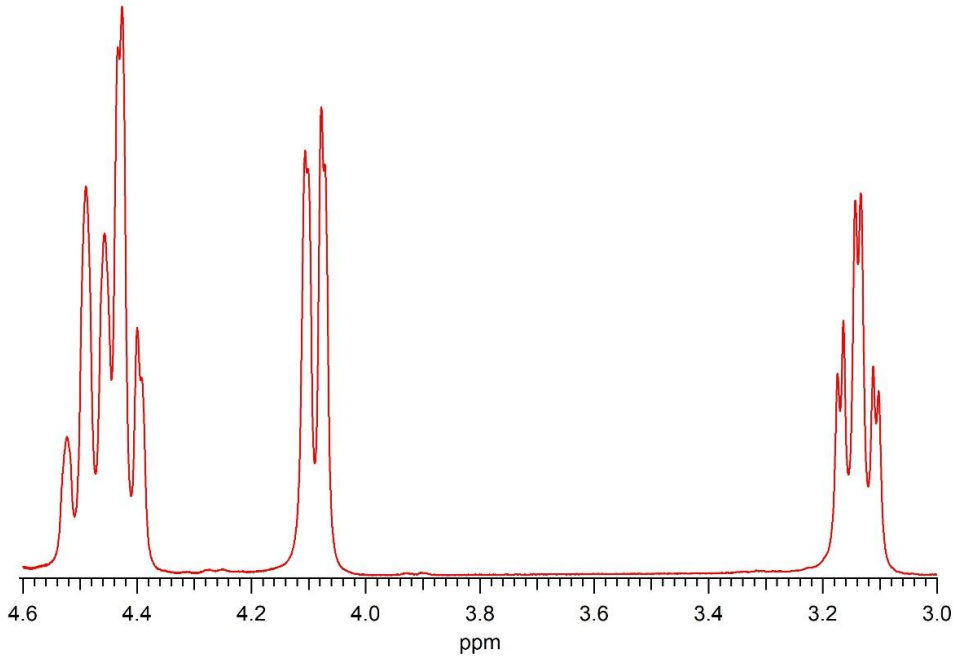

Figure 4.17. ^{1}H NMR spectra of $[(UO_2)(saldien\text{-}SO_3)]^{2-}$ in D_2O highlighting the chemical shifts of the ethylene backbone protons in the 3.0-4.6 ppm range.

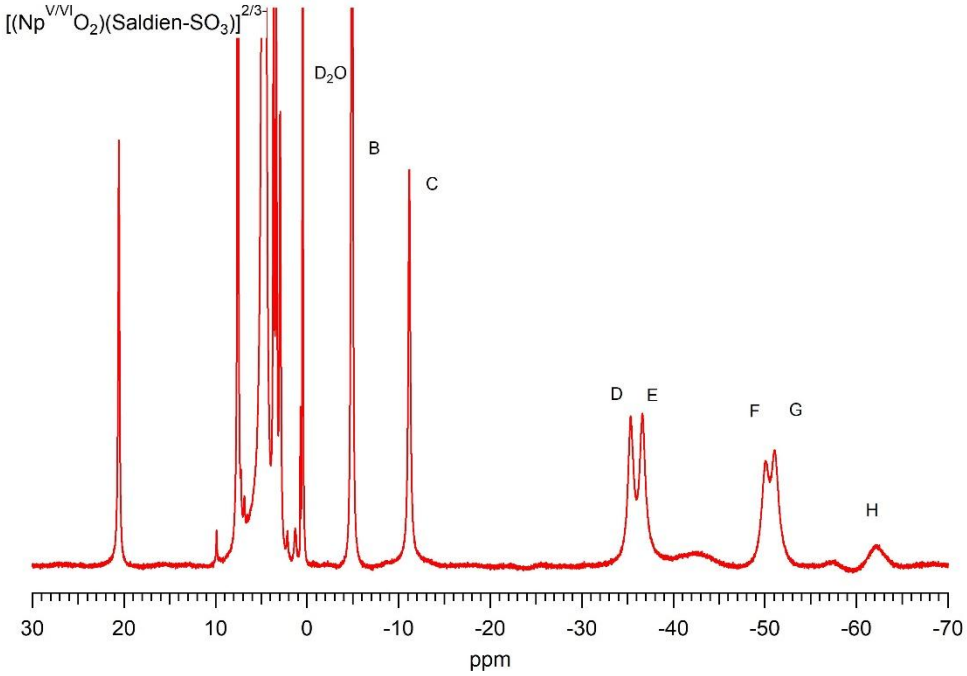

Figure 4.18. ^{1}H-NMR of $[(Np^{V/VI}O_2)(Saldien\text{-}SO_3)]^{2/3-}$ in D_2O.

4.2.3.3. IR and Raman Spectroscopy

Vibrational spectroscopy measurement were made on saldien-SO_3 and crystals of the uranium(VI)-saldien-SO_3 complex (Figure 4.19)). The Raman spectra of saldien-SO_3 exhibits bands at frequencies typical for C=N (1620 cm^{-1}) and C=C (1580 cm^{-1}) bonds. Upon complexation of uranium(VI) by the saldien-SO_3 there is a slight shift of the C=N stretch to 1640 cm^{-1} indicating interactions between the cation and the imine nitrogen. The Raman spectra for the complex shows bands of relatively low intensity at 790 and 820 cm^{-1}, which are not present in the Raman spectra of the free ligand, that can be attributed to the symmetric (v_1) uranyl stretching mode.[90] The uranyl(VI) symmetric stretch v_1 is sensitive to the ligand coordination about the equatorial plane as increasing uranium(VI)-ligand stability results in decreasing v_1 frequency.[90, 101] The comparatively low energy stretch would imply a weaker bond. The previously characterized uranium(VI) complex with the tetradentate salen-SO_3 yielded a "stepped" conformation which lowered the molecular symmetry.[75] Although the symmetric uranyl stretch is often inactive in the IR, the lowered symmetry is believed to make the symmetric stretch active in the IR through a change in the dipole moment. The uranyl(VI)-saldien-SO_3 appears to take an overall "boat" conformation as opposed to the "stepped" conformation, which would lower overall symmetry, therefore an active symmetric uranyl stretch in the IR is not expected. It can be noted that no symmetric uranyl stretch v_1 was reported for the (UO_2)(Saldien) complex in DMSO.[42] The IR spectra have bands at 790 and 820 cm^{-1} which could correspond to the v_1 symmetric uranyl stretch, possibly resulting from distortions caused by the saldien-SO_3 rather than lowered symmetry.[91] There is also a prominent stretch at 880 cm^{-1} in the IR spectra of the $[(UO_2)(\text{saldien-}SO_3)]^{2-}$ complex which is not present in the

spectra of the free ligand. This band is presumed to be the asymmetric uranyl stretch (ν_3) which is observed in 880-930 cm^{-1} in other salen-uranyl(VI) complexes.[91, 102] The asymmetric (ν_3) IR uranyl stretch is also reported at 895 cm^{-1} in the (UO_2)(Saldien) complex in DMSO.[42] Stretches in the 1039 - 1220 cm^{-1} range could correspond to the two sulfonate environments present in the unit cell, as was described for $[UO_2(Salen\text{-}SO_3)(OH_2)]^{2-}$.[75]

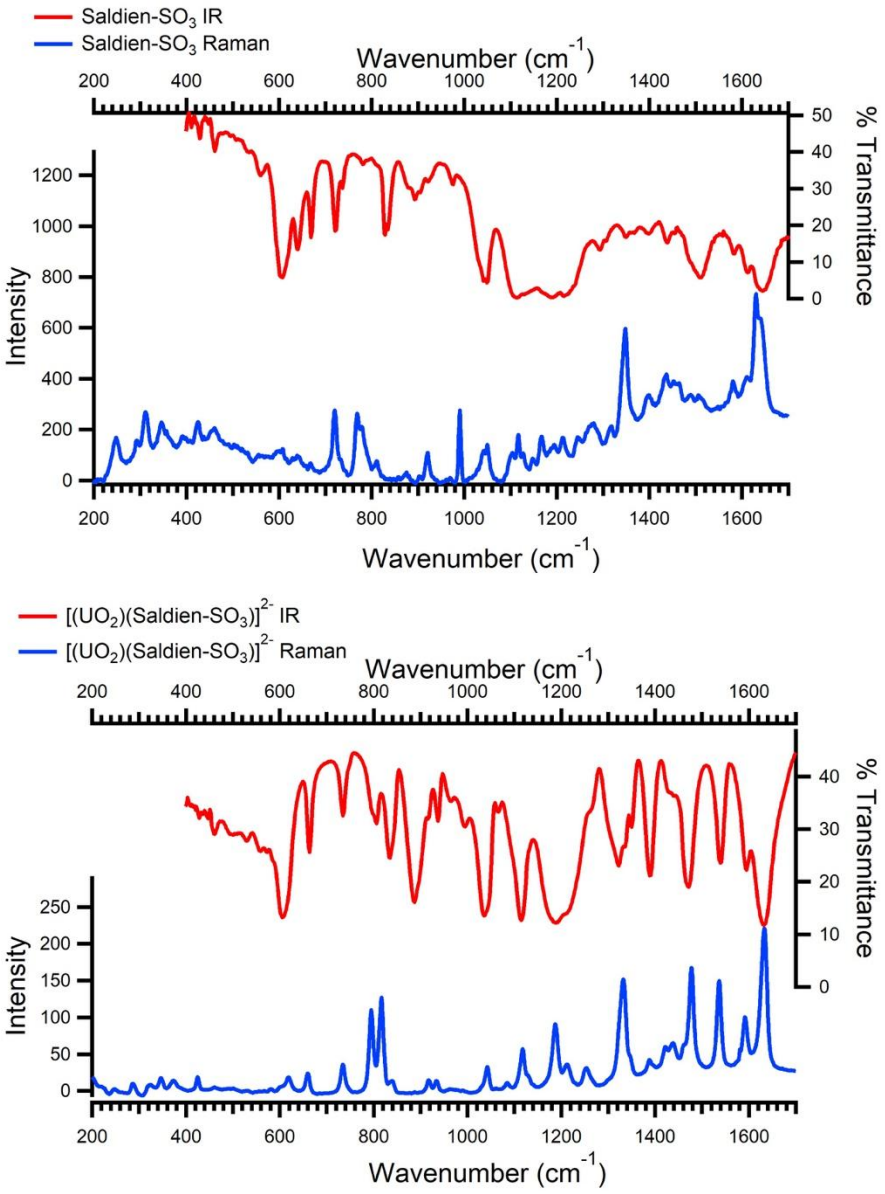

Figure 4.19. Overlay of IR and Raman spectra of free H_2Saldien-SO_3 (top) and crystalline solids of $[UO_2(saldien\text{-}SO_3)]^{2-}$ (bottom).

4.2. Solvent Extraction Studies

4.2.1. Optimized Diluent Mixture

Initial extraction experiments were carried out in order to optimize a diluent mixture that results in greater metal extraction and total mass recovery. Preliminary experiments with toluene indicated that there was significant precipitation of ligand-metal complex as indicated by low mass of metal recovery yields. Consequently, as long chained aliphatic alcohols are inhibitors of third-phase formation, studies where the organic diluent contained different ratios of 1-octanol to toluene was investigated.[103]

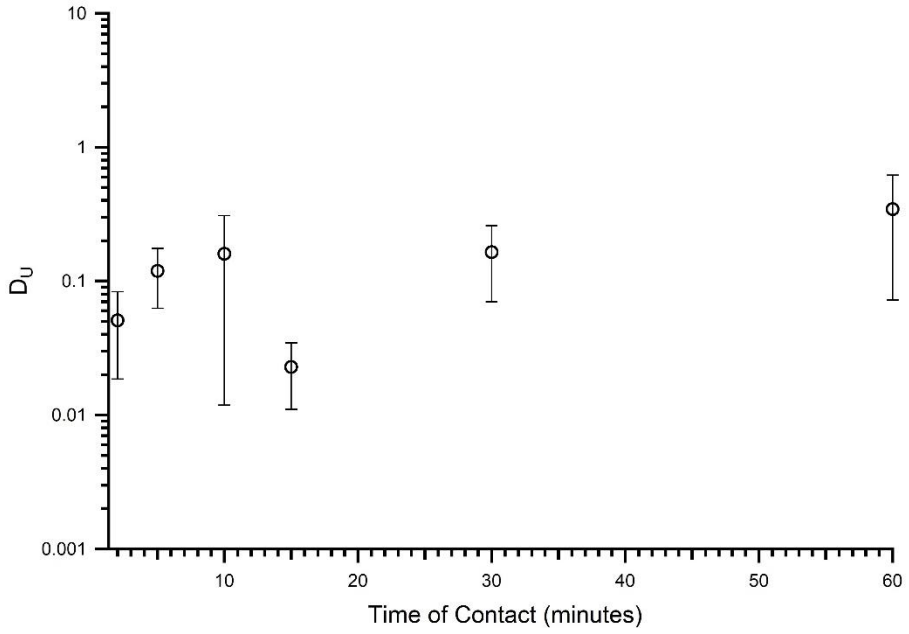

Figure 4.20. Distribution of the extraction of U(VI) from 0.1 M KNO_3 by 0.015 M di-t-butyl Salen in toluene.

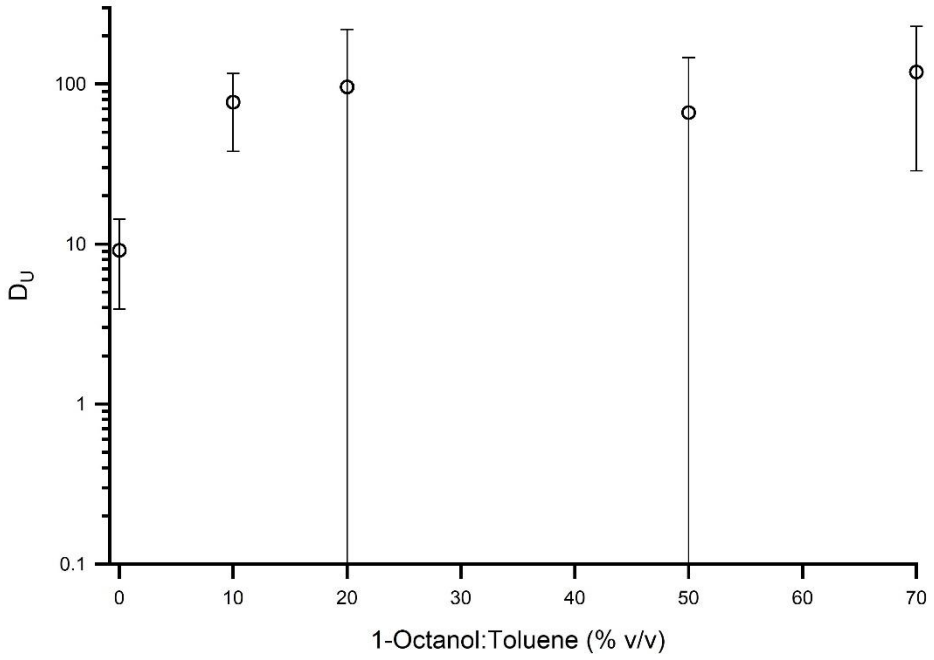

Figure 4.21. Distribution of the extraction of U(VI) from 0.1 M KNO_3 by 0.025 M di-t-butyl Salen at different ratios of 1-octanol to toluene.

In extraction studies with no 1-octanol present, the mass recovery of uranyl(VI) averaged from 25-40%. Although the distribution plot suggests a high D value at only 10% 1-octanol:toluene, mass recovery averaged 49%. It was a 7:3 1-octanol to toluene ration that resulted in the complete extraction of uranyl(VI) as well as complete recovery by mass. A high concentration of 1-octanol proved to prevent precipitation of the metal-ligand complex. All subsequent extraction studies were carried out in a diluent mixture of 7:3 1-octanol to toluene.

Table 4.3. Total recovery (%) of uranyl(VI) as increasing ratios of 1-octanol to toluene.

% of 1-Octanol to Toluene	Recovery by Mass (%)
0	29.15
10	49.63
20	80.79
50	89.93
70	98.50

4.2.2. Time Dependent Studies

4.2.2.1. Uranium Extraction

Results from time dependent extraction experiments for uranyl(VI) indicated that the di-t-butyl substituted ligands required approximately a contact time of 2 h to reach extraction equilibrium while unsubstituted Salen and Salophen achieved extraction equilibrium at a contact time of 5 and 60 minutes respectively (Figure 4.22). Salophen, although at a lower concentration (0.012 M) yielded D_U values greater than both di-t-butyl Salen and di-t-butyl Salophen. For a consistent comparison, a time dependent extraction plot of the ligands at 0.003 M is shown below in Figure 4.23. The extraction trend for D_U is Salen > Salophen > di-t-butyl Salen > di-t-butyl Salophen. Upon reaching extraction equilibrium, the extraction of uranyl(VI) by Salen presented D_U values are greater than one order of magnitude compared to that of Salophen, 3 orders of magnitude compared to di-t-butyl Salen and 4 orders of magnitude compared to di-t-butyl Salophen. The discrepancy in D_U values could be attributed to the steric constraints due to the combination of the 1,2-phenylenediamine and t-butyl groups.

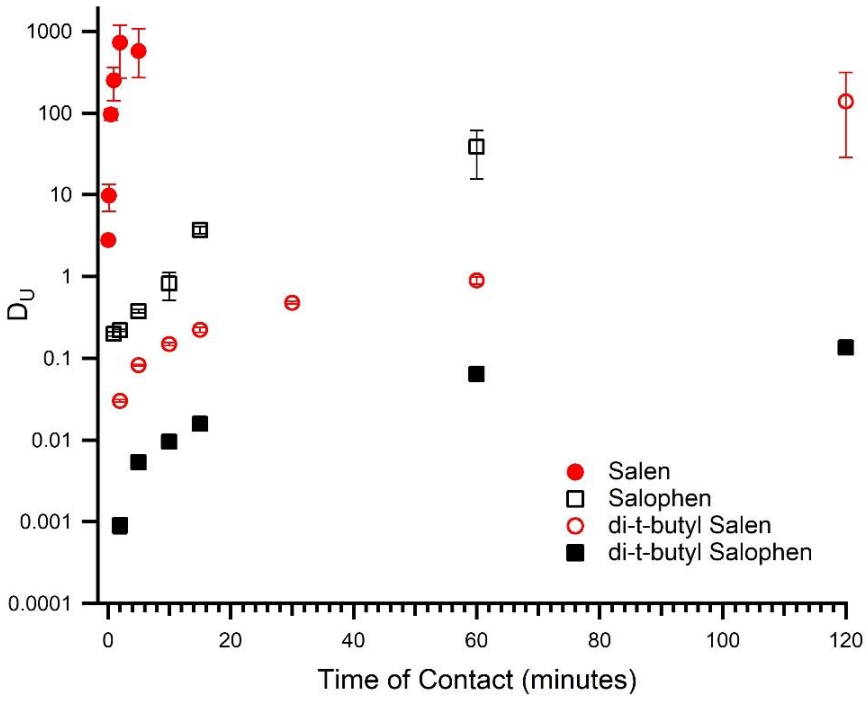

Figure 4.22. Extraction of U(VI) by 0.025 M Salen, di-t-buty Salen, di-t-butyl Salophen and 0.012 M Salophen

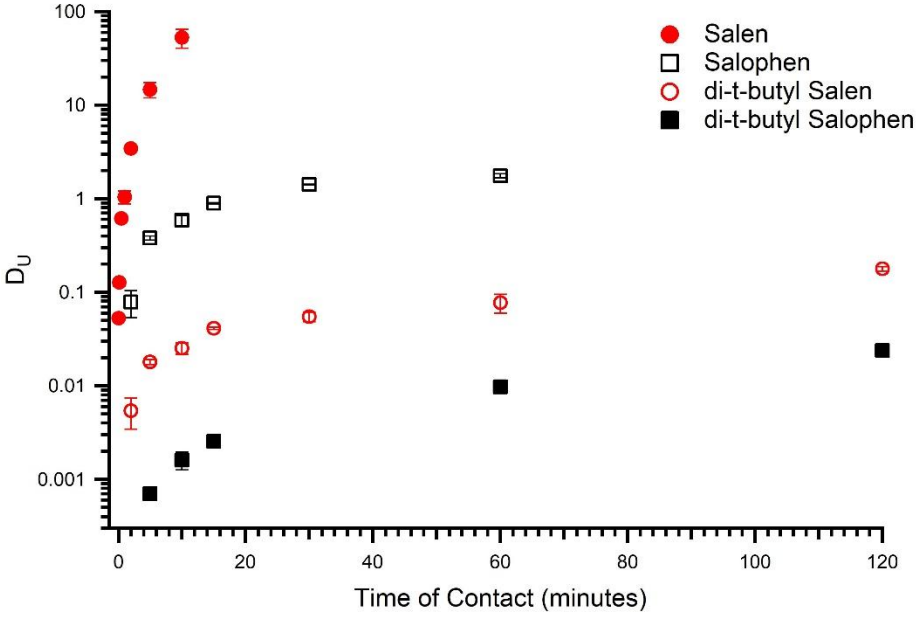

Figure 4.23. Distribution plot of the extraction of 0.001 M U(VI) by 0.003 M ligands

4.2.2.2. Plutonium Extraction

The extraction of plutonyl(VI) exhibited lower distribution ratios than those for uranyl(VI) (Figure 4.24). This result is expected since charge density decreases going across the hexavalent actinyl cation series leading to weaker coordination.[104] This trend ($D_U > D_{Pu}$) is also observed in the extraction of sodium bismuthate oxidized An(VI) by TBP[32] and dialkyl amide.[105] As observed with the extraction of uranyl(VI), the D_{Pu} is greater for Salen than di-t-butyl Salen. In regards to extraction by di-t-butyl Salen, it appears that a maximum distribution value of 0.2 is attained after 10 minutes of contact followed by a gradual decrease as the contact time increases to 2 h. This gradual decrease in distribution ratio could be attributed to the reduction of Pu(VI) to Pu(V) followed by disproportionation to Pu(IV) and Pu(VI).

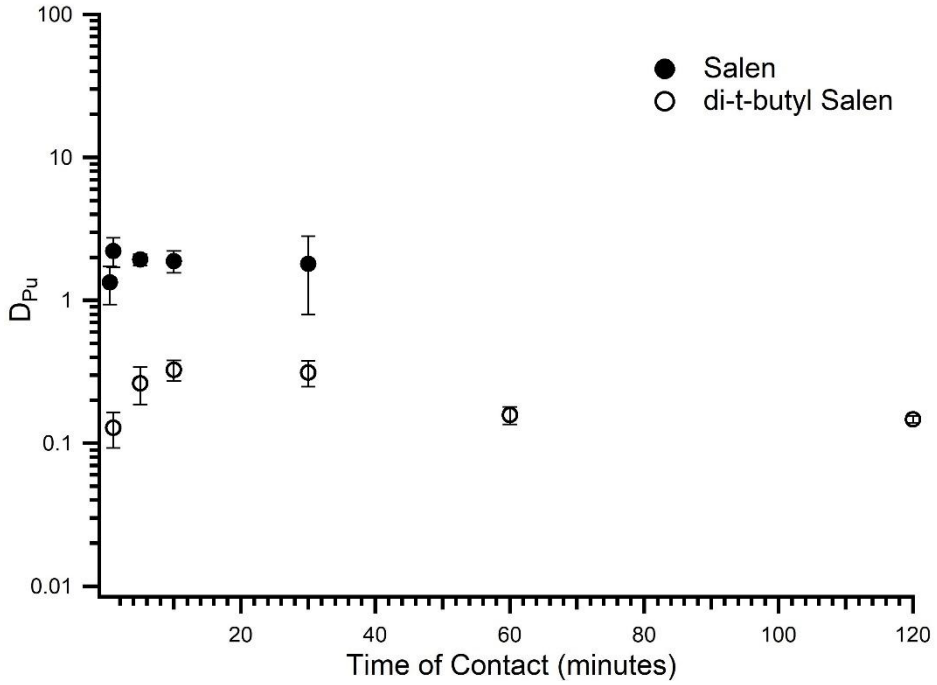

Figure 4.24. Distribution plot of the extraction 2.1×10^{-7} M plutonyl(VI) by 0.025 M Salen and di-t-butyl Salen.

4.2.2.3. Neptunium Extraction

Previous studies with the water-soluble Schiff base system indicated the rapid reduction of Np(VI) to Np(V) upon ligand-metal complexation.[76] However, complexation chemistry studies with di-t-butyl Salen proved to be successful in stabilizing Np(VI) in an organic medium consisting of only acetonitrile. Since Salen demonstrated relatively quick extraction kinetics, it was used for solvent extraction studies with Np(VI). It became apparent that the reduction of Np(VI) to Np(V) had occurred as evident by the low distribution values (Figure 4.25). The extraction behaviour of Np(VI) is similar to that of U(VI) and Pu(VI) and therefore expected to see significant Neptunium extraction if indeed it was in the +VI oxidation state.[32] For the time point of 5 minutes, D values for U and Pu were 569.27 and 1.93 respectively, while 0.024 Np.

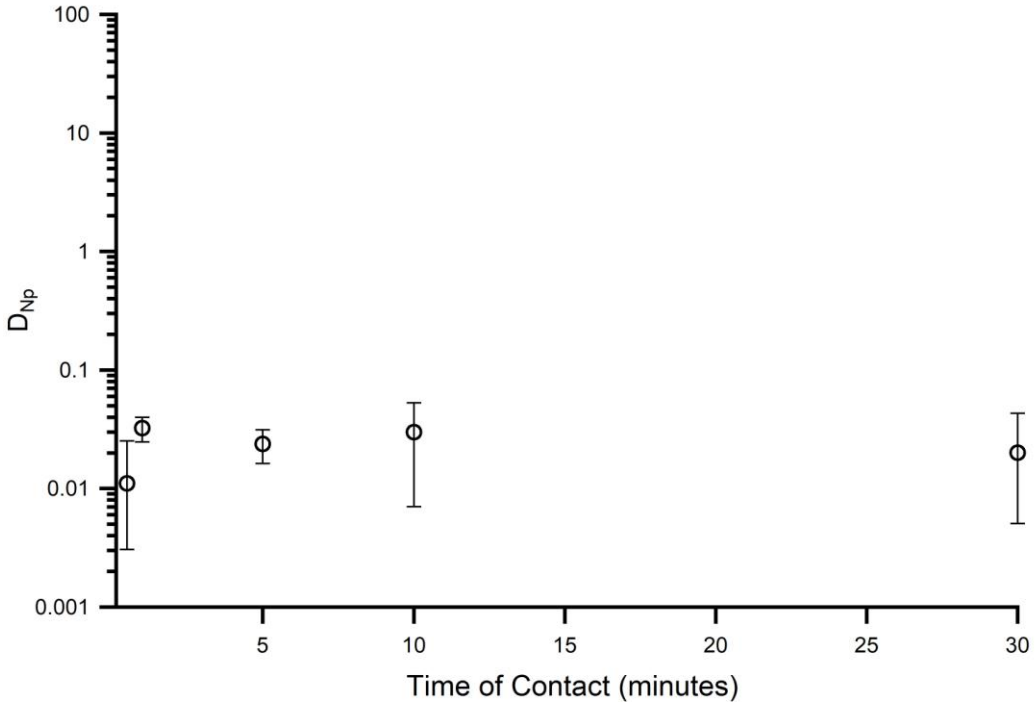

Figure 4.25. Distribution plot for the extraction of Np(V/VI) by 0.025 M Salen.

4.2.3. An(VI) Extraction Dependence on Ligand Concentration

4.2.3.1. Uranium

The distribution ratios (D_M) can be used to evaluate the extraction stoichiometry of the system, estimating the average number of ligand molecules bound to each metal ion. The assumption that the actinyl cations are extracted into the organic phase as neutral complexes, and the deprotonation of Salen-type ligands, results in the overall equilibrium reaction shown in eq. 8, and the corresponding equilibrium constant expression is shown in eq. 9:

$$(AnO_2^{2+})_{(aq)} + n(H_2L)_{(org)} \rightleftharpoons (AnO_2 \cdot L_n)_{(org)} + 2nH^+_{(aq)} \qquad \text{(eq. 8)}$$

$$K_{ex} = \frac{[AnO_2 \cdot L]_{(org)}[H^+]^2_{(aq)}}{[AnO_2^{2+}]_{(org)}[H_2L]^n_{(org)}} \qquad \text{(eq. 9)}$$

The distribution ratio is the total concentration of the actinyl cations in the organic phase divided by the total actinyl cations concentration in the aqueous phase (eq. 10)

$$D_M = \frac{[AnO_2 \cdot L]_{(org)}}{[AnO_2^{2+}]_{(aq)}} \qquad \text{(eq. 10)}$$

Using this expression for D and making the assumptions that the dominating species is free actinyl and the ligand-metal complex in the aqueous and organic phase, respectively and that changes in ionic strength (i.e. changes in nitrate concentration) can be neglected, eq. 9 can be rewritten as the following (eq. 11):

$$K_{ex} = \frac{D_M[H^+]^2_{(aq)}}{[H_2L]^n_{(org)}} \qquad \text{(eq. 11)}$$

Equation 11 can then be rearranged and rewritten in a linear form (eq. 12):

$$\log D_M = \log K_{ex} + n\log[H_2L]_{(org)} - 2\log[H^+]_{(aq)} \quad \text{(eq. 12)}$$

The stoichiometric number n in the extraction process was determined by slope analysis where the D_M values were calculated at different ligand concentrations and constant aqueous conditions of 0.1 M KNO_3 and pH_i=3.00 where the value n is the average number of ligand molecules coordinated to each metal ion. Figure 4.26 depicts the D_U values at varied concentrations of Salen, Salophen, di-t-butyl Salen and di-t-butyl Salophen.

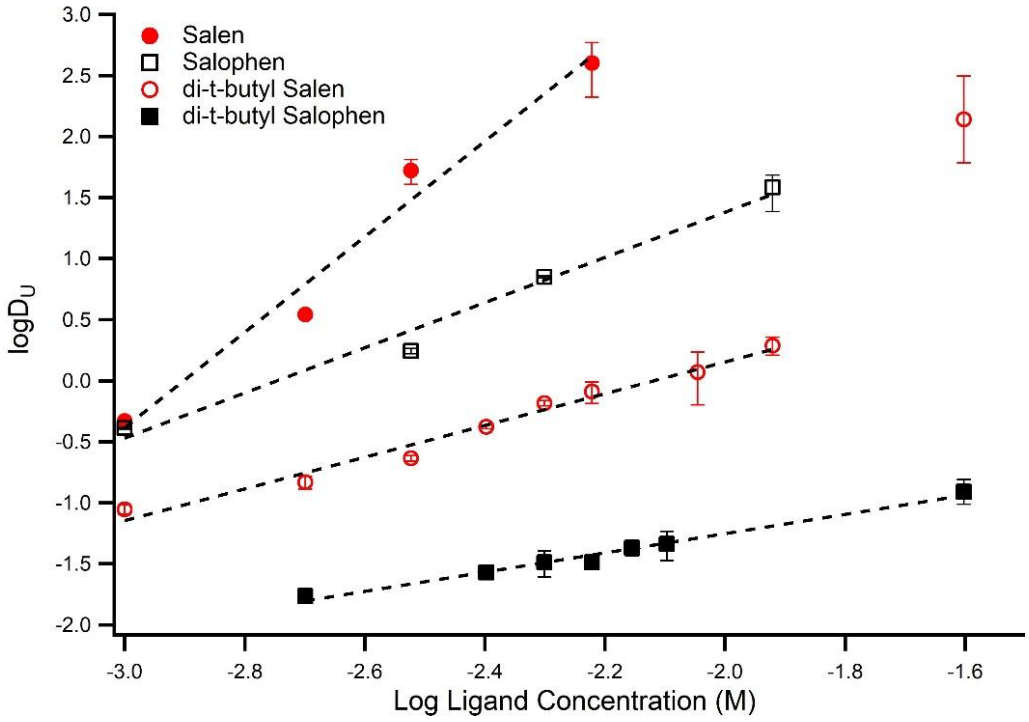

Figure 4.26. Extraction stoichiometry study for U(VI) (0.001 M) using varying amounts (0.001 - 0.025 M) of ligand.

Given the geometry of the actinyl cation, which has 5 equatorial positions available for coordination[46,42], it would be expected that a single Salen ligand would bind to the uranyl(VI)

cation during extraction. Previous solvent extraction studies with muti-dentate Schiff base ligands with uranyl(VI) have demonstrated the presence of a single ligand molecule in the extracted complex.[53] The values attained from slope analysis were 3.91 ± 0.45 for Salen, 0.786 ± 0.043 for di-t-butyl Salophen and 1.85 ± 0.18 for Salophen. For di-t-butyl Salen, a slope of 1.3 ± 0.08 in the ligand concentration range of 0.001 - 0.012 M followed by a sharp increase in D_U at 0.025 M. The di-t-butyl Salophen ligand yields a slope close to 1, confirming expected complex stoichiometry. However, Salophen and Salen yielded slopes close to 2 and 4 suggesting 2:1 and 4:1 ligand to metal complex stoichiometry. The di-t-butyl Salen ligand may also extract the uranyl cation as a 1:1 complex in the lower ligand concentration range and aggregated ligand-metal complexes could dominate at higher ligand concentrations. Diglycolamides also demonstrated extraction stoichiometries that appeared to exceed the inner-sphere coordination positions of trivalent actinides in non-polar diluents with low polarizability/dielectric constant (n-dodecane).[106,107] Since the same extraction behaviour is not observed in more polar solvents such as 1-octanol, the extraction stoichiometry for An(III) is attributed to extraction by aggregates in dodecane.[108] Since our diluent system consists of 2 different solvents, with different polarities, it could be possible that the extraction of uranyl(VI) is dominated by ligand-metal aggregates. EXAFS studies can help in uncovering details of the actinyl coordination environment. Recently a set of EXAFS data was collected for these extraction systems and the analysis is pending.

Since there is a change in pH at extraction equilibrium, distribution values were normalized to a single value, pH= 3.3, for a more accurate comparison between the ligand systems (Figure 4.27). This value was chosen since equilibrium pH for extraction studies in the lower ligand concentration range (0.001 - 0.003) averaged 3.3. Normalizing to a single pH value

resulted in slightly lower distribution values, especially at higher ligand concentrations. Slope analysis of these plots reveal extraction stoichiometry of 2:1 for Salen and Salophen and 1:1 stoichiometry for di-t-butyl Salen and di-t-butyl Salophen (Table 4.4).

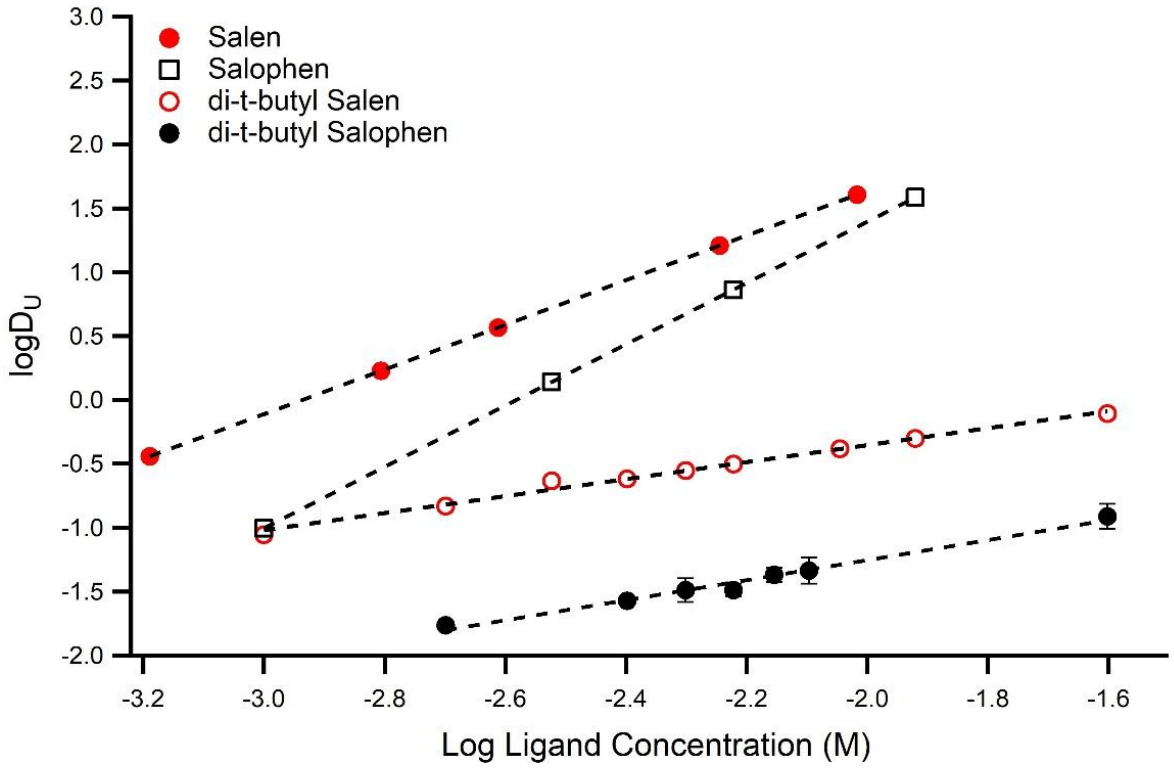

Figure 4.27. Distribution values for ligand concentration dependency studies for the extraction of U(VI) (0.001 M) normalized to pH= 3.3.

Table 4.4. Extraction Stoichiometry values obtained from normalization of distribution values to pH= 3.3.

	Stoichiometry
Salen	$1.7 \pm 2.6 \times 10^{-5}$
Salophen	$2.4 \pm 5.0 \times 10^{-5}$
di-t-butyl Salen	0.67 ± 0.025
di-t-butyl Salophen	0.79 ± 0.043

4.2.3.2. Plutonium

Ligand dependency extraction studies for Pu(VI) revealed different stoichiometry than that for U(VI) (Figure 4.28). Solutions of Salen and di-t-butyl Salen at different concentrations were contacted with Pu(VI) for limited to 10 minutes. A slope of 0.63 ± 0.067 for Salen and 0.43 ± 0.010 for di-t-butyl Salen, a deviation from ligand to metal ratios, at normalized pH, of 2:1 for Salen and 1:1 for di-t-butyl Salen. Metal loading experiments (Figure 4.30) indicated that uranyl(VI) distribution values are higher at low metal concentration and gradually decrease with increasing uranyl(VI) concentration. During ligand dependency studies, the concentration of uranyl(VI) was 0.001 M while the concentration of Pu(VI) was 3.14×10^{-7} M. Since the concentration of Pu(VI) is about 3 orders of magnitude lower than that of uranyl(VI), and D_U values greater than 10 are obtained at 0.001 M Salen vs 1×10^{-4} uranyl(VI) (last figure), we expected to see greater D_{Pu} values at this plutonyl(VI) concentration. As observed with the time dependent study (Figure 4.24), the presence of Pu(V) in the aqueous solution could suppress D_{Pu} values. Reduction of Pu(VI) to Pu(V), and possible subsequent disproportionation to Pu(IV) and Pu(VI), would lower D_{Pu} values and alter the expected extraction stoichiometry. Although di-t-butyl Salen proved to complex and stabilize Pu(VI) in a single organic phase (acetonitrile) (Bustillos, May, Nilsson et al), redox stability in a bi-phasic system with this ligand class proves more challenging.

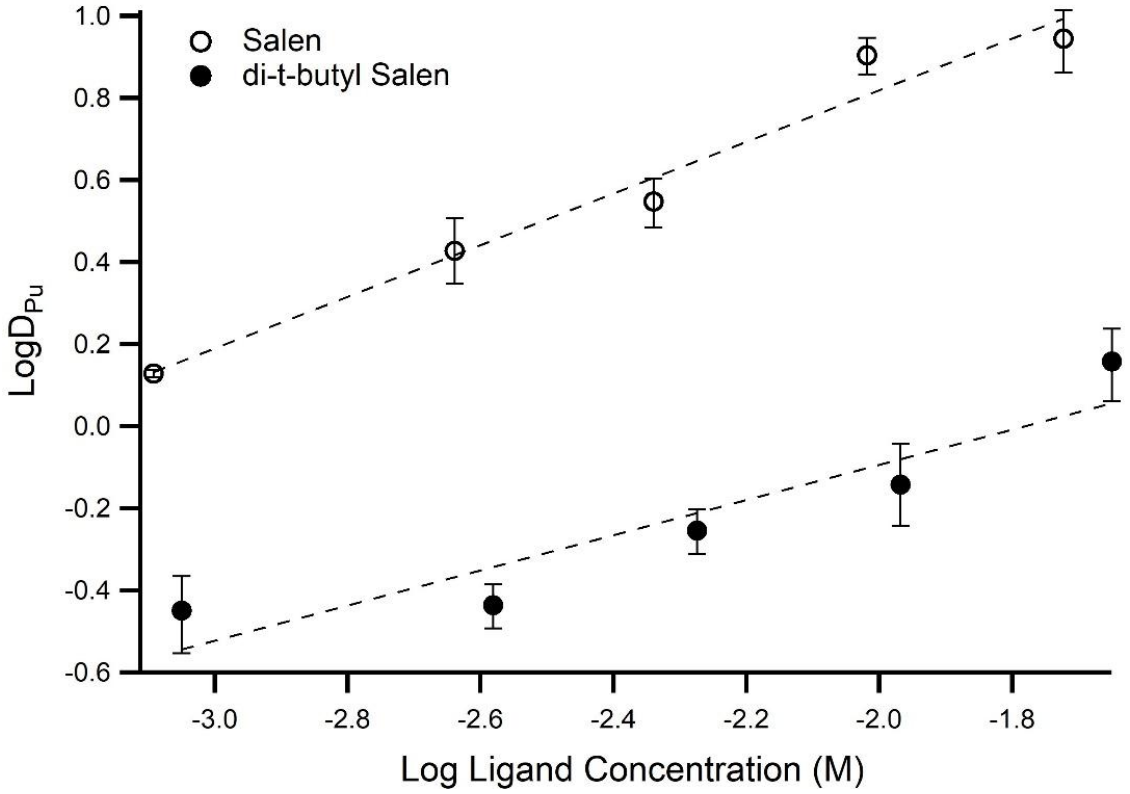

Figure 4.28. Extraction stoichiometry study for the extraction of Pu(VI) (0.314 μM) using varied amounts of Salen and di-t-butyl Salen

Table 4.5. Extraction stoichiometry values obtained for extraction studies with Pu(VI)

	Stoichiometry
Salen	0.63 ± 0.067
di-t-butyl Salen	0.43 ± 0.098

4.2.4. An(VI) Extraction Dependence on pH

4.2.4.1. Uranium

Since the ligands are deprotonated during complexation with actinyl cations[54, 73, 75-76] extraction experiments where the pH was varied would provide valuable insight into the extraction mechanism of U(VI). Since concentration of the ligands are being held constant, the slope of the plot of the uranyl(VI) distribution and the recorded equilibrium pH should provide

the number of H atoms exchanged during the extraction process (eq. 4). The dependency of D_U values on pH_{eq} for the ligands is depicted in the figure below. It is apparent that there is a steep dependency on pH since distribution values greatly increase with increasing pH. Structural data collected from X-ray crystallography in a single solvent system does suggest that complexation between the Schiff base ligand and metal occurs through the deprotonation of the phenolic oxygens. Figure 4.29 indicates that the slope of the pH dependence is close to 2 for di-t-butyl Salen and Salen, suggesting the deprotonation of both phenolic protons on a single ligand molecule during extraction. The slope of 2.4 for Salen could be a result of an average of 2 protons released during the extraction, suggesting a possible 1:1 ligand to metal complex, although results from ligand dependency studies suggested a 2:1 ligand to metal extraction complex. Previous studies have also demonstrated the release of 2 protons by Salen, in benzene, during the extraction of uranyl(VI).[55] Surprisingly, due to the lack of flexibility expected from the aromatic backbone, slopes obtained from solvent extraction suggest that Salophen and di-t-butyl Salophen exchange only one H atoms during the extraction process. Ligand dependency studies suggested that uranyl(VI) was extracted by only 1 ligand molecule of di-t-butyl Salen. This would imply that the uranyl cation is extracted as either a mononitrate species as (UO_2)(Hdi-t-butyl Salophen)(NO_3) or possibly as a hydrolyzed cation as (UO_2)(OH)(Hdi-t-butyl Salophen). Previous studies have reported the extracted species of uranyl(VI), from perchlorate solutions, by Salen, dissolved in benzene, to be (UO_2)(OH)(HSalen).[53] In addition, ligand dependency studies suggested that uranyl(VI) was extracted by an average of 2 Salophen molecules. In conjunction with results from pH dependence, the uranium cation could be extracted into the aqueous phase as $(UO_2)(HSalophen)_2$ where the actinyl cation is bound by two mono basic Salophen molecules. It could be possible that pi stacking from the aromatic rings

facilitates this process. Previous studies in non coordinating solvents showed that dimers were formed during complexation, where the uranyl cation was coordinated by 2 ligands, where the equatorial position was filled by a phenolic oxygen of another (UO_2)(HSalophen) complex.[109] As previously stated, pending analysis of EXAFS data was collected from ligand dependency studies can assist in determining the structure of the extracted species.

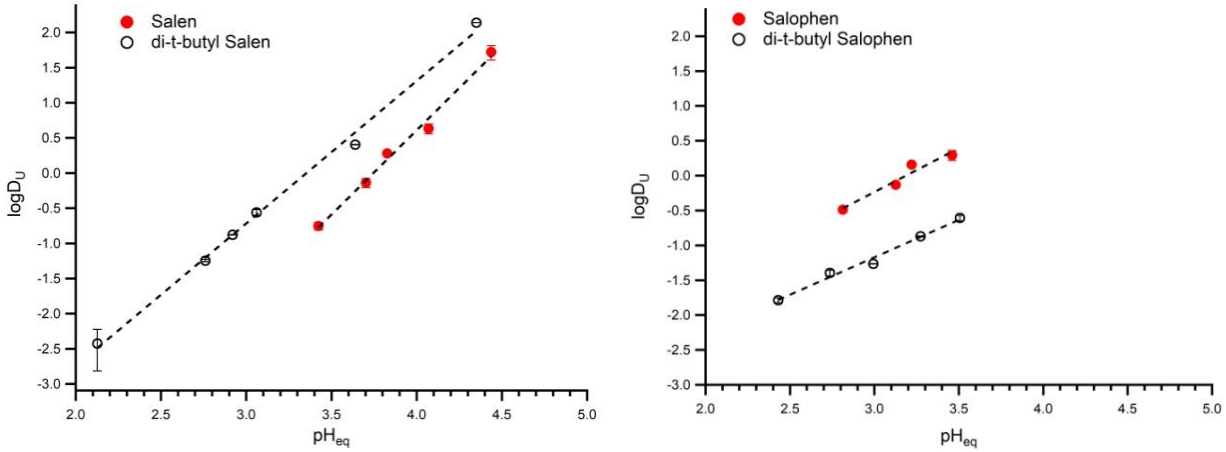

Figure 4.29. Distribution ratios for the extraction dependence of U(VI) on pH_{eq} by di-t-butyl Salen (0.025 M), Salen (0.003 M), Salophen (0.003 M), and di-t-butyl Salophen (0.025 M).

Table 4.6. Slopes obtained from D_U dependency on pH_{eq}

	Slope
Salen	2.4 ± 0.12
Salophen	1.25 ± 0.21
di-t-butyl Salen	2.03 ± 0.07
di-t-butyl Salophen	1.07 ± 0.07

4.2.5. Effect of Metal Concentration

4.2.5.1. Uranium

Experiments were carried out where the uranyl concentration was varied ($1x10^{-4}$ to 0.08 M) with 0.001 and 0.006 M Salen as the extractants in order to quantify the effect of metal

concentration on distribution values. For concentrations of 0.001 M and 0.006 M Salen there is an overall suppression of D_U values as the metal concentration is increased (Figure 4.30). When the uranyl concentration was increased from $1x10^{-4}$ to 0.08 M, distribution values for uranyl decreased by about 2 orders of magnitude.

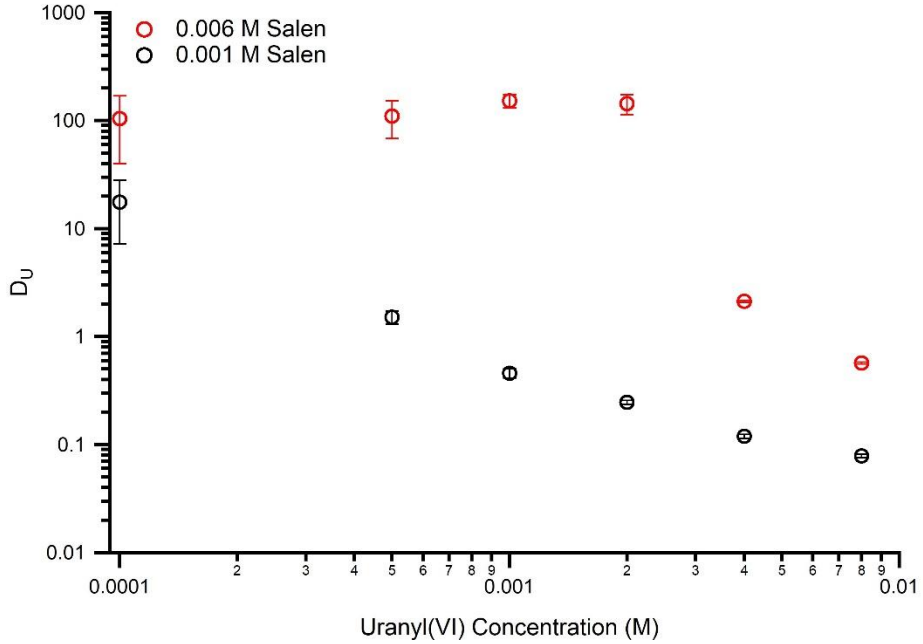

Figure 4.30. Distribution plot for the extraction of uranyl(VI) from 0.1 M KNO_3 at varying uranyl concentrations by 0.001 and 0.006 M Salen.

A plot of the total uranium concentration in the organic phase versus total uranium concentration will yield the extraction capacity of the ligand solutions.[23] Solvent saturation for uranyl is observed for both 0.001 and 0.006 M Salen solutions within this metal concentration range. Capacity curves (Figure 4.31) reveal that there is an increase by a factor of 6 when the ligand concentration is increased by a factor of 6.

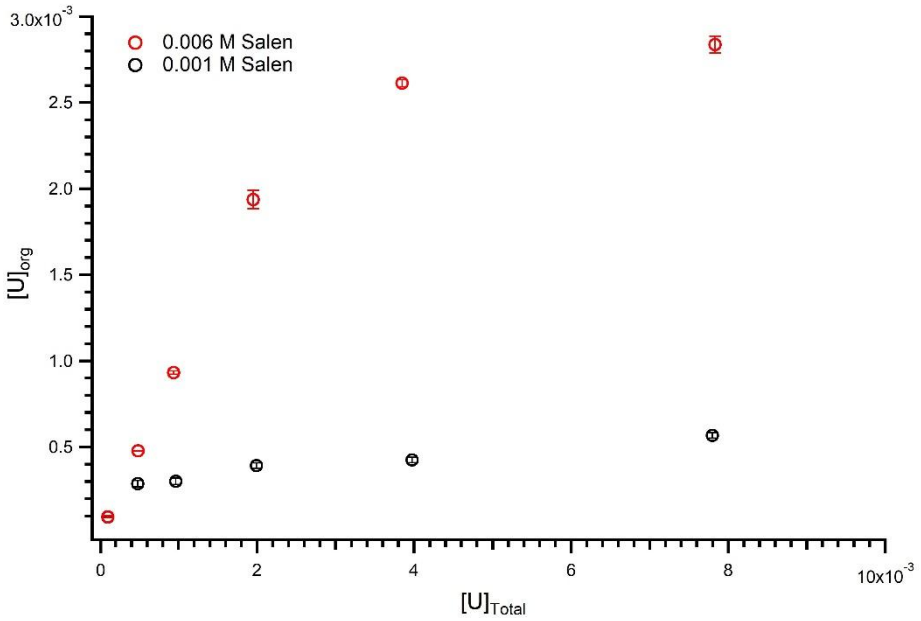

Figure 4.31. Capacity curve for the extraction of uranyl by 0.001 and 0.006 M Salen (1:1 volume ratios).

4.2.6. Kinetic and Thermodynamics of Uranyl(VI) Extraction

4.2.6.1. Kinetic Studies

The effect of ligand concentration on the extraction rate of uranyl(VI) was investigated. If the extraction of uranyl(VI) follows first order kinetics, a plot of the natural log of concentration vs time should result in a straight line. This was observed for the 4 different ligands, allowing us to confirm that extraction of uranyl(VI) is a first order (Figure 4.32). The observed rate constants (k_{obs}) were calculated based on the estimated remaining uranyl(VI) concentration in the aqueous phase. The slope of a plot of the natural log on the remaining uranyl(VI) aqueous concentration vs time will give k_{obs}. The figure below displays first-order plots for different concentrations of the different salen-type ligands. Unsurprisingly, observed rate constants increases with increases ligand concentration. Ligands with bulky butyl groups also demonstrated slower extraction kinetics than non substituted ligands. The slope of a line in

a log-log plot of the observed rate constants and ligand concentration can give an estimated order dependence of the extraction.

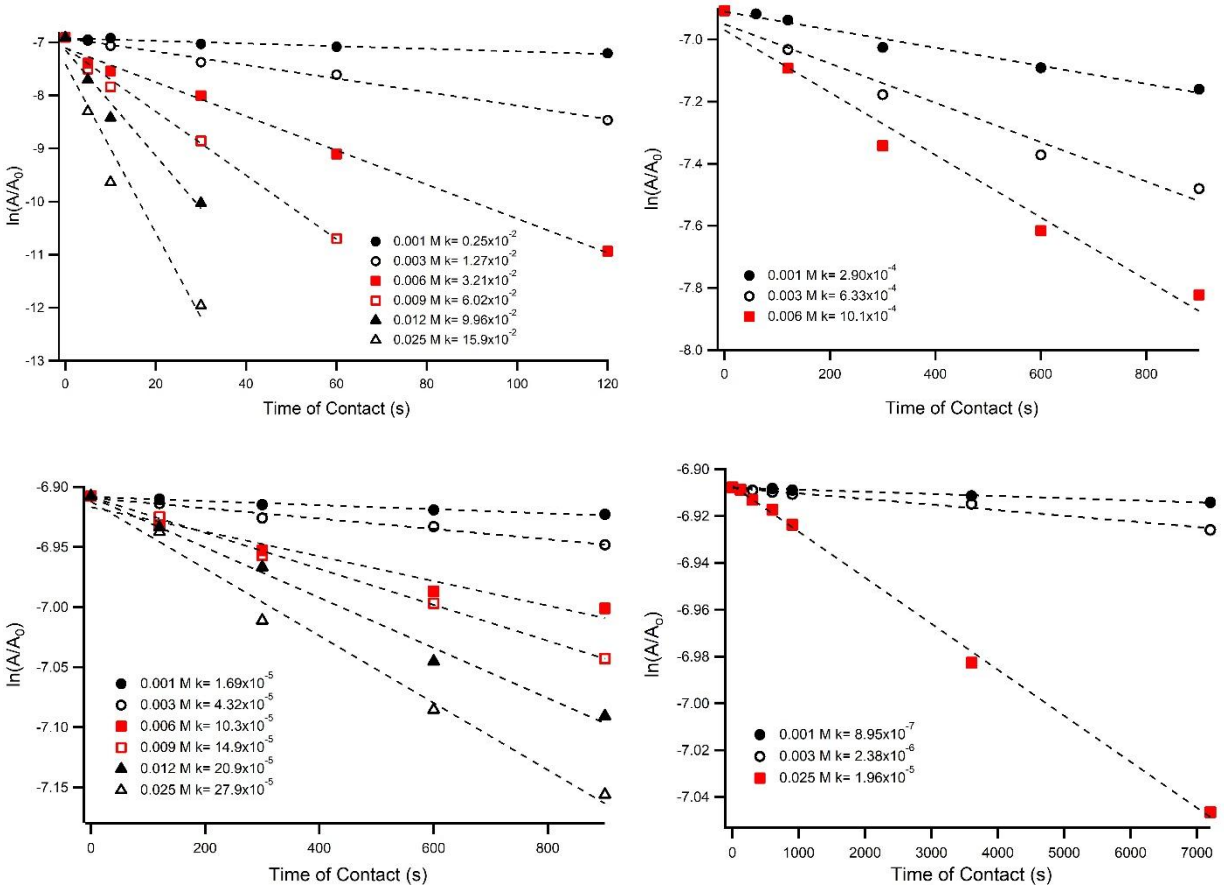

Figure 4.32. First-order plots for the extraction of Uranium(VI) from 0.1 M KNO_3 at varying ligand concentrations for Salen (top left), Salophen (top right), di-t-butyl Salen (bottom left) and di-t-butyl Salophen (bottom right).

Table 4.7. Observed rate constants calculated for varied concentrations of tetradentate Schiff Base ligands

	k_{obs} (s^{-1})			
Concentration (M)	Salen	Salophen	di-t-butyl Salen	di-t-butyl Salophen
0.001	$0.25x10^{-2} \pm 2.5x10^{-4}$	$2.90x10^{-4} \pm 2.1x10^{-5}$	$1.69x10^{-5} \pm 1.4x10^{-6}$	$8.95x10^{-7} \pm 4x10^{-8}$
0.003	$1.27x10^{-2} \pm 5.3x10^{-4}$	$6.33x10^{-4} \pm 6.4x10^{-5}$	$4.32x10^{-5} \pm 3.6x10^{-6}$	$2.38x10^{-6} \pm 1.6x10^{-7}$
0.006	$3.21x10^{-2} \pm 1.4x10^{-3}$	$10.1x10^{-4} \pm 9.2x10^{-5}$	$10.3x10^{-5} \pm 1.3x10^{-5}$	
0.009	$6.02x10^{-2} \pm 3.1x10^{-3}$		$14.9x10^{-5} \pm 3.3x10^{-6}$	
0.012	$9.96x10^{-2} \pm 1.2x10^{-2}$		$20.9x10^{-5} \pm 1.1x10^{-5}$	
0.025	$15.9x10^{-2} \pm 2.6x10^{-2}$		$27.9x10^{-5} \pm 1.6x10^{-5}$	$1.96x10^{-5} \pm 3.9x10^{-7}$

Salen exhibits overall much faster extraction kinetics, as calculated observed rate constants are 2 orders of magnitude greater than those corresponding to Salophen and over 3 orders of magnitude greater than those for di-t-butyl Salen and di-t-butyl Salophen. It's apparent that the tert-butyl substituted ligands exhibit slower extraction kinetics than the non bulky substituted group. Within those two groups, the more flexible ethylene backbone ligands extracted uranyl(VI) at a faster rate than the phenylenediamine group. The combination of rigidity and the presence of bulky tert-butyl groups, unfavorable steric constraints, lead to the slow extraction kinetics by di-t-butyl Salophen. A similar trend is observed in the BTBP ligand group, as the addition of a t-butyl group slows extraction kinetics.[110]

Since the total ligand and nitrate concentration were held constant at each calculated rate constant, a plot of the log(k_{obs}) vs the log of ligand concentration should give the order of the rate of extraction with respect to the ligand concentration.[111] The slope for the ligands were all close to 1, suggesting that the rate of extraction for uranyl(VI) with respect to ligand concentration is first order (Figure 4.33).

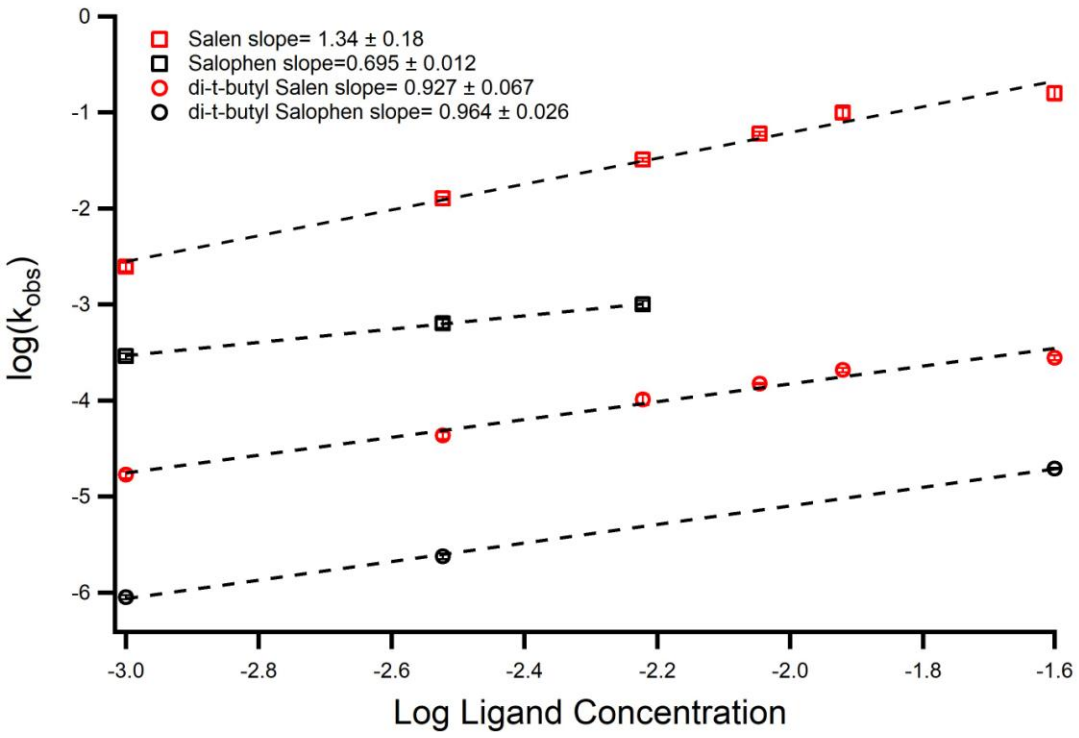

Figure 4.33. Dependence on the rate of extraction of uranyl(VI) with respect to ligand concentration.

4.2.6.2. Temperature Dependent Studies

The definition of Gibbs free energy (eq. 13) and the relationship between Gibbs free energy (eq. 14) and the equilibrium constant are expressed as follows:

$$\Delta G = \Delta H - T\Delta S \qquad \text{(eq. 13)}$$

$$\Delta G = -RT\ln(K_{eq}) \qquad \text{(eq. 14)}$$

From the combination of the two equations, the linear form of the Van't Hoff equation can be derived:

$$\ln(K_{eq}) = -\frac{\Delta H}{RT} + \frac{\Delta S}{R} \qquad \text{(eq. 15)}$$

Temperature dependent solvent extraction data is usually treated using the van't Hoff method, where the thermodynamics parameters of change in enthalpy (ΔH) and entropy (ΔS) can be

calculated and obtained by plotting the equilibrium constant (K_{ex}) of the extraction process at varied temperature. In order to asses a rigorous thermodynamic evaluation of the extraction process, the equilibrium constants must be accurately calculated for the system. Due to the complicated nature of the bi-phasic solvent extraction process, calculating equilibrium constants is not necessarily a trivial task. However, a conditional relationship between the equilibrium constant and distribution ratio can provide some insight into the overall thermodynamic trends of the extraction process. The extraction equilibrium can be expressed as (eq. 17) (Bustillos, May, Nilsson 2018):

$$(AnO_2^{2+})_{(aq)} + n(H_2L)_{(org)} \rightleftharpoons (AnO_2 \cdot L)_{(org)} + 2H^+_{(aq)} \quad \text{(eq. 16)}$$

$$K'_{ex} = \frac{[AnO_2 \cdot L]_{(org)}[H^+]^2_{(aq)}}{[AnO_2^{2+}]_{(aq)}[H_2L]^n_{(org)}} \quad \text{(eq. 17)}$$

where K'_{ex} is a conditional extraction constant assuming that the activity coefficients in both organic and aqueous phase are constant. Given that the distribution ratio is the total concentration of the actinyl cations in the organic phase divided by the total actinyl cations concentration in the aqueous phase (eq. 18)

$$D_M = \frac{[AnO_2 \cdot L]_{(org)}}{[AnO_2^{2+}]_{(aq)}} \quad \text{(eq. 18)}$$

and changes in ionic strength and changes in nitrate concentration can be neglected, eq. 2 can be rewritten as the following (eq. 19):

$$K'_{ex} = \frac{D_M[H^+]^2_{(aq)}}{[H_2L]^n_{(org)}} \quad \text{(eq. 19)}$$

Therefore, with the presumption that D_U is proportional to K'_{ex}, van't Hoff analysis can be performed in which $\ln(D_U)$ vs T is analyzed and calculated thermodynamic values can be used to reveal overall trends of the extraction process.[112] Because of its rather slow kinetics and reasonable uranyl distribution values (D_U not too high or too low), temperature dependence

studies were carried out with di-t-butyl Salen. Time dependence studies at room temperature (19° C) indicated that the extraction equilibrium for uranyl(VI) was reached at a contact time of 2 h. Extraction studies were carried out with different concentrations of di-t-butyl Salen at varying temperatures (10, 19, 22, 30, 35 and 40° C) for a contact time of 2 h. Figure 4.34 depicts the affect that temperature has on the extraction of uranyl(VI). Since the partitioning of uranyl(VI) increases with increasing temperature, the extraction of uranyl(VI) in a bi-phasic solvent extraction system by di-t-butyl Salen is an endothermic process. Temperature dependent studies on the extraction of Pd(II) by a tetradentate pyrazole derived Schiff base revealed an inverse relationship between temperature and distribution values, although the decrease in extraction at higher temperatures was attributed to the dissociation of the ligand at higher temperatures.[113] This was not observed with di-t-butyl Salen (I'm not sure if this is entirely relevant). Conditional enthalpy and entropy values can be calculated from the slope and interesct of the line and are listed in table 4.8.

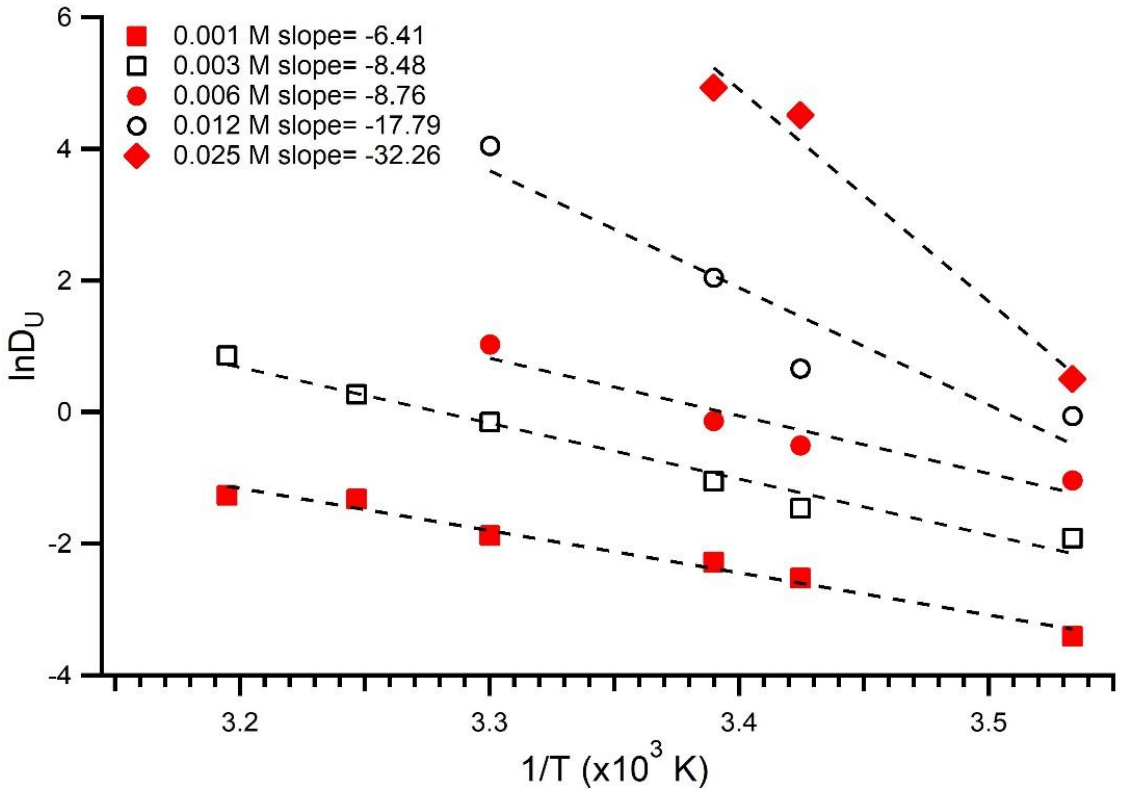

Figure 4.34. Temperature dependence of the extraction of U(VI) by varied concentrations ofdi-t-butyl Salen.

Table 4.8. Thermodynamic parameters for the extraction of uranyl(VI) by di-t-butyl Salen

Concentration (M)	ΔH (kJ mol^{-1})	ΔS (kJ mol^{-1} K^{-1}	ΔG (kJ mol^{-1})
0.001	53.3 ± 3.9	0.16 ± 0.01	6.2 ± 0.7
0.003	70.5 ± 5.6	0.23 ± 0.02	2.7 ± 0.3
0.006	72.9 ± 14.2	0.25 ± 0.05	0.42 ± 0.12
0.012	147.9 ± 34.3	0.52 ± 0.12	-4.04 ± 1.31
0.025	268.2 ± 40.1	0.95 ± 0.14	-10.9 ± 2.3

Although we can infer from the extraction data that the overall extraction is endothermic, detailing the interpretation of the thermodynamic parameters is difficult due to numerous processes occurring. Contributions to change in enthalpy and entropy values can arise from complexation of the metal ion, dehydration of the metal ion, dissolution of the complex in the

organic phase, protonation equilibria and ligand-ligand interactions. Since a single ligand class of extractant is under investigation, and no functional groups are varied, a direct comparison can be made as ligand concentration is varied. Bonds in soft acid soft base complexes results in the sharing of an electron pair while bonds in hard acid hard base complexes is characterized by electrostatic interactions.[25] In relation to solvent extraction, the interactions between "hard" cations, such as An(III) and An(VI), and "hard" donor (O, N) ligand form complexes which are often characterized by both positive enthalpy and entropy changes.[25] Effectively, the extraction of uranyl(VI) by di-t-butyl Salen resembles the extraction mechanism of a chelating acidic extractant. The driving force of the extraction of a metal cation by a chelating acidic extractant is the replacement of water molecules. These interactions are referred to as entropy driven due to the loss of hydration of the cations. As water molecules are displaced from the metal cation, there is an overall increase in the disorder and randomness of the system resulting in positive entropy contribution. The dehydration results in endothermic enthalpy contribution as energy input is required for the breaking of water-metal bonds. During complexation of the actinyl cation by the ligand, a negative enthalpy contribution should be expected due to bond formation. The bond formation should also result in negative entropy contribution since the randomness of the system decreases as the metal-ligand complex forms. Calculated entropy and enthalpy values are listed in Table 4.8 and represent thermodynamic parameters for the overall extraction system. The solvent extraction of uranyl(VI) is described by endothermic enthalpy change for all ligand concentrations and positive entropy contribution. Entropy values increase with increasing ligand concentration. These values indicate that dehydration of the actinyl cation is the most significant step in the solvent extraction process.[114] The contribution to change in entropy due to the release of protons upon ligand deprotonation and the formation of hydrolytic products can not be

discounted. The extraction of uranyl(VI) by neutral organo-phosphorous compounds has demonstrated exothermic heats of extraction and negative entropy contributions.[115] Exothermic heats of extraction are also typical for the extraction of trivalent actinides by solvating extractants.[116] Results obtained from extraction studies of uranyl(VI) by di-t-butyl Salen are similar to the extraction of trivalent lanthanides by chelating acidic extractants.[117,118]

The plot below depicts the extraction of uranyl(VI) at varying di-t-butyl Salen Salen concentration and increasing temperature (Figure 4.35). The slope at T= 10° suggests that the extraction stoichiometry appears to be a 1:1 ligand to metal ratio through the entire tested ligand concentration range. At T= 20°, a 1:1 stoichiometry is presumed through the concentration range 0.001 - 0.006 M and D_U values increase drastically at concentrations above 0.006 M possibly due to a change in the extraction mechanism. When the temperature is increased to 30° C, in the 0.001 - 0.006 M range, a slope of 1.62 is obtained, suggesting a mixture of 1:1 and 2:1 ligand to metal complexes. At T= 35° C, it appears that a 2:1 ligand to metal complex dominates the extraction in the same ligand concentration range. As temperature is increased, it is possible that sufficient energy becomes available in order to form higher order ligand to metal complexes.

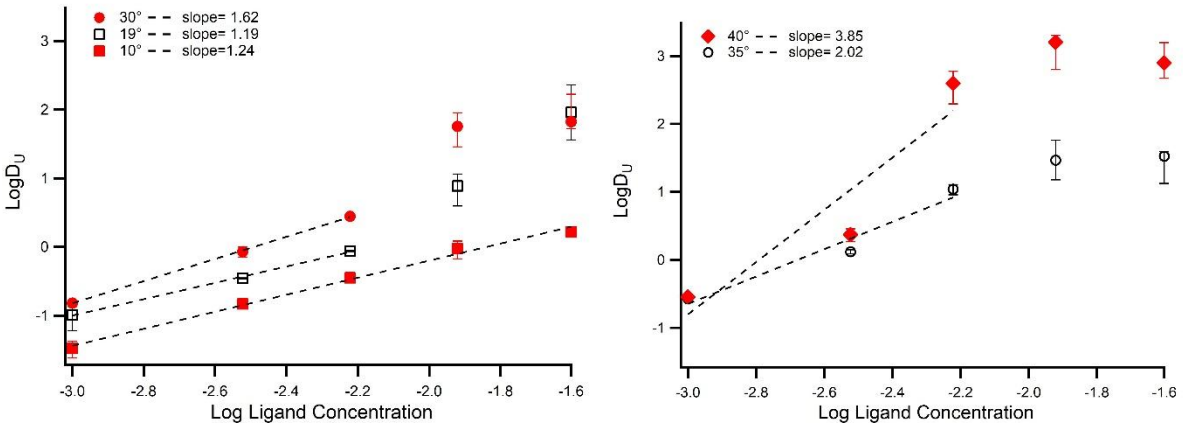

Figure 4.35. Effect of di-t-butyl Salen concentration dependency on uranyl(VI) extraction at varied temperatures.

Additional kinetic experiments were pursued with di-t-butyl Salen at different temperatures in order to uncover further details in regards to the kinetics of the initial uptake of uranyl(VI). Extraction k_{obs} were calculated for different concentrations of di-t-butyl Salen at different temperatures of 10, 20, 30 and 40 ˚C (Figure 4.36). Calculated observed rate constants are listed in table 4.9. At low ligand concentration, as the temperature increases by 10 °C, the k_{obs} appears to more or less double. As temperature is increased from 10 to 40 ˚C, the k_{obs} roughly increases by an order of magnitude. At higher ligand concentration the changes in k_{obs} at higher temperatures are relatively larger.

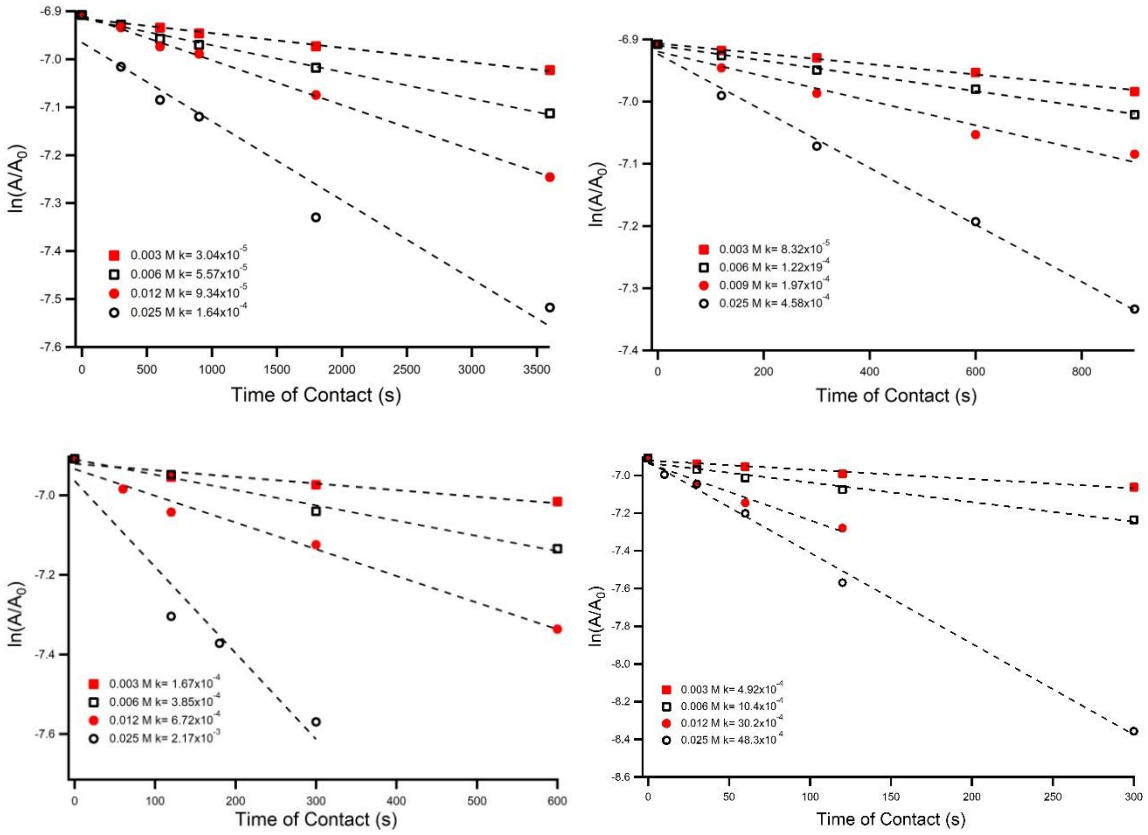

Figure 4.36. Effect of temperature on observed rate constants for different concentration of di-t-Bu Salen (0.003 - 0.025 M) at 10° (top left), 20° (top right), 30° (bottom left) and 40° (bottom right).

Table 4.9. Observed rate constants for the uptake of uranyl(VI) by varied di-t-butyl Salen at different temperatures.

	k_{obs}			
Concentration (M)	10°	20°	30°	40°
0.003	$3.04x10^{-5} \pm 1.7x10^{-6}$	$8.31x10^{-5} \pm 3.7x10^{-6}$	$1.67x10^{-4} \pm 3.1x10^{-5}$	$4.92x10^{-4} \pm 4.5x10^{-5}$
0.006	$5.57x10^{-5} \pm 2.3x10^{-6}$	$12.2x10^{-5} \pm 4.0x10^{-6}$	$3.85x10^{-4} \pm 2.9x10^{-5}$	$10.4x10^{-4} \pm 9.0x10^{-5}$
0.012	$9.34x10^{-5} \pm 1.8x10^{-6}$	$19.7x10^{-5} \pm 1.9x10^{-5}$	$6.72x10^{-4} \pm 4.9x10^{-5}$	$30.2x10^{-4} \pm 3.8x10^{-4}$
0.025	$16.4x10^{-5} \pm 1.7x10^{-5}$	$45.8x10^{-5} \pm 1.8x10^{-5}$	$21.7x10^{-4} \pm 3.6x10^{-4}$	$48.3x10^{-4} \pm 1.5x10^{-4}$

The linear relationship between k_{obs} and inverse temperature can be obtained from the Arrhenius equation:

$$k_{obs} = Ae^{-E_a/RT} \qquad \text{(eq. 20)}$$

where R is the universal gas constant, T is the absolute temperature and A in the frequency factor and E_a is the possible activation energy.[119] The figure below (4.37) plots $\ln(k_{obs})$ vs 1/T where the slope is the energy of activation of the extraction process. Calculated energy of activation for the extraction system are listed in Table 4.

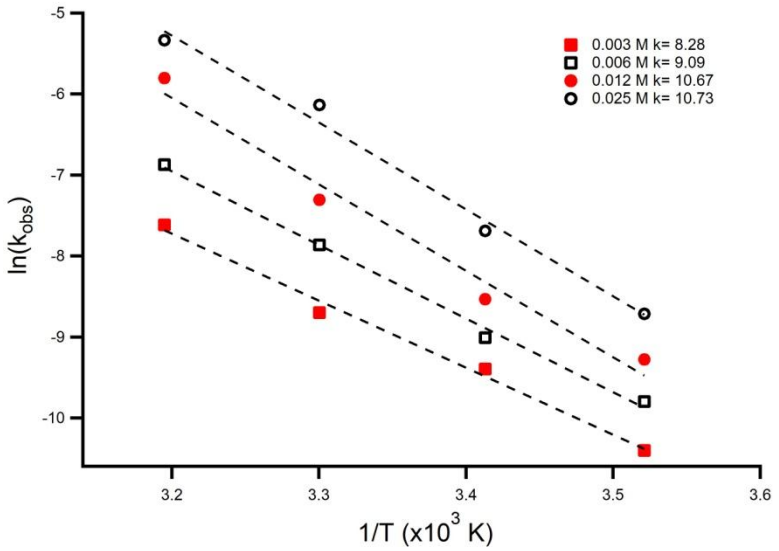

Figure 4.37. Observed rate constants as varying temperatures for varied concentrations of di-t-butyl Salen

As mentioned previously, it was apparent that energy barriers were present in the extraction of uranyl(VI) by the di-t-butyl Salen. Calculated activation energy increases with increasing ligand concentration, suggesting states which require larger energy input at higher ligand concentrations. Slope analysis results suggested the formation of 2:1, and possibly higher, extraction stoichiometry of uranyl(VI) by di-t-butyl Salen at higher temperatures. An energy of activation greater than 20 kJ mol^{-1} suggests the transfer of the metal cation into the organic phase is carried out mostly through chemical reactions rather than diffusion.[119b] Calculated energy of activation values help illustrate the energy associated with the possible formation of higher order ligand to metal complexes. Previous work on solvent extraction of Cu(II) by the reagent LIX 64N indicate that there is a slight increase in the energy of activation for increasing extractant concentration, although no reason for this observation was given.[119a]

Table 4.10. Calculated energy of activation for the extraction of uranyl(VI)

Concentration (M)	E_a (kJ mol^{-1})
0.003	68.8 ± 4.5
0.006	75.6 ± 3.5
0.012	88.7 ± 9.5
0.025	89.2 ± 6.7

In similar fashion, the calculated observed rate constants at different temperatures can also be used in determining the enthalpy and entropy of activation through the Eyring equation:

$$k_{obs} = \frac{RT}{Nh} e^{\frac{\Delta S^{\ddagger}}{R}} e^{\frac{-\Delta H^{\ddagger}}{RT}} \qquad \text{(eq. 21)}$$

Where R is the universal gas constant, T is absolute temperature, N is avogadros number, h is Plancks constant, $\Delta S^{\ddagger}$ is entropy of activation and $\Delta H^{\ddagger}$ is enthalpy of activation. From the linear relationship, the enthalpy and entropy of activation can be calculated:

$$\ln\left(\frac{k_{obs}}{T}\right) = \ln\left(\frac{R}{Nh}\right) + \frac{\Delta S^{\ddagger}}{R} - \frac{\Delta H^{\ddagger}}{RT} \qquad \text{(eq. 22)}$$

Enthalpy of activation values can be calculated from the slope of the plot of the natural log of the observed rate constant over temperature vs inverse temperature while entropy of activation can be calculated from the intercept. The plot and table with calculated values are shown below.

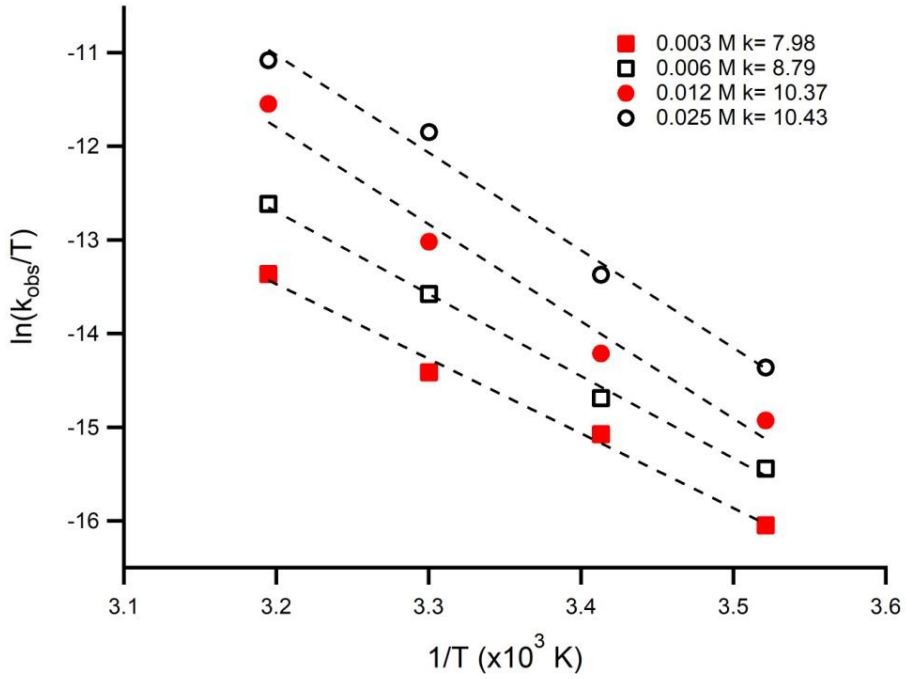

Figure 4.38. Observed rate constants over temperature vs temperature for di-t-butyl Salen.

Table 4.11. Enthalpy and Entropy of activation values calculated for the extraction of 0.003 - 0.025 M di-t-butyl Salen.

Concentration (M)	$\Delta H^{\ddagger}$ (kJ mol^{-1})	$\Delta S^{\ddagger}$ (J mol^{-1} K^{-1})
0.003	66.3 ± 4.5	-97.2 ± 14.5
0.006	73.1 ± 3.5	-69.2 ± 6.4
0.012	86.2 ± 9.5	-19.6 ± 3.5
0.025	86.7 ± 6.7	-11.7 ± 1.4

As mentioned previously, the equilibrium extraction of uranyl(VI) is characterized by endothermic enthalpy values and a positive entropy contribution. It is believed that these values are largely due to the dehydration of the metal cation as energy inputs break the metal-water bond and the overall increase in disorder of the system. Activation values indicate that the initial uptake of uranyl(VI) involves endothermic change in enthalpy and negative contributions to entropy although entropy becomes less negative as ligand concentration increases. The activation endothermic heats of extraction reflect the breaking of metal-water bonds. However, negative activation entropy values suggest an ordered activated system. This could reflect complexation of the metal by the ligand, leading to a decrease in the degrees of freedom by the ligand (loss of configurational entropy) but dehydration of the metal has not occurred. As the ligand concentration increases, change in entropy becomes more positive suggesting that the system is becoming more disordered. Although multiple ligand binding to a metal cation would lead to negative entropy contributions, the increase in change in entropy values could be due to dehydration by multiple ligands. Again, change in entropy contributions from deprotonation and the formation of hydrolytic products can not be discounted nor ignored.

4.2.7. Continuous Extraction Studies- Retention of Cation in Aqueous Phase

4.2.7.1. Uranium

Extraction studies with uranyl(VI) with Salen-SO_3 and Saldien-SO_3 acting as holdback reagents have been studied and is reported in (Hawkins et. al.).[75]

4.2.7.2. Neptunium

Extraction studies with the neptunyl cations with Salen-SO_3 and Saldien-SO_3 acting as holdback reagents has been studied and is reported in (Hawkins et. al).[76]

4.2.7.3. Plutonium

Competitive continuous extraction studies were carried out, in separate experiments, with Salen-SO_3 and Saldien-SO_3 as holdback reagents in the aqueous phase and an organic phase consisting of HDEHP as in toluene. The figure below (4.39) plots the distribution values calculated at different time points for the extraction of Pu(VI) by HDEHP with and without Salen-SO_3 present in the aqueous phase. Extraction of Pu(VI) with no Salen-SO_3 yields distribution values close to 10 after 30 minutes of contact. However, when the Salen-SO_3 is present in the aqueous phase, extraction of Pu(VI) decreased by almost an order of magnitude and remains in the aqueous phase for the duration of the experiment. Complexation studies with Pu(VI) revealed no apparent reduction of Pu(VI) in an aqueous medium. Under the assumption that there was also no reduction of Pu(VI) in this experiment, we can conclude that the tetradentate Salen-SO_3does function as an efficient holdback reagent for Pu(VI). In the likelihood that there was reduction to Pu(V), distribution values for the +V oxidation state would be expected to be much lower.

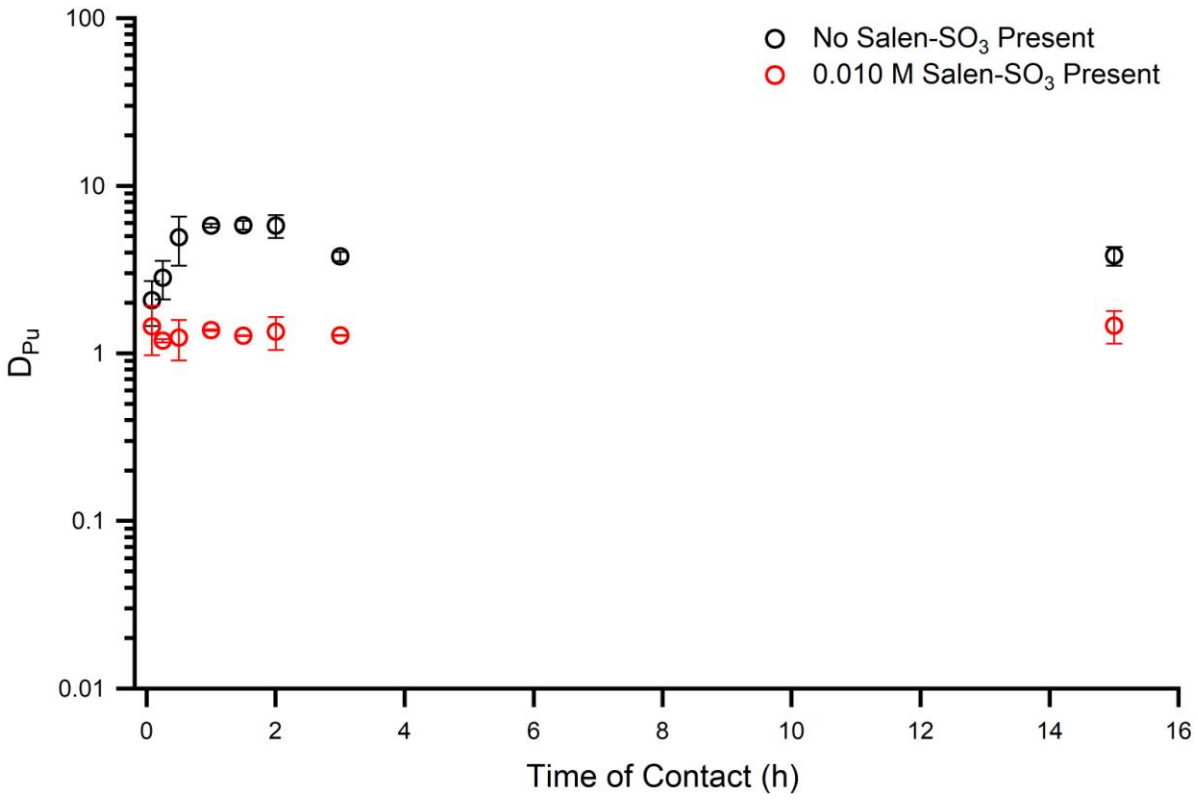

Figure 4.39. Distribution ratio of the extraction of Pu(VI) ($1x10^{-7}$ M) from 0.1 M KNO_3 as a function of contact time by 0.01 M HDEHP with 0.01 M SO_3-Salen present and not present.

Studies with the pentadentate Saldien-SO_3 demonstrated overall similar retention of the Plutonyl(VI) cation as the tetradentate system (Figure 4.40). It appears that when the Saldien-SO_3 is present, at a contact time of 15 h, there is an increase in the distribution ratio. Similar to the Salen-SO_3, Saldien-SO_3 showed no reduction of Pu(VI) to Pu(V), and we would expect Pu(V) to suppress distribution values. The spike is the partitioning of plutonium in the organic phase could be due to the hydrolysis and breakdown of the ligand itself.

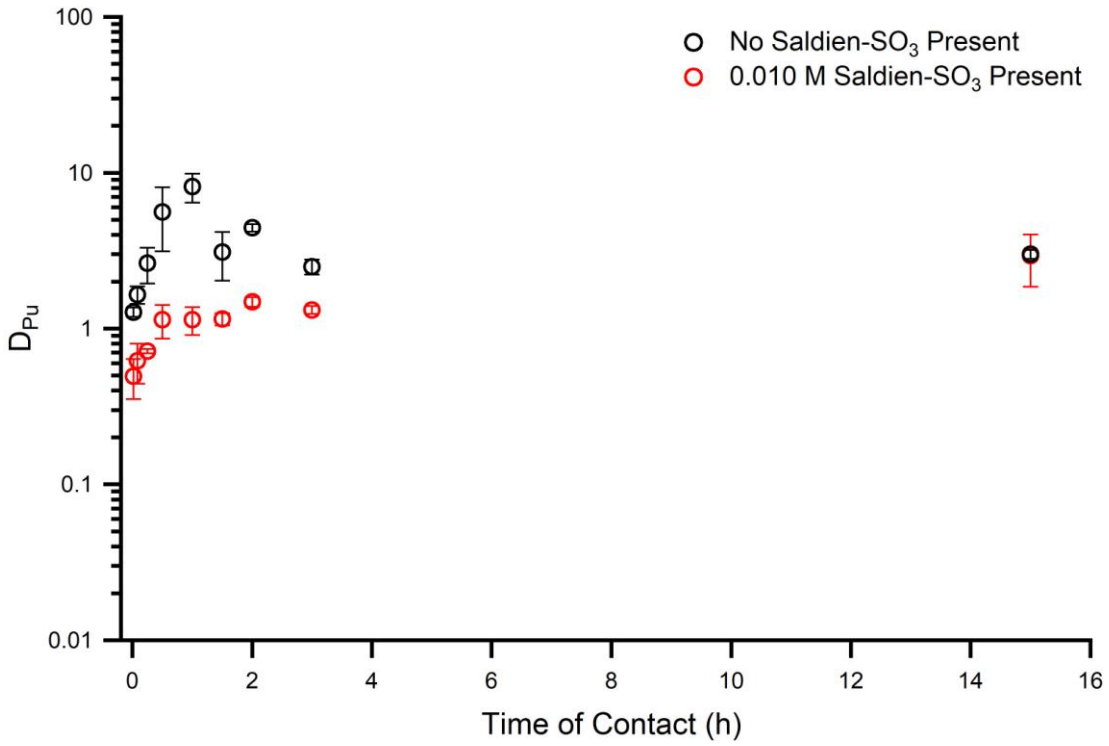

Figure 4.40. Distribution ratios for the extraction of Pu(VI) by 0.010 M HDEHP with Saldien-SO_3 (0.010 M) present and not present.

4.2.7.4. Americium

Competitive biphasic continuous extraction studies were continued with Americium oxidized to the pentavalent state. The extraction behavior of Am(V) and Am(VI) has been observed to exhibit similar extraction behavior as other the hexavalent and pentavalent mid actinides.[32,105] The pentavalent actinyl cation, due to its low charge density, is difficult to extract, similar to Np(V). Similar to previous experiments, HDEHP served as the extractant and Salen-SO_3 served as the holdback reagents. Experiments were carried out with and without aqueous soluble ligands present. Results indicate that there is immediate extraction of the Am when there is no Salen-SO_3 in the aqueous phase (Figure 4.41). When the water soluble Schiff base is incorporated in the aqueous phase, distribution values for Am are similar, and greater, than those with no holdback reagent present in the aqueous phase. Americium is essentially

completely extracted into the organic phase, exhibiting distribution values similar to the extraction of Am(III) by 0.010 M HDEHP. The extraction of Am with Salen-SO_3 present in the aqueous phase also exhibits similar distribution values and extraction trend as the extraction of Cm(III) in the same system.[76] This leads us to believe that significant, if not complete, reduction of Am(V) to Am(III) occurs in this system. Since extraction of Am is greater when the water-soluble Schiff base, we can assume that the presence of the ligand contributes to the reduction of Am(V). Reduction of high valency americium is not surprising, and more accurate result could have been collected with shorter contact times. Additionally, without proper spectroscopic analysis, accurate extraction behavior of high valency americium is difficult.

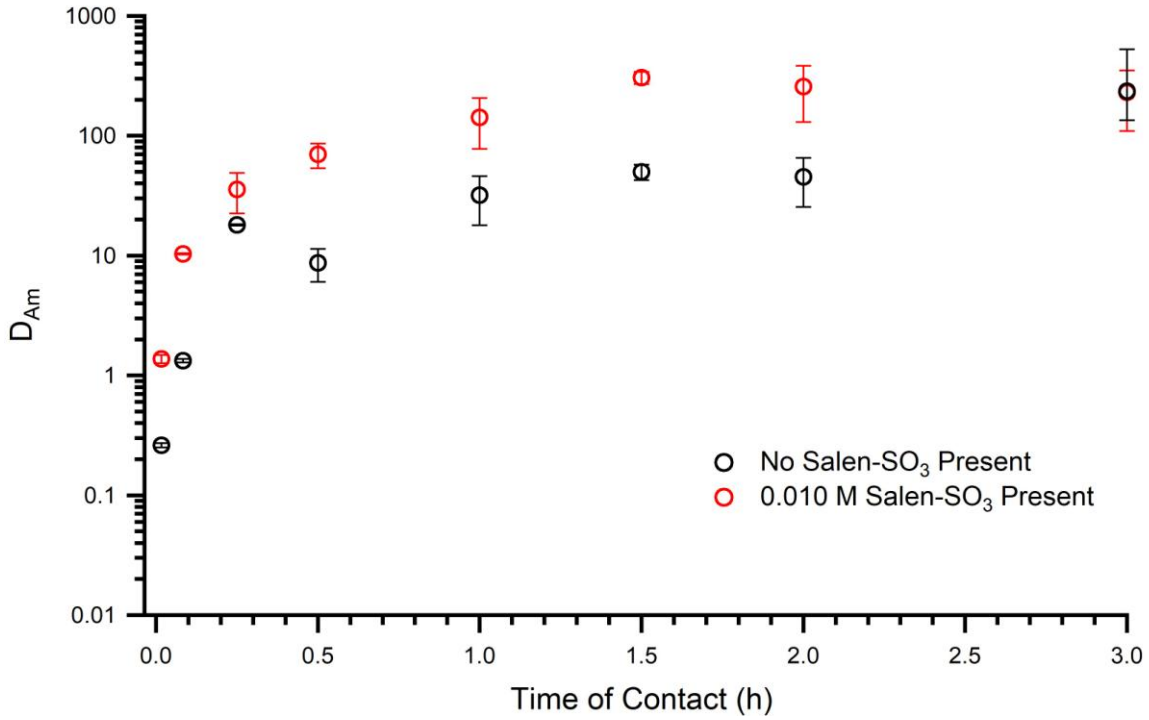

Figure 4.41. Extraction of Am(V) by 0.010 M HDEHP in toluene with and without Salen-SO_3 in 0.10 M KNO_3 present.

4.3. Degradation Studies

4.3.1. Hydrolysis

Although it is understood that the imine position on Schiff base ligands is readily susceptible to hydrolysis, especially at pH<2[120], it's important to investigate the extent of hydrolysis of di-t-butyl Salen in the diluent mixture of 1-octanol/toluene (7:3 v/v). The hydrolytic stability of a 0.025 M solution of tBu Salen was tested by contacting the organic solution, in separate experiments, with aqueous solutions at different pH for a varied amount of time. Contact times of up to 2 h, and greater, were chosen since solvent extraction studies with di-t-butyl Salen and actinyl(VI) cations were contacted for 2 h. The absorption spectra of the organic ligand solutions were recorded at each pH after each contact.

The absorption spectra for contacts at pH ranges 2-6 are characterized by a slight, gradual decrease of the intensity of the band at 330 nm. Along with the decrease in intensity, there is a slight shift of the band to a longer wavelength (Figure 4.42). One of the possible hydrolytic products, and starting material in the synthesis of the ligand, is 3,5-di-tert-butyl salicylaldehyde, which has an absorption band at 345 nm and would remain soluble in the organic phase. The slight shift of the 330 nm band to lower energy could be attributed to the formation of a hydrolytic product. When the 0.025 M di-t-butyl Salen solution was contacted with an aqueous solution at pH= 9 there was also a decrease in intensity of the absorption band at 330 nm. However, instead of the band shifting to a longer wavelength as observed with contacts with pH= 3 and 6, there is a shift of the band to a shorter wavelength. This could be attributed to addition of OH groups on the imine carbon.

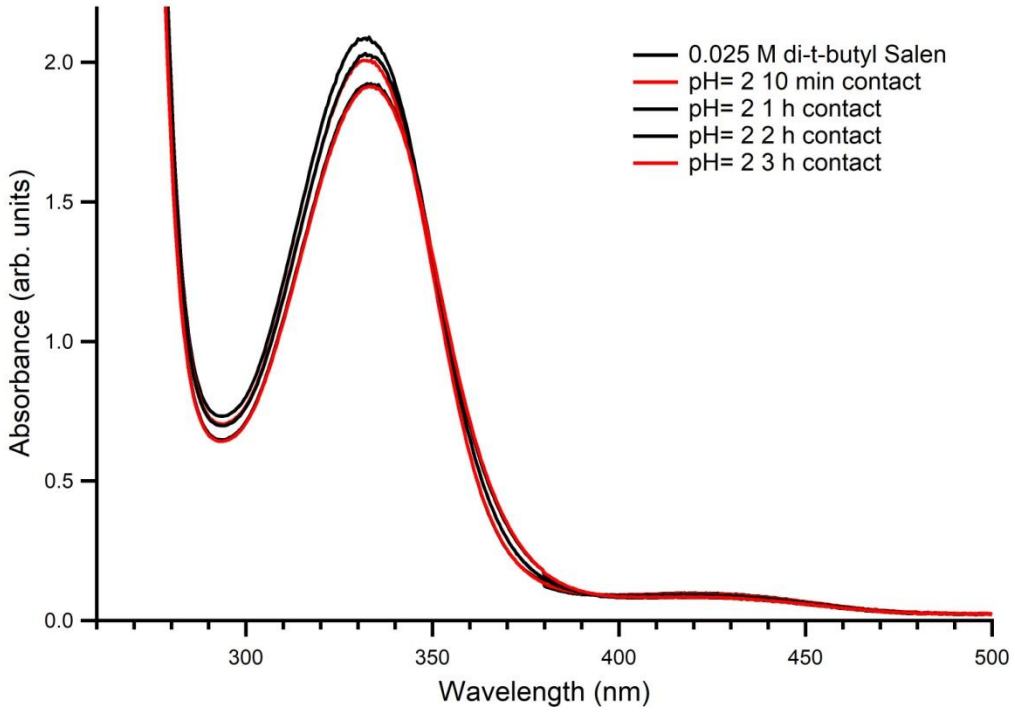

Figure 4.42. Absorption spectrum of 0.025 M di t-butyl Salen contacted with aqueous solutions at pH= 2 for varied time collected in a 1 cm path length cell.

Although the ligand demonstrated somewhat stability in neutral pH ranges for extended period of time, that was not the case when the organic solutions came into contact with more acidic aqueous solutions. The absorption spectra of contact with a pH of 2.0 solution displays a more pronounced decrease in the intensity of the band at 330 nm after 2 h (Figure 4.42). This feature is even more evident when the ligand solution is contacted with an aqueous solution at a pH of 1 or lower (Figure 4.43). When the organic solution is contacted with an aqueous solution of a pH of 0.52, there is a more pronounced decrease and shift of the absorption band to lower energy after only 5 minutes of contact. After 30 minutes of contact, there is almost a complete discoloration of the organic solution from bright yellow to pale yellow. The intact ligand in organic solvent is bright yellow and 3,5-di-tert-butyl salicylaldehyde in organic solvent is pale

yellow and almost colorless. This result, and absorption spectra, suggest that the ligand undergoes significant hydrolysis at this low pH range.

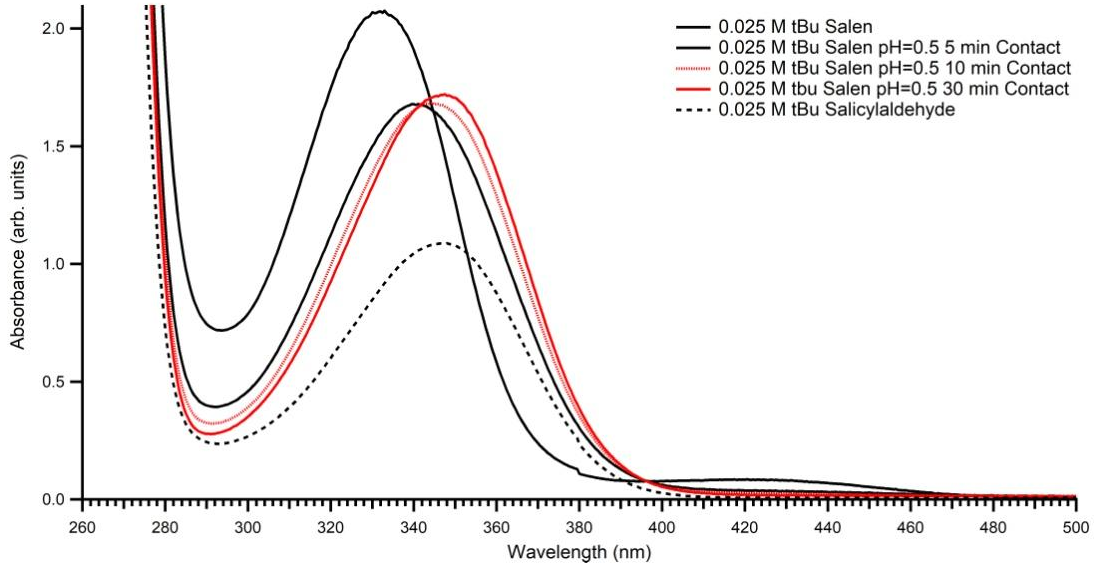

Figure 4.43. Absorption spectrum of di-t-butyl Salen contacted with an aqueous phase of pH=0.52 in 1 cm path length cell

The rate of hydrolysis can be quantified if the concentration of the remaining ligand in organic solution is known. Although the absorption band decreases in intensity and shifts, the absorbance at 330 nm can allow an estimate of the apparent remaining ligand concentration. Concentrations were calculated for each time point for each pH and are plotted against the time of contact. A plot of the natural log of ligand concentration versus time results in a straight line, indicating that the rate of hydrolysis of di-t-butyl Salen follows a first-order kinetics. First order rate of hydrolysis constant can be calculated, or estimated, from the slope of If we believe that the overall hydrolysis follows first order kinetics, the hydrolysis constant can be calculated, from the slope of the natural log of ligand concentration versus time. Calculated observed first-order rate constants and exponential constants indicate that the rate of hydrolysis of the 0.025 M di-t-butyl Salen solution at pH= 0.52 is an order of magnitude greater than at the other pH points.

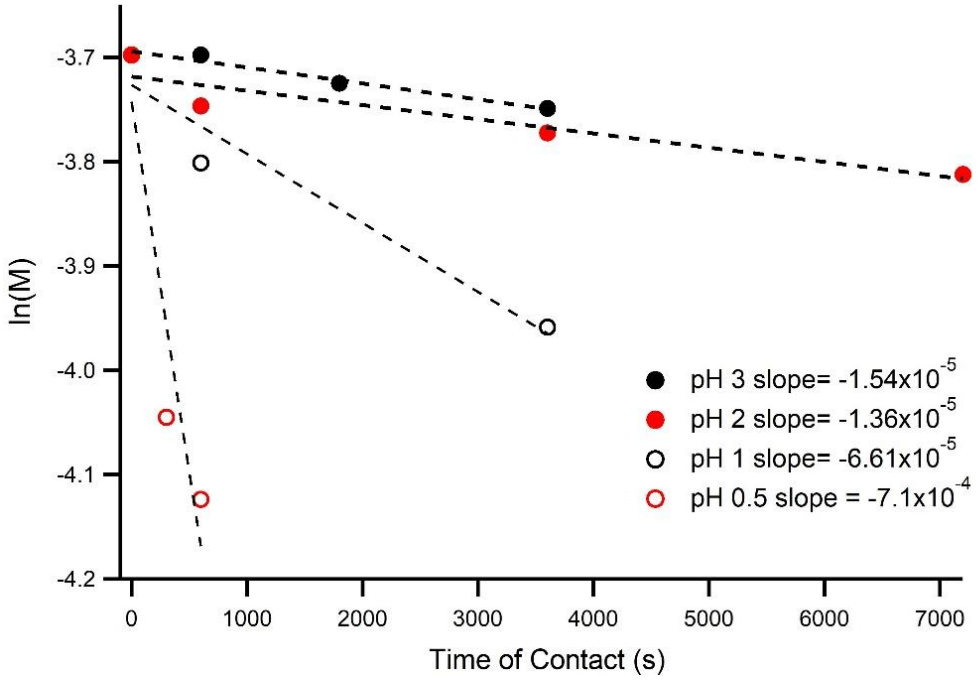

Figure 4.44. First-order plot of the change in apparent concentration of 0.025 di-t-butyl Salen at varying pH

Table 4.12. Calculated first-order observed rate constants (k_{obs}) for the hydrolysis of di-t-butyl Salen

	k_{obs} (s^{-1})
pH= 3	$1.54x10^{-5} \pm 1.91x10^{-6}$
pH= 2	$1.36x10^{-5} \pm 3.66x10^{-6}$
pH= 1	$6.61x10^{-5} \pm 1.68x10^{-5}$
pH= 0.5	$7.1x10^{-4} \pm 2.59x10^{-4}$

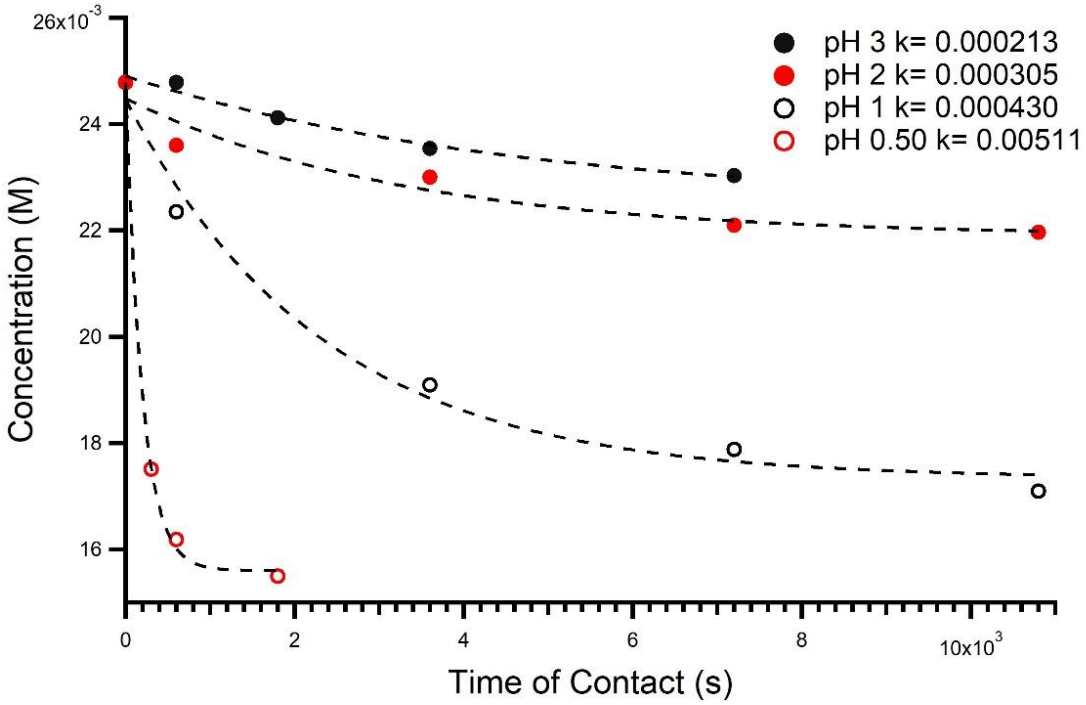

Figure 4.45. Change in apparent concentration of 0.025 M tBu Salen at varing pH

4.3.1.1. Identification of Hydrolytic Products Through ESI-MS

Since organic solutions of 0.025 M di-t-butyl Salen contacted with aqueous solutions of pH= 0.52 exhibited significant apparent hydrolysis, they were analyzed by ESI-MS in order to identify and confirm the possible organic soluble hydrolytic products. ESI-MS spectra of 0.025 M di-t-butyl Salen contact with an aqueous solution of pH= 0.52 at contact times of 5, 10, and 30 minutes and shown below (Figures 4.46-4.48). The peak at (m/z)= 493 corresponds to protonated di-t-butyl Salen ($M+H^+$). After only 5 minutes of contact, the most abundant peak is (m/z)= 277.20 which corresponds to the ligand having undergone partial hydrolysis. After a contact time of 10 minutes, (m/z)= 277 and (m/z)= 493 are the only dominant identifiable peaks, with the same relative abundance as in t= 5 min. After 30 minutes, the (m/z)= 493 peak is still present in siginificant quantities although (m/z)= 277 remains the most abundant peak. More peaks are also present in greater abundance than there were at t= 5 and 10 min. The (m/z)= 235

peak corresponds to (3,5)-di-tert-butyl salicylaldehyde, a starting material in the synthesis of di-t-butyl Salen. Although it is a primary hydrolytic product, it did not appear at t= 5 and 10 min.

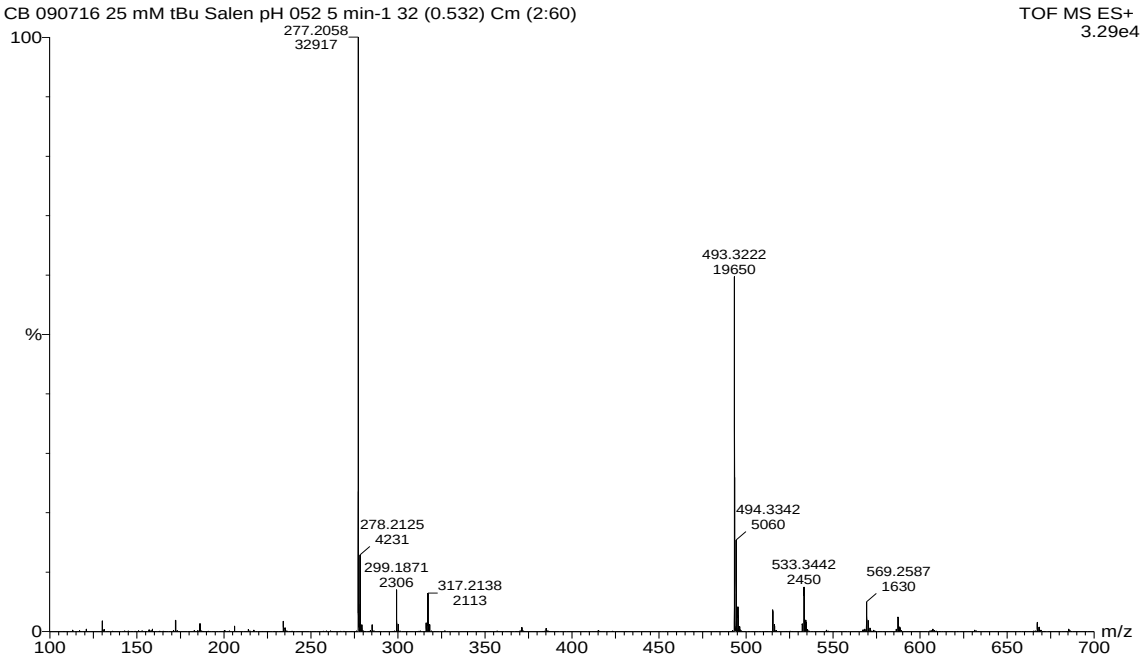

Figure 4.46. 25 mM Salen contacted with pH = 0.52 after 5 minutes

(m/z)= 277

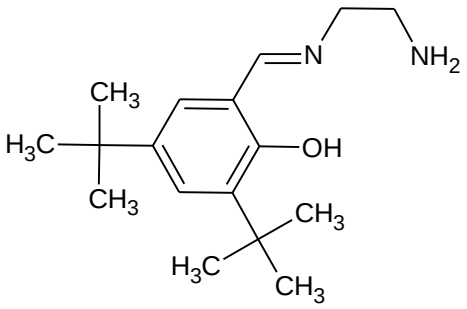

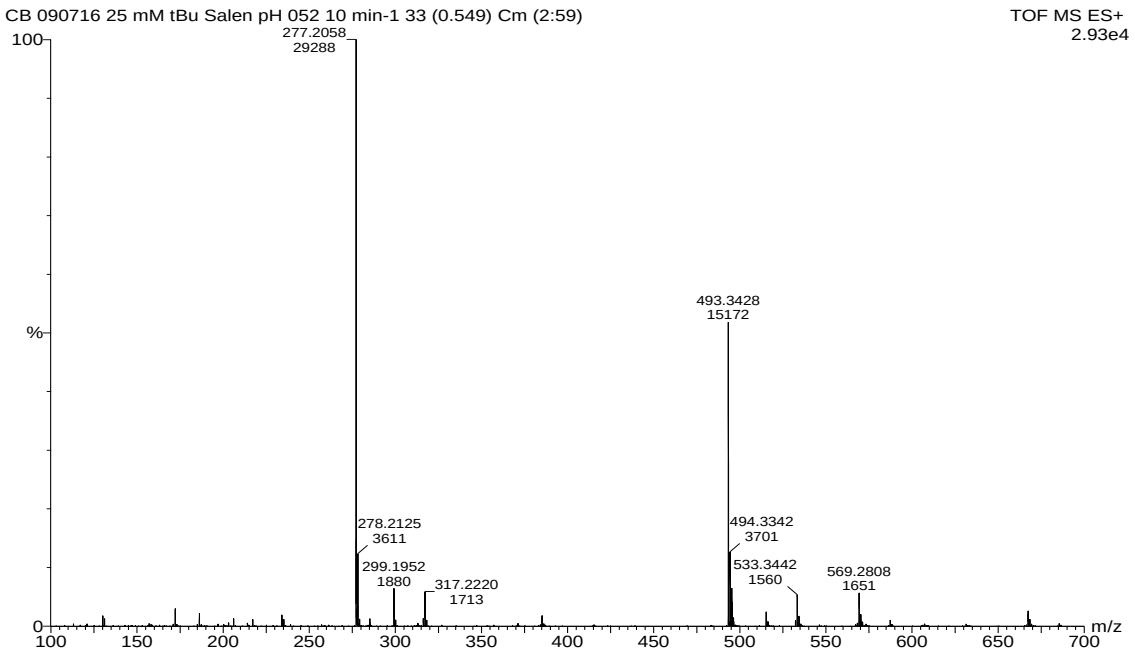

Figure 4.47. 25 mM Salen contacted with pH = 0.52 after 10 minutes

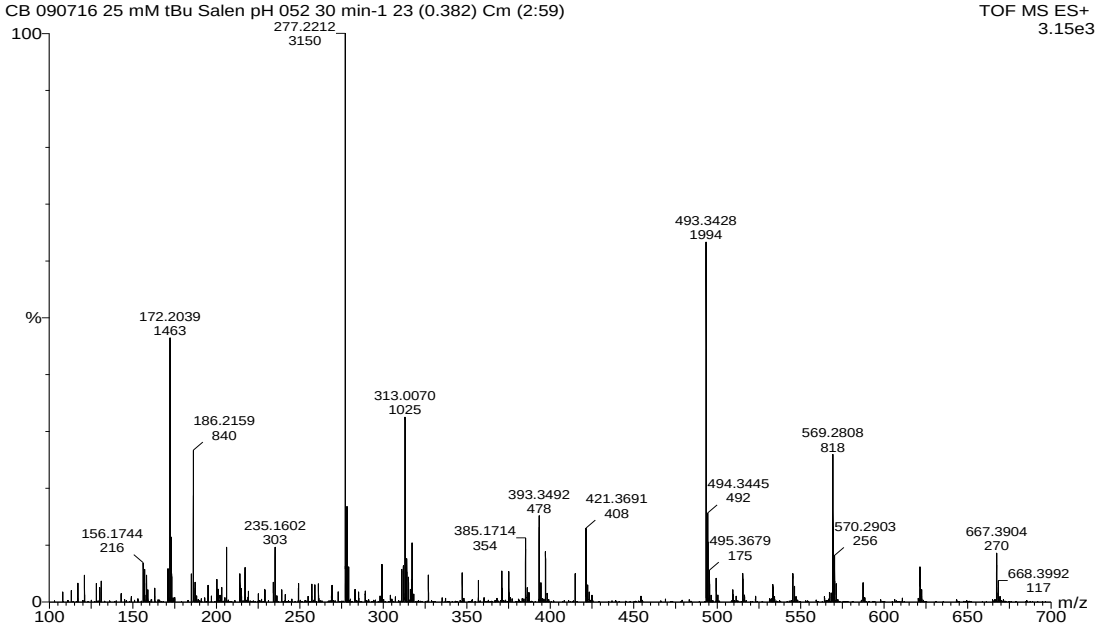

Figure 4.48. 25 mM Salen contacted with pH = 0.52 after 30 minutes

(m/z)= 235

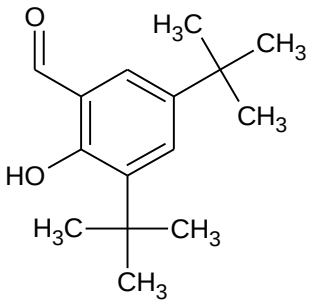

4.3.2. Radiolytic Studies

Solutions of 0.025 M Salen, 0.025 M tBu Salen and 0.012 M tBu Salophen were irradiated in a Cs-137 source at a dose rate of 2 kGy h^{-1} for an extended period of time. The extent and quantification of ligand degradation was predominantly studied by absorption spectroscopy and concentrations were calculated from absorptions at $\lambda_{abs,\ max}$= 318 for Salen, $\lambda_{abs,\ max}$= 330 for tBu Salen and $\lambda_{abs,\ max}$=340 nm for tBu Salophen. The absorption spectrums for the irradiated ligands are shown below in figure 4.49. The absorption spectrum of 0.025 M Salen is characterized by an intense band at 318 nm, and a lower energy band at 420 nm and a higher energy band at 280 nm. As the total dose absorbed increases, there is a gradual decrease in intensity of the band at 318 nm, likely due to the radiolytic degradation of the ligand, but there is no pronounced shift of the band. Although the bands at 318 and 420 nm decrease in intensity with increasing absorbed dose, the band at 280 nm increases in intensity. The increase in intensity could be due to the formation and accumulation of a specific radiolytic product or a charge transfer band. Similar to Salen, the absorption spectra of the radiolytic degradation of tBu Salen is characterized by a gradual decrease in intensity of its absorption band at 330 nm with increasing total absorbed dose. The decrease in intensity of the band was not accompanied by a dramatic shift in the band as it was observed in hydrolytic studies (Figure 4.49). A notable feature of irradiated tBu Salen is the growth of a shoulder around 280-290 nm, similar to the

band present in the absorption spectrum of Salen. This band was not present in spectra collected from hydrolytic studies, suggesting the band could correspond to a radiolytic product. If it is a radiolytic product, it could correspond to a fragment which hast-butyl groups. Similar to the other ligands, the absorbance band corresponding to tBu Salophen at 340 nm decreases in intensity with increasing absorbed dose. Initially the band at 340 nm is a broad feature, multiple shoulders/bands appear at a high absorbed dose.

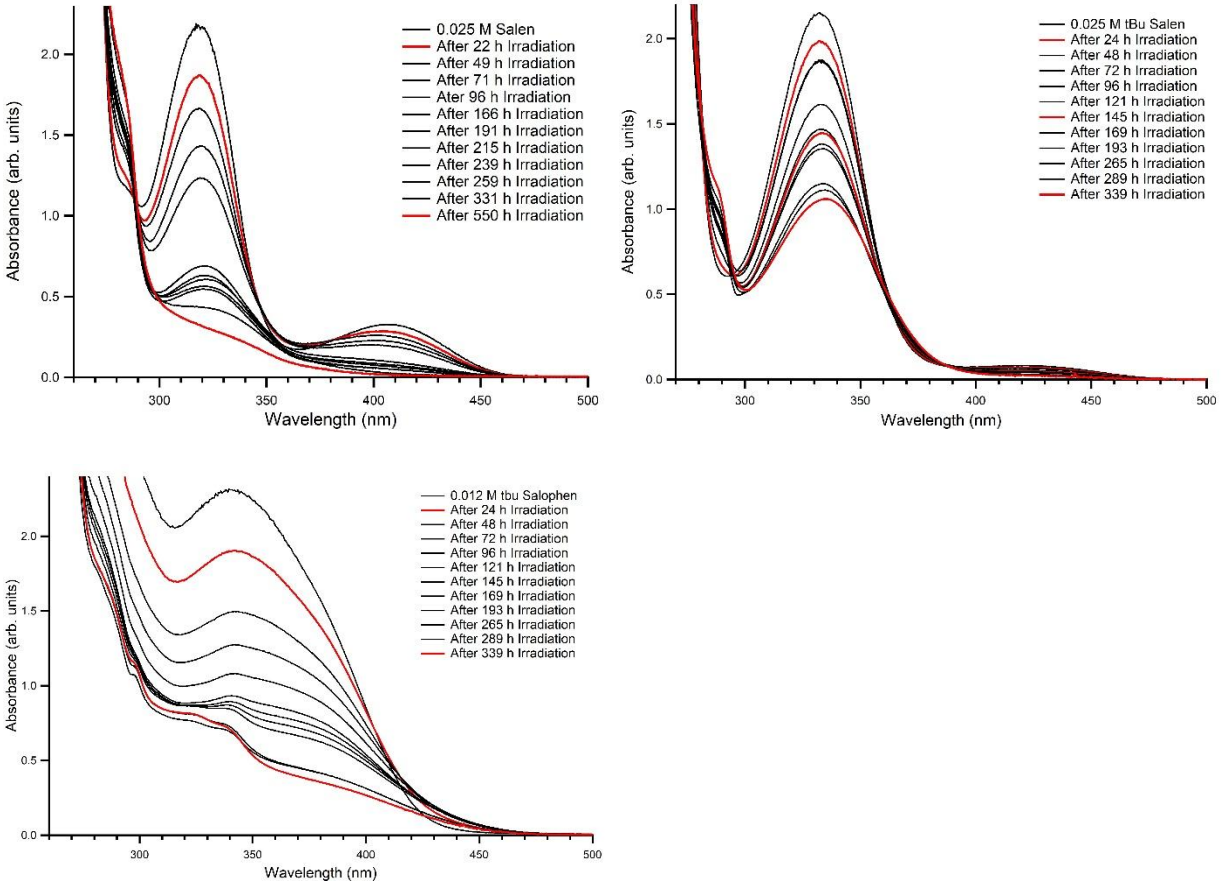

Figure 4.49. Absorption spectra for irradiated 0.025 M Salen (top left), 0.025 M tBu Salen (top right) and 0.012 M tBu Salophen (bottom left) recorded in a 1 cm path length cell

The degradation of organic solutions subjected to irradiation have been described by series of first-order reactions.[62] Degradation of tributyl phosphate (TBP) due to gamma irradiation has been described by the following equation:

$$C_T = C_{T_0} e^{-k_\gamma D_\gamma t} \qquad \text{(eq. 23)}$$

Where C_{To} is the initial concentration at zero dose, D_γ is the gamma dose rate, t is irradiation time and k_γ is the degradation constant. If the degradation of our ligand solutions would appear to follow first-order kinetics, then the above equation can be applied in order to calculate a k_γ degradation constant. Concentrations of the apparent ligand concentration remaining in organic solution were calculated at their λ_{max} throughout the entire irradiation time. A plot of the natural log of the ligand concentration against the time of irradiation in seconds yields a straight line, suggesting that the radiolytic degradation of the ligands follow first-order kinetics (Figure 4.50). Calculated observed rate constants indicate di-t-butyl Salen undergoes the least degradation by radiolysis.

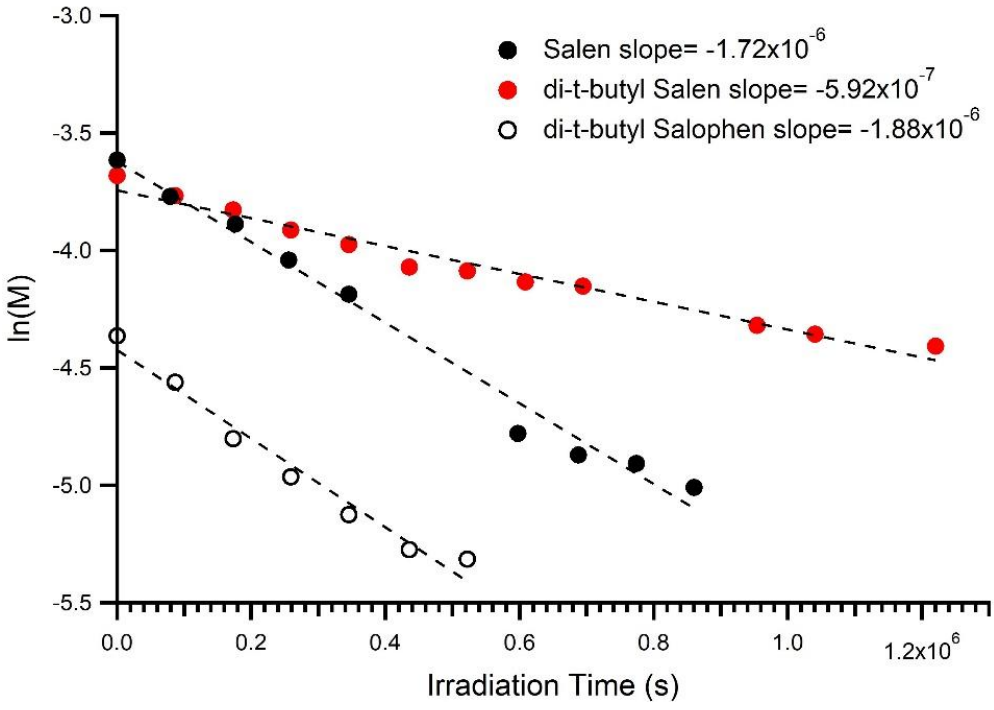

Figure 4.50. First-order plot of the change in apparent concentration of 0.025 M Salen, 0.025 di-t-butyl Salen, and 0.012 M di-t-butyl Salophen

Table 4.13. Calculated first-order observed rate constants (k_{obs}) for the radiolysis of the ligands

	k_{obs} (s^{-1})
Salen	$1.72x10^{-6} \pm 3.11x10^{-8}$
di-t-butyl Salen	$5.92x10^{-7} \pm 7.83x10^{-9}$
di-t-butyl Salophen	$1.88x10^{-6} \pm 1.44x10^{-7}$

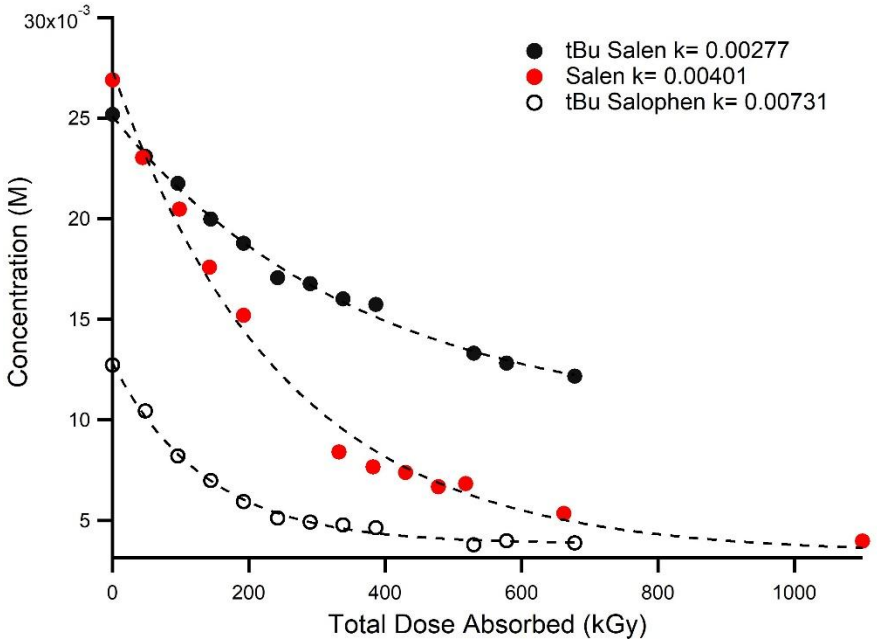

Figure 4.51. Calculated degradation constants for irradiated ligands (0.025 Salen, 0.025 di-t-butyl Salen and 0.012 M di-t-butyl Salophen)

The concentration of the observed ligand concentration remaining in the organic solution was plot against the total absorbed dose in kGy (Figure 4.51). From this analysis, calculated dose constants further indicate that di-t-butyl Salophen was the most susceptible to degradation while di-t-butyl Salen was the least susceptible. However, di-t-butyl Salophen contains an extra aromatic ring that Salen and di-t-butyl Salen do not possess. The slight increase in overall aromaticity of the ligand should provide more stability and resistance to radiolytic degradation as

aromatic compounds scavenge reducing free radicals.[61] A comparison of G-values could provide a better comparison in regards to their radiolytic susceptibility (Figure 4.52). G-values can be obtained from the derivative of concentration versus absorbed dose, and are listed in the table below (Table 4.14). Calculated G-values indicate that Salen is the most susceptible to gamma irradiation.

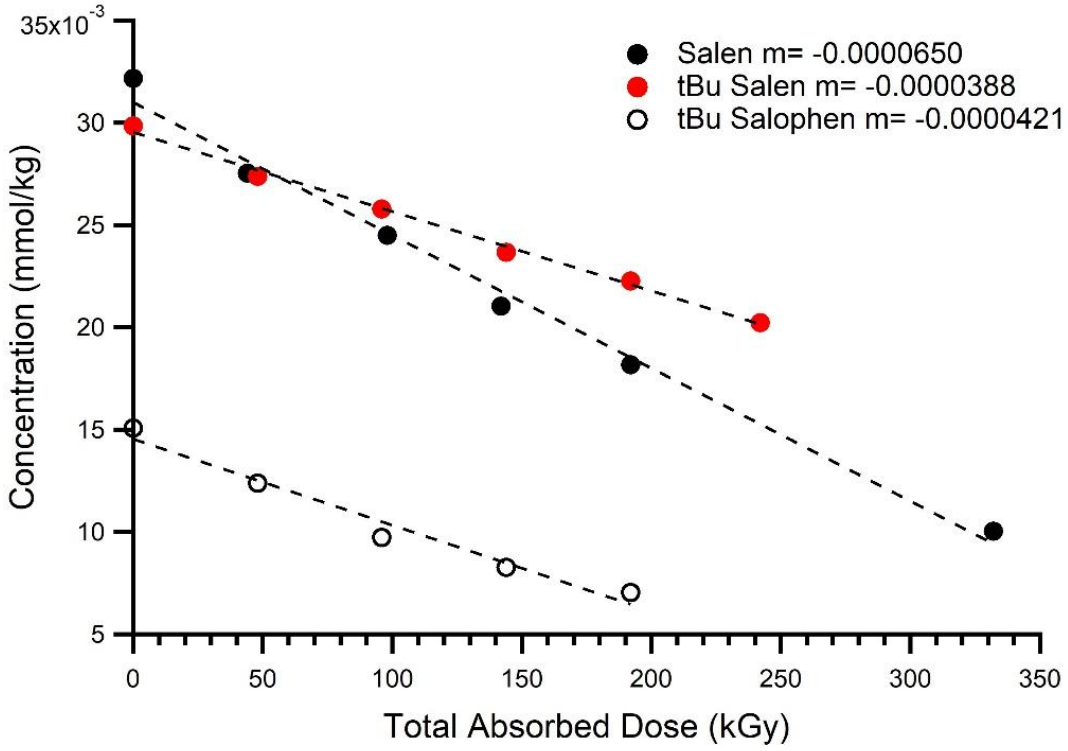

Figure 4.52. Degradation of Salen, di-t-butyl Salen and di-t-butyl Salophen where the slope of the line represents the G-value

Table 4.14. Calculated G-values for Ligand Radiolysis

	G-value (μmol J^{-1})
Salen	$-6.50 \times 10^{-5} \pm 3.15 \times 10^{-6}$
di-t-butyl Salen	$-3.88 \times 10^{-5} \pm 1.32 \times 10^{-6}$
di-t-butyl Salophen	$-4.21 \times 10^{-5} \pm 4.32 \times 10^{-6}$

During reprocessing conditions, both the organic and aqueous phases are in constant contact and are both exposed to ionization radiation emitted from spent nuclear fuel. With the presence of both aqueous and nitric compounds also exposed to radiation, overall radiolysis of the ligand solutions could be affected differently. Since experiments utilizing a continuous flow-loop exposed to gamma radiation is not feasible, a solution of 0.025 M Salen was contacted with 0.010 M HNO_3 and exposed to low LET radiation. The contacted solution was exposed to the same dose rate (2 kGy/h) and total irradiation time as non contacted 0.025 M Salen. The absorption spectra of 0.025 M Salen and acid contacted 0.025 M Salen are shown below in Figure 12. The spectra of the acid contacted Salen is overall similar to that of non contacted Salen. There is a decrease in intensity at $\lambda_{abs,\ max}$= 318 nm with increasing absorbed dose with no significant shift by the band. However, features in the range of 270-310 nm differ in intensity, which could be attributed to the formation of different radiolytic products. Calculated degradation constants (Figure 4.54) indicate a solution of 0.025 M Salen that was contacted with 0.01 M HNO_3 is slightly less resistant to radiation than the non contacted solution of 0.025 M Salen. Working under the assumption that the density of the 0.025 M Salen solution does not change drastically after contact with 0.010 M HNO_3, obtained G-values indicate that the acid contacted solution is slightly more stable than the non contacted solution (Figure 4.55). The slight stability could be attributed to possible presence of a nitrate (NO_3^-) ion which can rapidly scavenge hydrated electrons.[121]

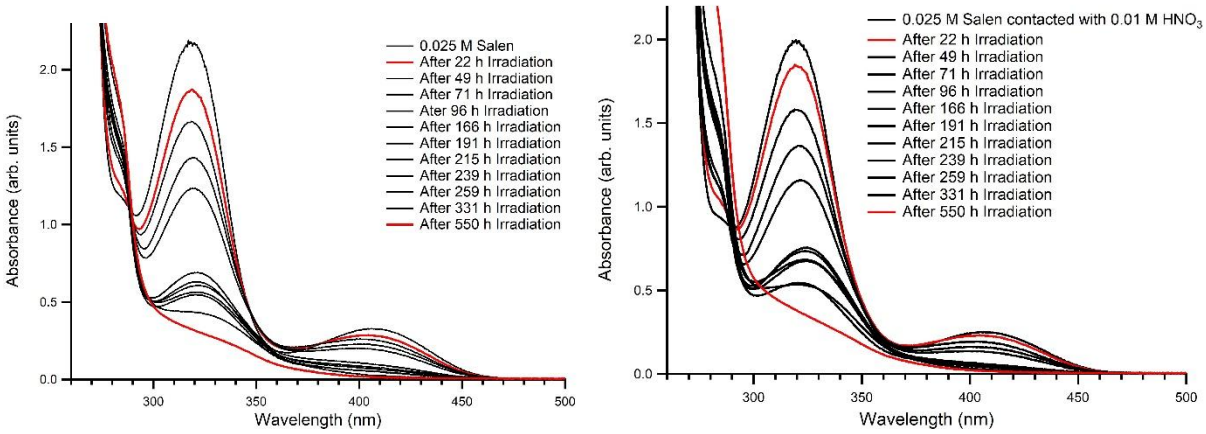

Figure 4.53. Absorption spectra of irradiated 0.025 M Salen and 0.010 M HNO_3 contacted 0.02 M Salen recorded in a 1 cm path length cell

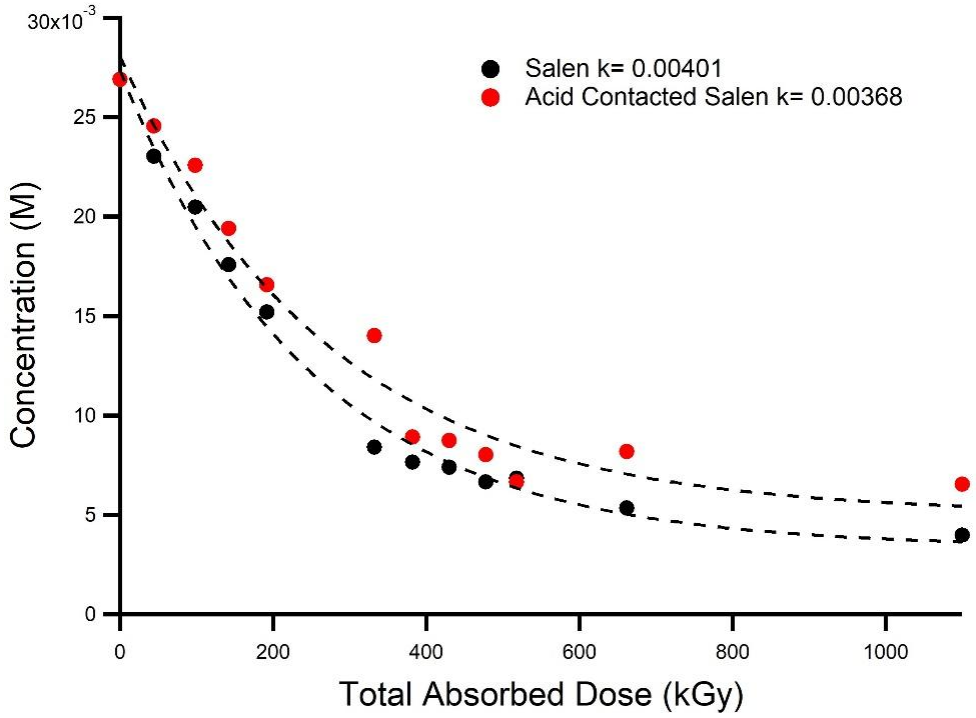

Figure 4.54. Calculated degradation constants for 0.025 M Salen and 0.01 M HNO_3 contacted 0.025 M Salen

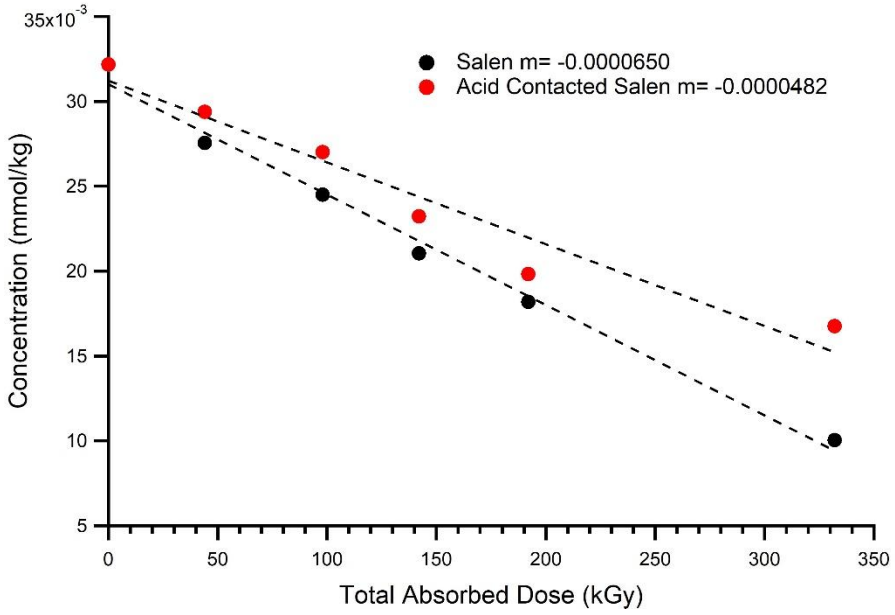

Figure 4.55. G-values for 0.025 M Salen and 0.025 M Salen contacted with 0.010 M NO_3

4.3.2.1. Effect of Degradation on Extraction Properties

In figure 4.56 the extraction of UO_2^{2+} is plotted against dose received by 0.025 M tBu Salen and 0.025 M Salen. The extraction of UO_2^{2+} decreases with increasing absorbed dose, suggesting that significant ligand degradation occurs enough to decrease extraction efficiency.[122,123] In order for the UO_2^{2+} cation to be extracted into the organic phase, the ligand metal complex must be charge neutral and the equatorial positions must be occupied in order to make the complex more soluble in the lipophilic phase. Tetradentate Schiff base ligands complex and extract to UO_2^{2+} by coordinating each O atom, to neutralize the charge, and each N atom. A decreasing D_U implies that the incoming ionization radiation is rupturing the tetradentate integrity of the ligand. This rupturing could be occurring at the imine position, on the ethylene backbone or between the imine carbon and the aromatic ring. Although Salen was the most susceptible to degradation due to gamma radiation, as determined from G-values, Salen maintains D_U values greater than tBu Salen for higher absorbed dose. For di-t-butyl Salen, D_U

values decrease to 0.1 at a dose of 700 kGy but Salen required a dose of 1100 kGy to drop down to that distribution value. Analysis of degradation products utilizing mass spectrometry can help identify specific products.

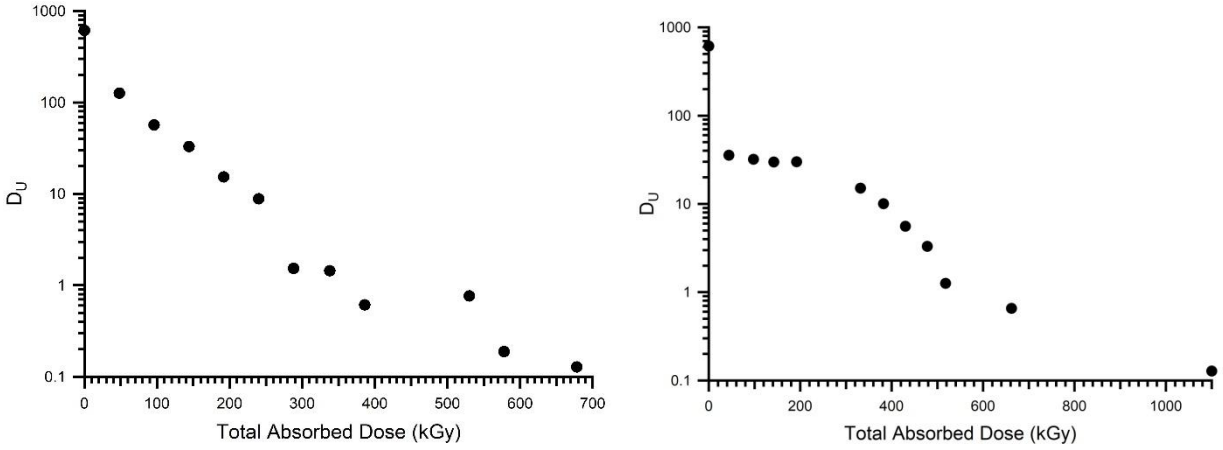

Figure 4.56. Distribution plot of the extraction of uranyl(VI) by irradiated 0.025 M tBu Salen and 0.025 M Salen

4.3.2.2. Identification of Degradation Products Through ESI-MS

The concentrations used for tBu Salen, Salen and tBu Salophen in 70% 1-octanol/toluene (0.025 M, 0.025 M and 0.012 M) are relatively low. The probability of direct interaction between the incoming ionizing radiation and the salen type ligands is therefore rather low and the majority of interaction takes place between the incoming ionization radiation and the diluent mixture. Chemical species formed from this direct radiolysis can then proceed in additional chemical reactions as indirect, or secondary, radiolysis.[124] This suggests that the decomposition of the salen type ligands is caused by reactive species formed in the radiolysis of the diluent, likely a 1-octanol/octane radical.[125,58, 126] The formation of free radicals from alcohols is described by the following equations. The most important products resulting from the direct radiolysis of alkanes and alcohols are solvated electrons, hydrogen gas radical, alcohol radical cation and carbon-centered α-hydroxy radicals which are able to react with the ligands.[58]

$$RCH_2OH + \gamma \rightarrow [RCH_2OH]^* \quad \text{(eq. 24)}$$

$$[RCH_2OH]^* \rightarrow e^-_{solv} + [RCH_2OH]^+ \quad \text{(eq. 25)}$$

$$[RCH_2OH]^+ \rightarrow RC^{\bullet}HOH + H^+ \quad \text{(eq. 26)}$$

Functional groups present in the organic molecules will then largely affect the composition of the radiolytic products.[57] In compounds containing polar functional groups, a rupturing of the bond in the α-position to the functional group tends to predominate.[59] The presence of unsaturated bonds and aromatic also increase the overall radiolytic stability of compounds.[60,61,62] Therefore it is expected to identify to find 1-octanol adducts, reduction of unsaturated bonds from reactions with formed reductive species. Since distribution values for uranyl(VI) decrease with increasing absorbed dose, there should also be fragments resulting from the direct radiolysis of the ligands. Noted trends can aid in identifying the possible chemical structure of radiolytic products. For direct comparison, identification of radiolytic products for the acid contacted 0.025 M Salen solution was also attempted.

Below are the ESI-MS spectrums of the organic solutions after irradiation at set periods of time. The spectra are generally characterized by a decrease in the relative abundance of peaks corresponding to the intact ligands and an increase in numerous radiolytic products, most of which are 1-octanol adducts. MS-ESI spectra indicate that most of the degradation of the ligand seems to occur from attacks from hydrogen and 1-octanol radicals rather than direct radiolysis from the ionization radiaition.

di-t-butyl Salen

Mass spectrometry spectra at select absorbed dose for the irradiation of 0.025 M di-t-butyl Salen are shown below along with structures of possible radiolytic products. As the absorbed dose increases, there is a decrease in the relative abundance of (m/z)=493 which

corresponds to the protonated ligand ($M+H^+$) and gradual increase of numerous degradation products. In the solution irradiated for 24 h, masses that we are confident belong to degraded ligand are at (m/z)= 277.0820, 387.1346 and 623.1767. The (m/z)= 516.0792 corresponds to intact ligand with a sodium adduct. ($M+Na^+$) Suggested structures are shown below.

(m/z)= 277.0820 ($M+H^+$)

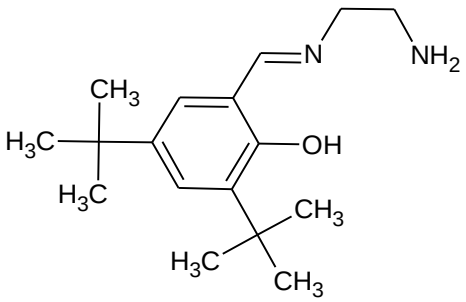

(m/z)= 387.1346 ($M+H^+$)

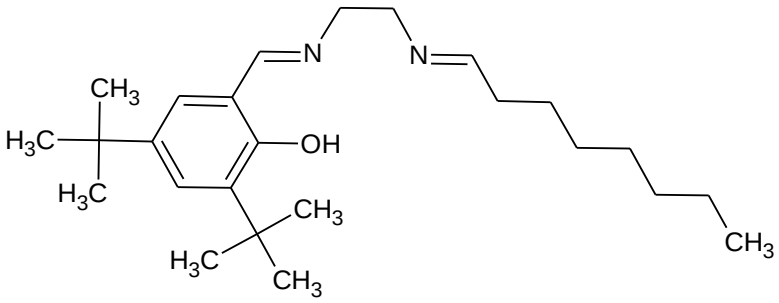

(m/z)= 623.1767 ($M+H^+$)

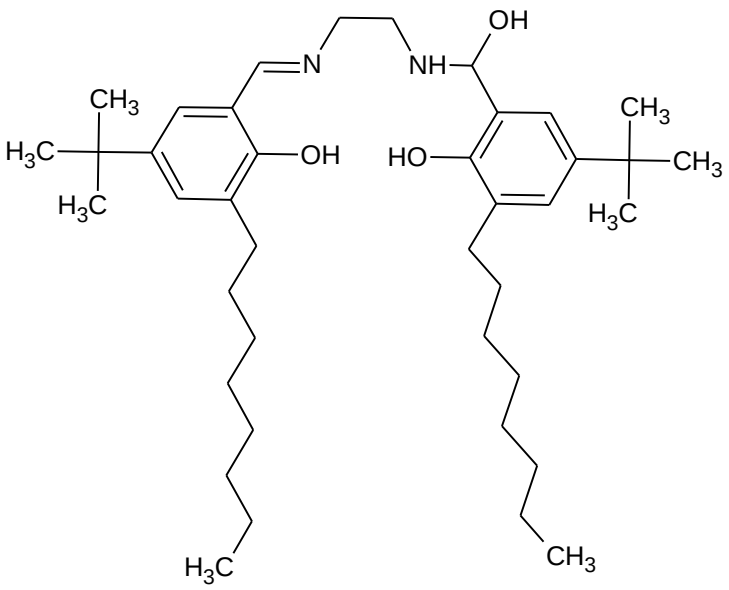

Figure 4.58 shows m/z peaks after 48 h of irradiation. Peaks that were present at 24 h of irradiation are also present. Figure 18 shows the presence of more degradation products after 72 h of irradiation, specifically at (m/z)=169.1202, 311.2091, 401.2033, 409.1727 and 499 which correspond to fragments formed by the recombination of degraded ligand and solvent compounds. The (m/z)=323.1755 and 457.0740 appear in a blank spectra. Suggested structures are shown below.

(m/z)= 169.1202

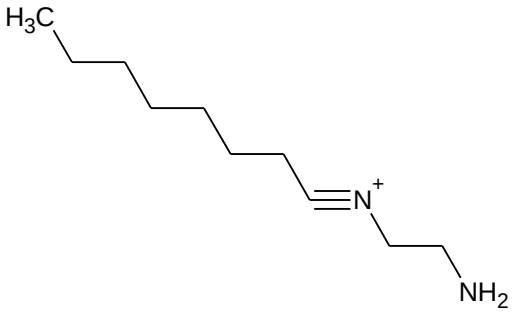

(m/z)= 401.2033 (An extra C atom added to the (m/z)= 387 fragment)

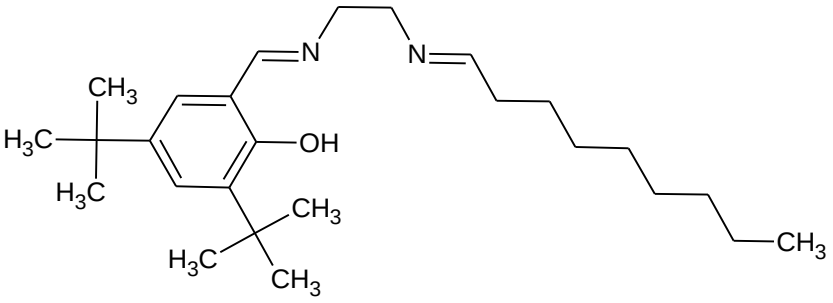

Figure 4.60 shows the increase in the relative intensity of the aforementioned degradation fragments after 96 h of irradiation and the decrease in the relative intensity of the (m/z)= 493.1984 and the growth of (m/z)= 169, a condensation product between 1-octanol and ethylenediamine. Towards longer irradiation times (196 and 339 h, Figure 4.69 and 4.62) the (m/z)=169 continues to increase in relative intensity, becoming the most abundant product. At 339 h, a peak present at (m/z)= 259 is the second most abundant product present. This peak could correspond to a 1-octanol dimer.

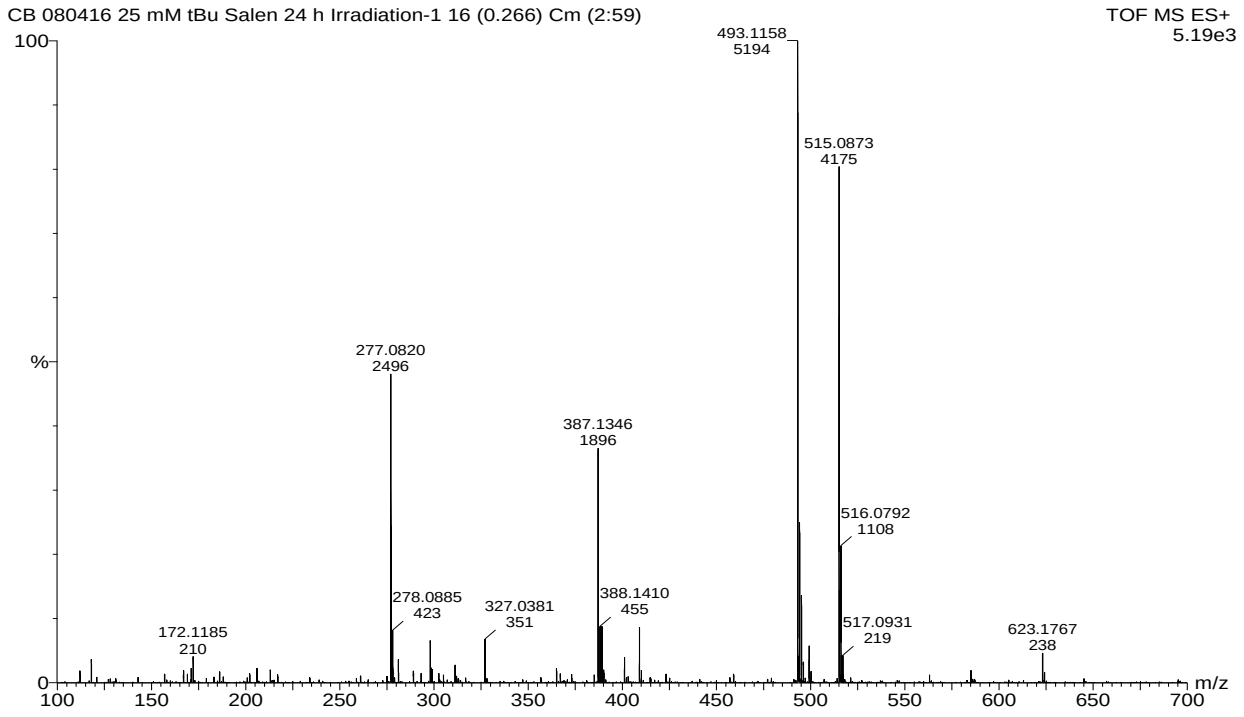

Figure 4.57. 25 mM tBu Salen after 24 h irradiation

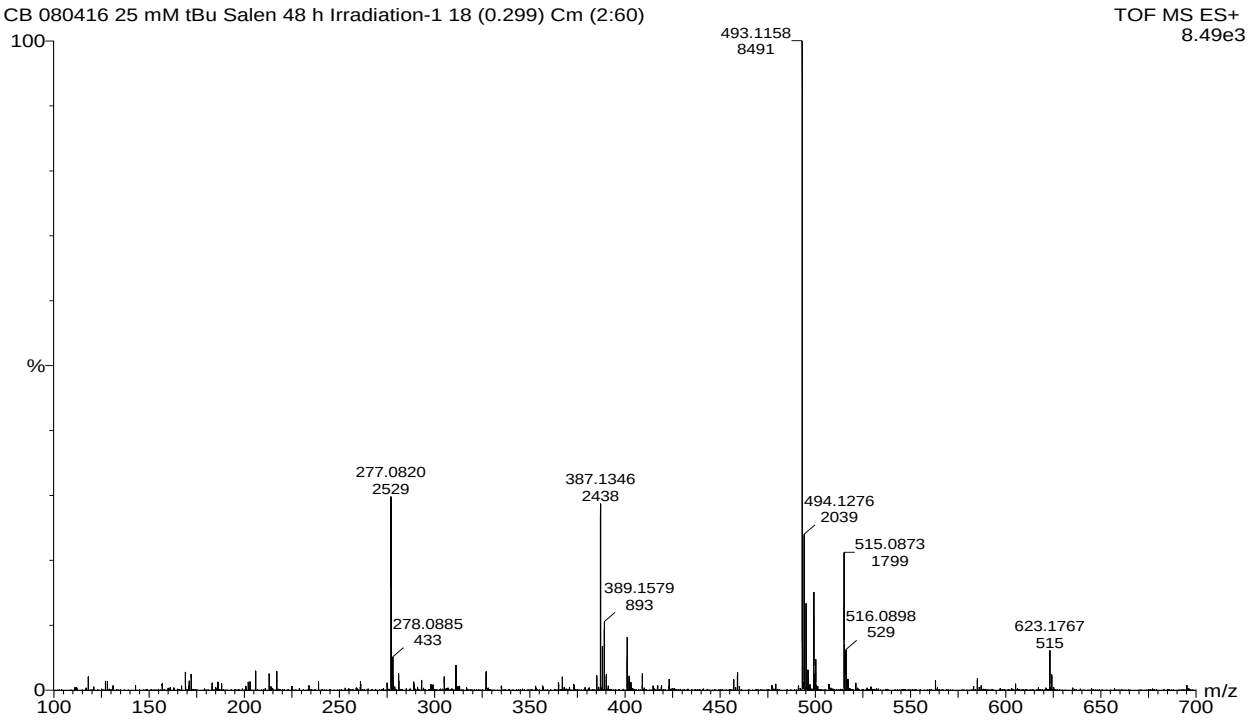

Figure 4.58. 25 mM tBu Salen after 48 h irradiation

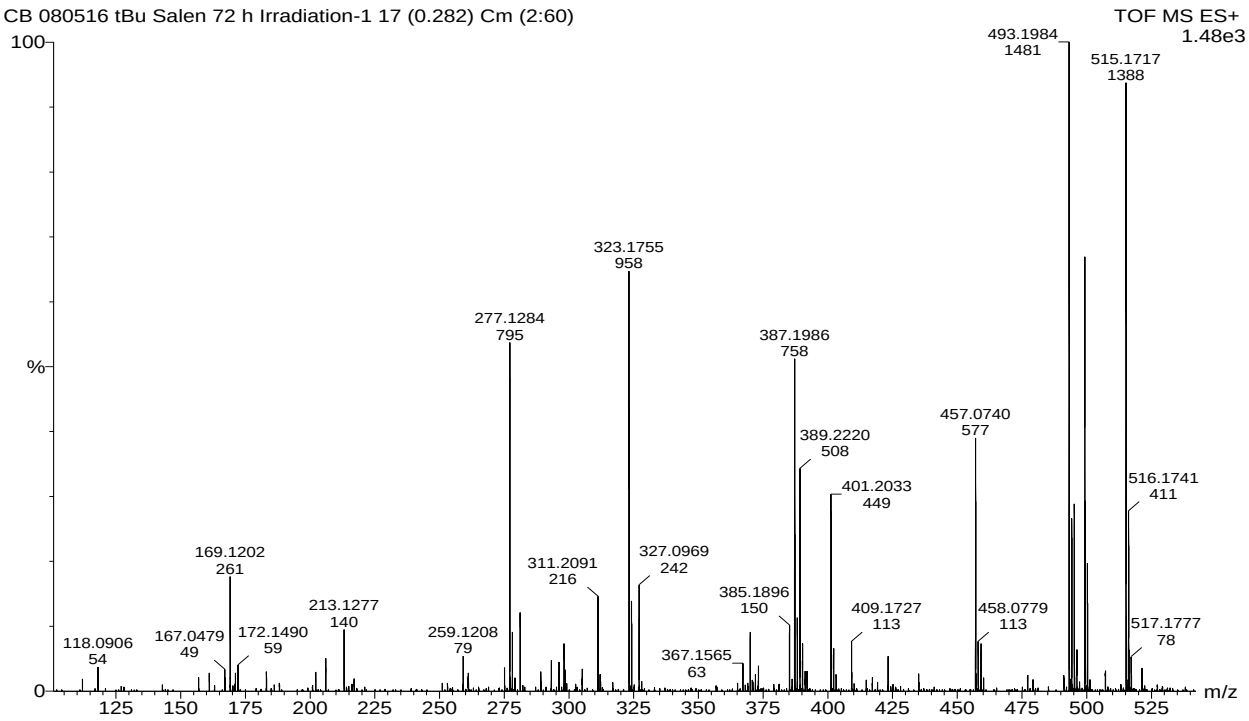

Figure 4.59. 25 mM tBu Salen after 72 h irradiation

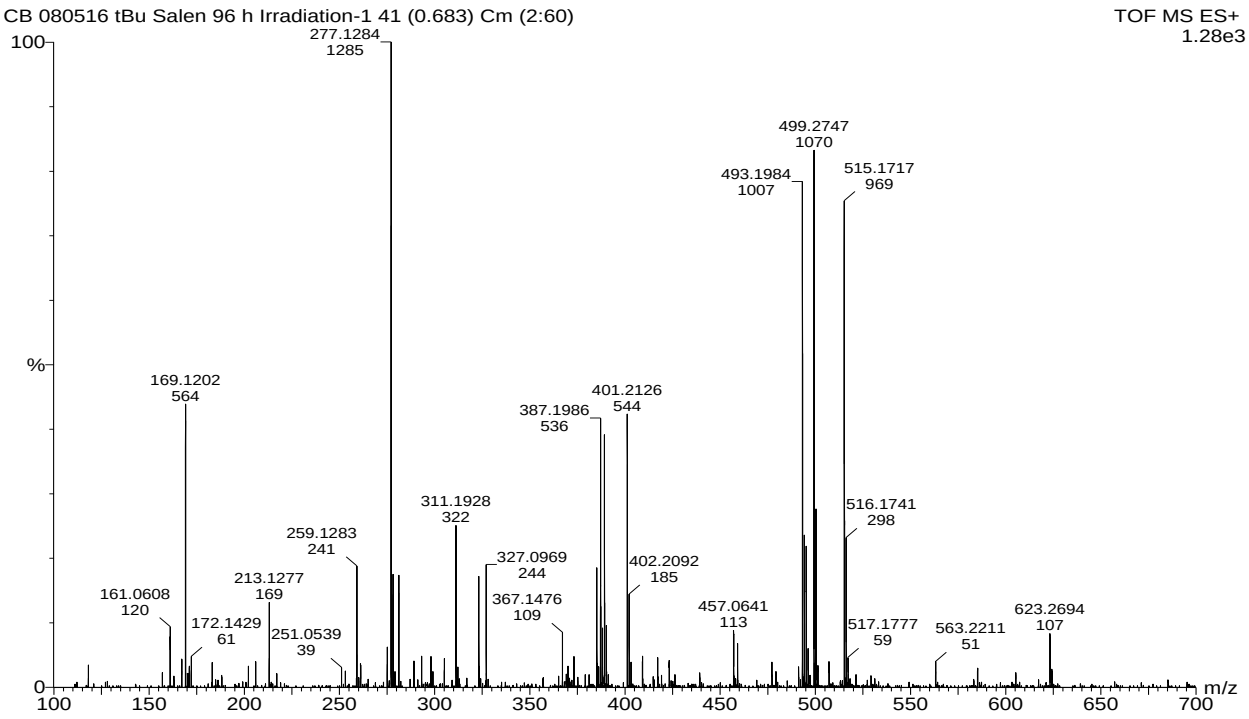

Figure 4.60. 25 mM tBu Salen after 96 h irradiation

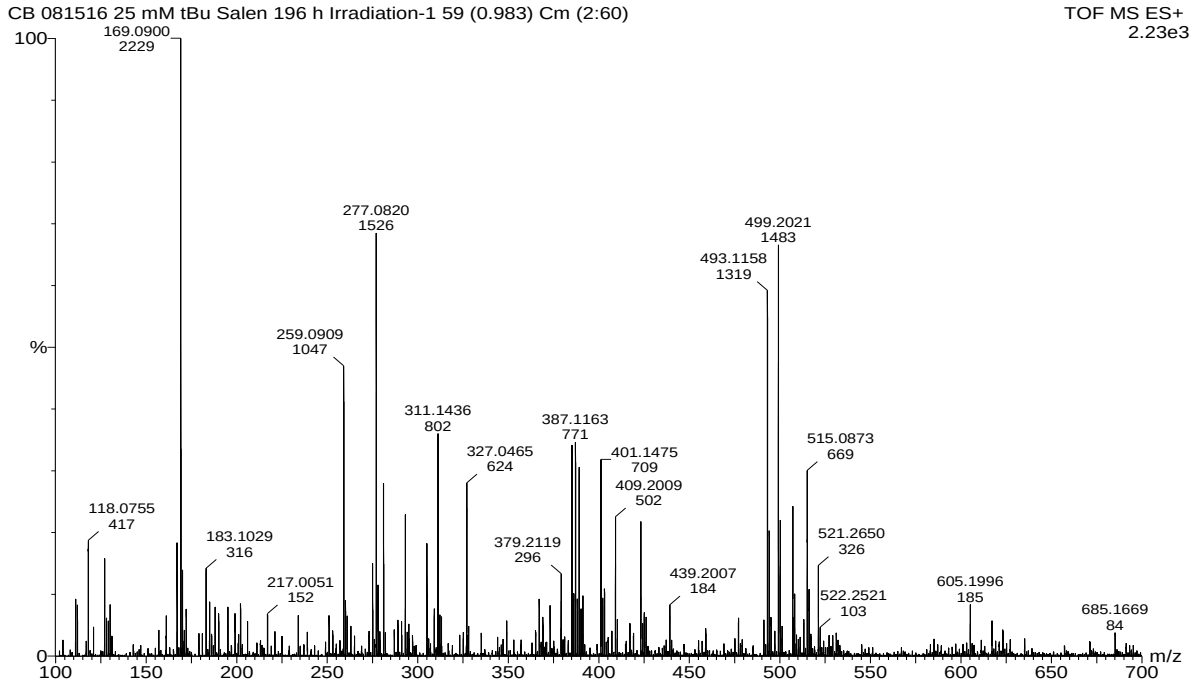

Figure 4.61. 25 mM tBu Salen after 196 h irradiation

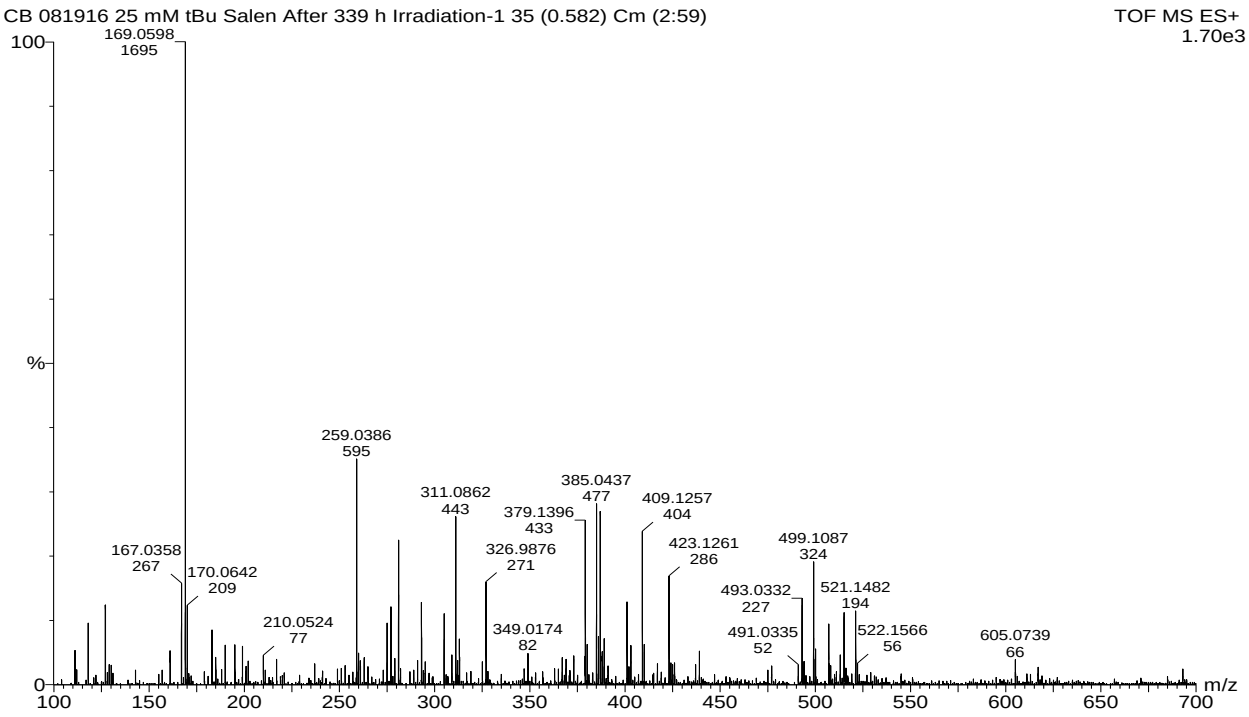

Figure 4.62. 25 mM tBu Salen after 339 h irradiation

di-t-butyl Salophen

ESI-MS spectra are shown below for the irradiation of 0.012 M di-t-butyl Salophen along with the structures of possible radiolytic product. As the absorbed dose increases, there is a decrease in the relative abundance of (m/z)=541 which corresponds to the ligand ($M+H^+$) and gradual increase of numerous degradation products and (m/z)=563.5078 corresponds to the sodium adduct ($M+Na^+$). Most notably, as total absorbed dose increases, the (m/z)=217 increases in intensity eventually becoming the predominant product. This peak corresponds to the condensation between 1-octanol and phenylenediamine.

In the 12 mM tBu Salophen solution that was irradiated for 24 h, the fragments in which we are confident belong to radiolytic degradation products are at (m/z)=217.2310, 325.3177, 281.3214, 325.3177 and possibly 669.6614 and 671.6831.

(m/z)=217.2310

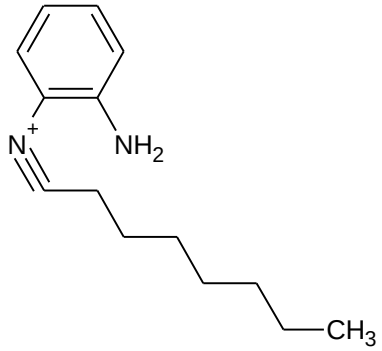

(m/z)=281.3214

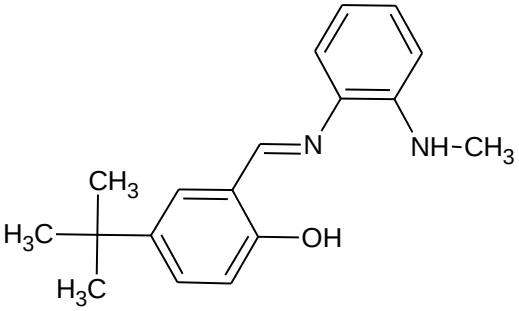

(m/z)=325.3177 ($M+H^+$)

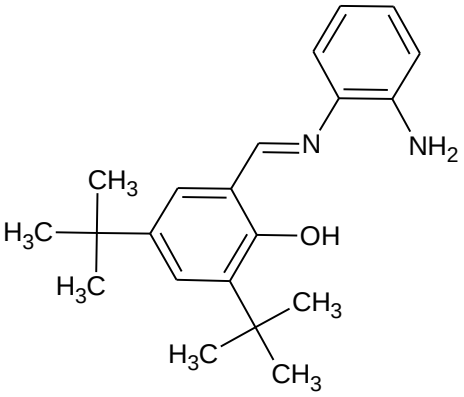

(m/z)= 669.6614 ($M+H^+$)

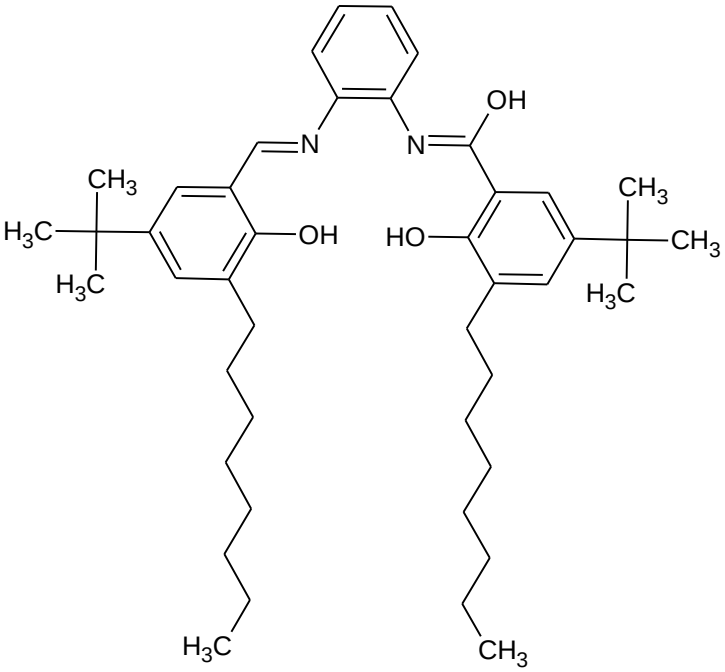

(m/z)= 671.6831

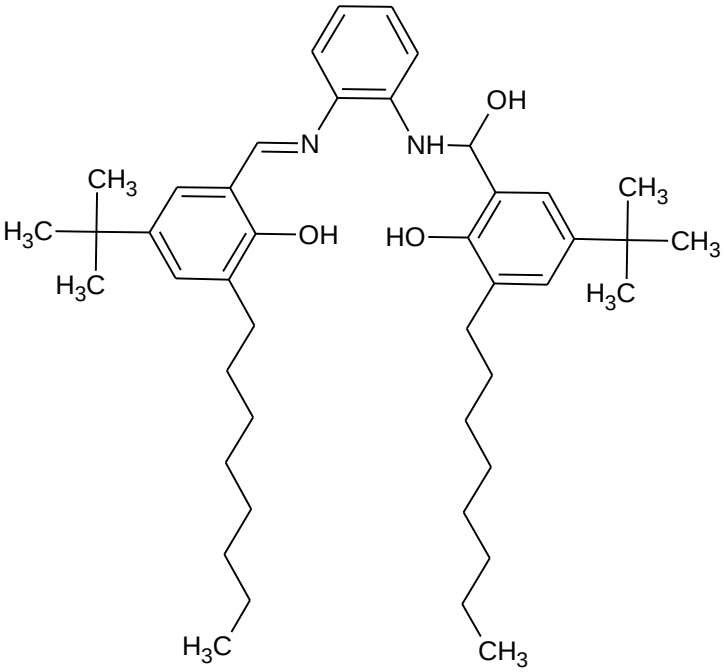

After only 48 h of irradiation, the fragment corresponding to the peak at (m/z) = 217 becomes the abundant radiolytic product. As the total absorbed dose increases, the (m/z) = 217 remains the most abundant while the peaks at higher (m/z) decrease in intensity. After 339 h of

irradiation, the peak at (m/z) = 540 (corresponding to intact di-t-butyl Salophen) is no longer present in significant quantities in the spectra.

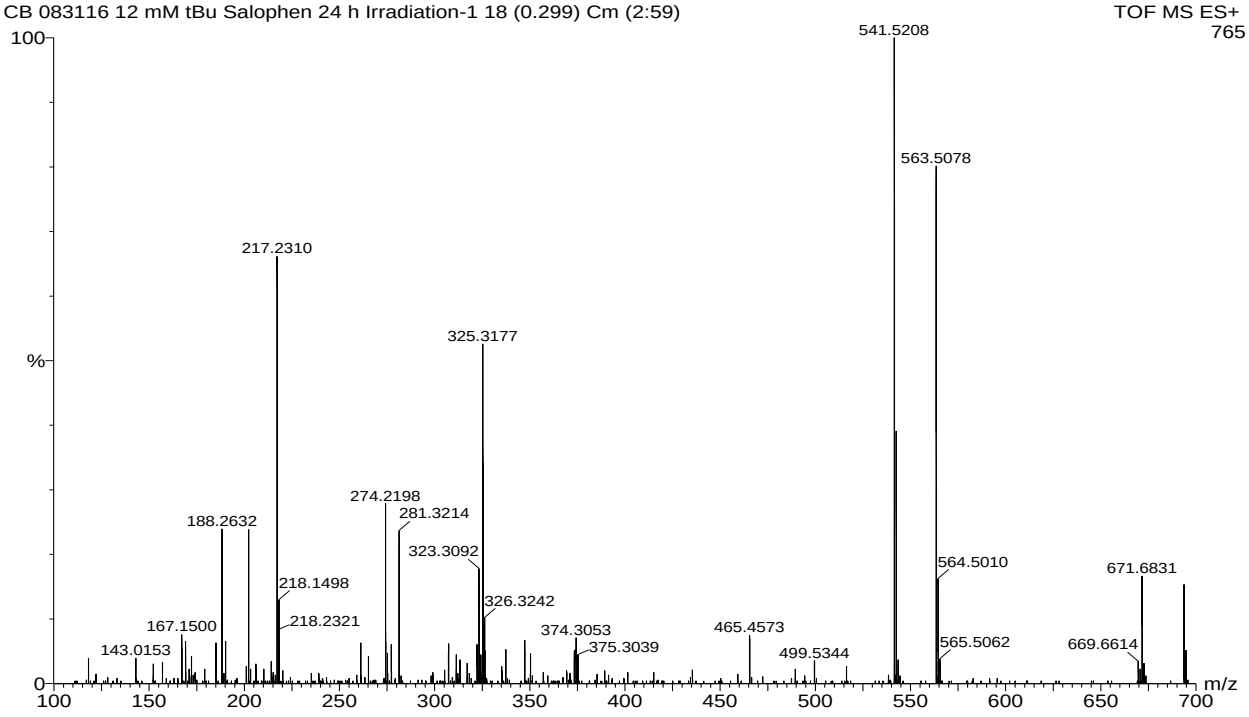

Figure 4.63. 12 mM tBu Salophen after 24 h irradiation

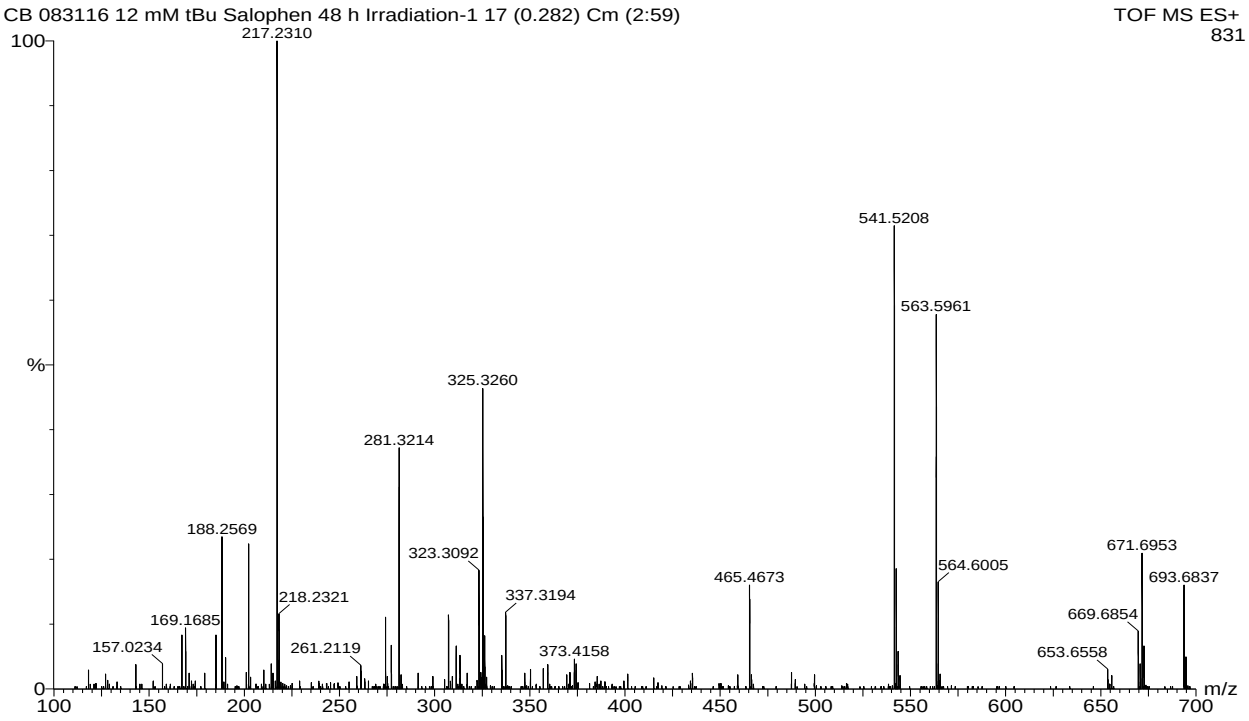

Figure 4.64. 12 mM tBu Salophen after 48 h Irradiation

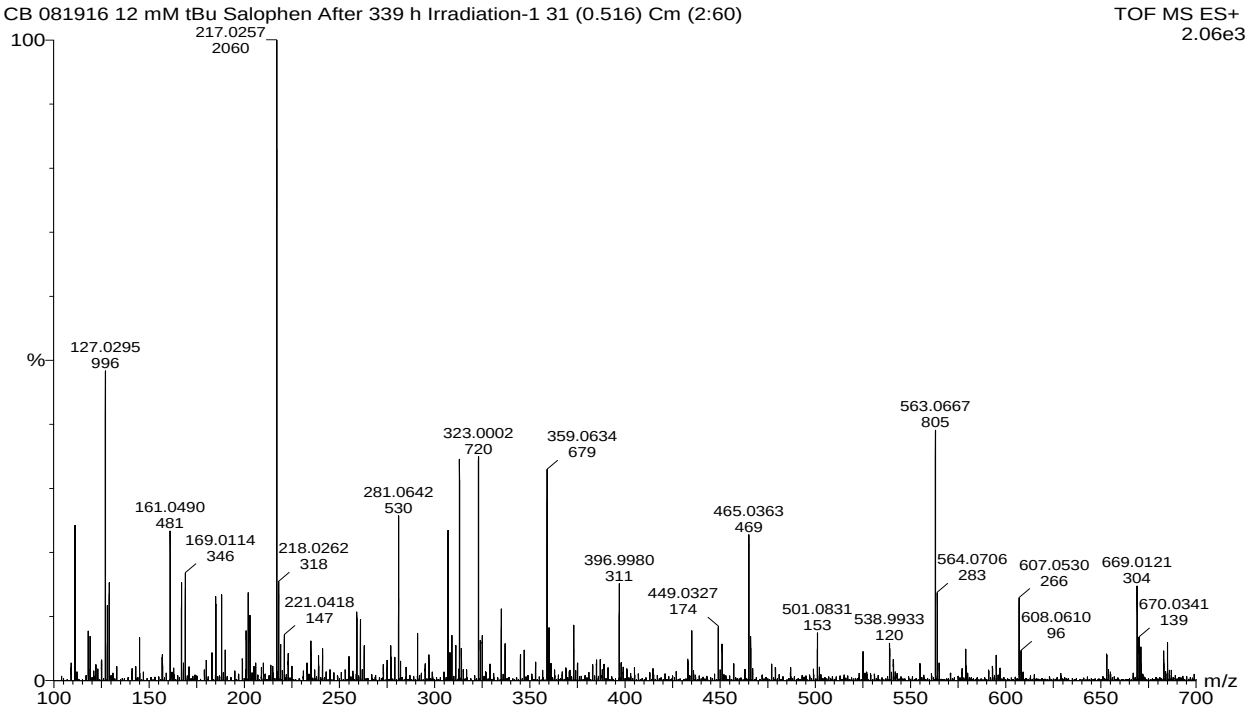

Figure. 4.65. 12 mM tBu Salophen after 339 h

Salen

ESI-MS spectra are shown below for the irradiation of 0.025 M Salen along with the structures of potentially corresponding radiolytic product. As the absorbed dose increases, there is a decrease in the relative abundance of (m/z)=268 and (m/z)= 291 which corresponds to the protonated ligand ($M+H^+$) and sodium adduct ($M+Na^+$) and gradual increase of numerous degradation products. Although acid contacted Salen solution did demonstrate slight resistance to degradation as calculated from G values, similar ESI-MS spectra indicates that there was no difference in possible radiolytic products formed.

After only 22 h of irradiation, peaks at (m/z)= 165 and (m/z)= 277 are present in significant quantities.

(m/z) = 165.0797 ($M+H^+$)

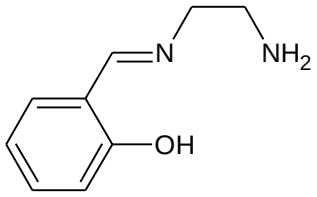

(m/z) = 277.2003 ($M+H^+$)

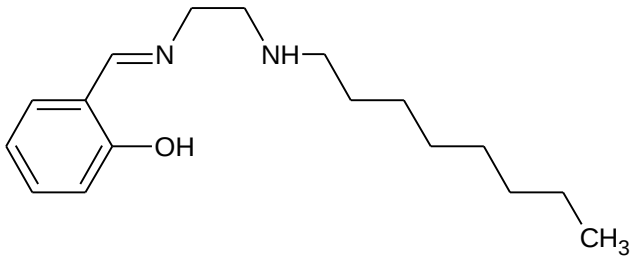

After 96 h of irradiation there is a significant presence in the condensation product between 1-octanol and etyhelenediamine.

(m/z) = 169.1527

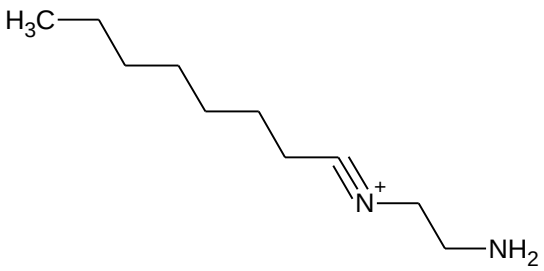

25 mM Salen after 96 h

After 96 h of irradiation, (m/z) = 277 becomes the most intense band indicating that it is the most abundant fragment.

(m/z) = 377.3488 ($L+H^+$)

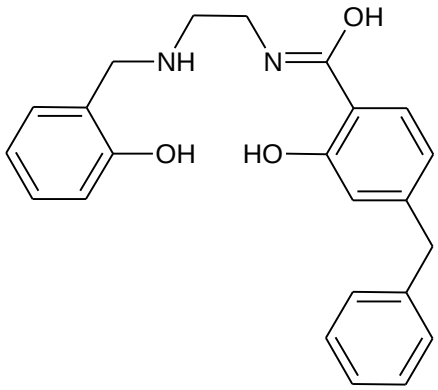

After 166 h of irradiation, the peak at (m/z) = 267 and 291, corresponding to the intact ligand, is no longer present in significant quantities.

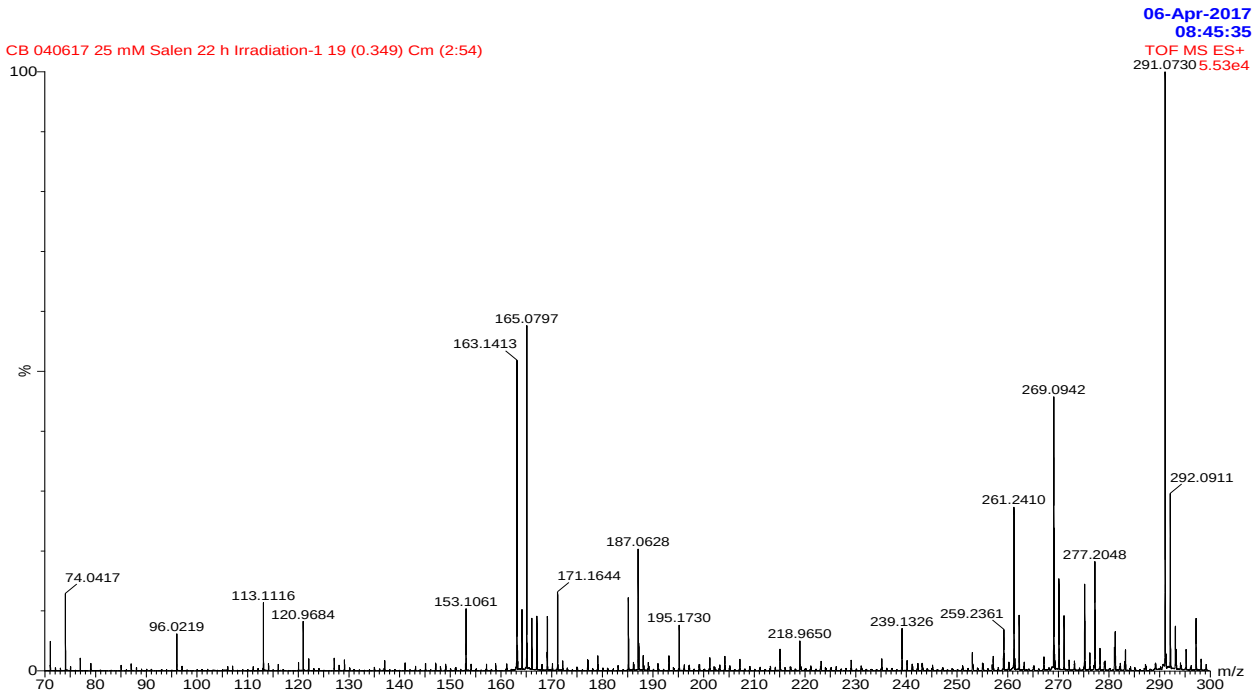

Figure 4.66. 25 mM Salen after 22 h irradiation

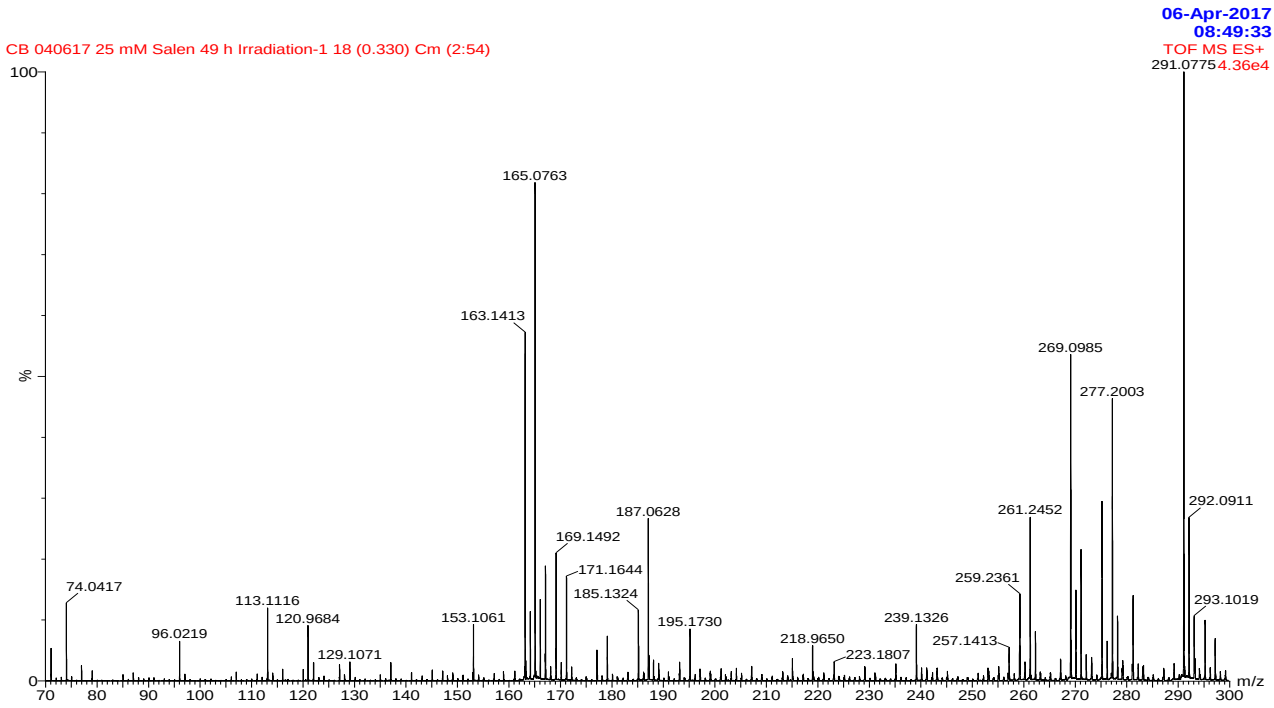

Figure 4.67. 25 mM Salen after 49 h irradiation

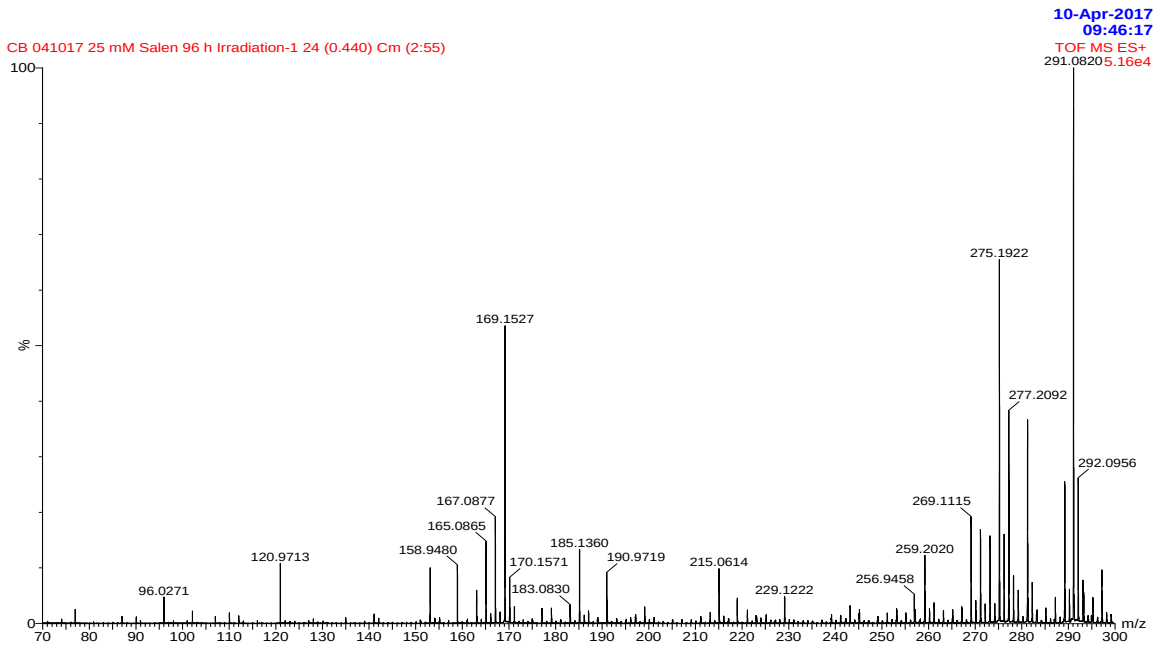

Figure 4.68. 25 mM Salen after 96 h irradiation

5. Conclusion

The development of novel reagents for application in the reprocessing of spent nuclear fuel for the specific removal and separation of the mid actinides is a step closer towards closing the nuclear fuel cycle. The objective of this work was to develop a novel separation scheme for the selective separation of the mid actinide cations in their penta and hexavalent oxidation states utilizing functionalized Schiff base ligands. Complexation and solvent extraction studies were carried out in order to study the feasibility of such separation scheme.

The redox chemistry of the actinide cations in solution can be complicated, and complexation studies with the actinyl cations were instrumental in understanding their redox behavior with the ligands that were studied in a single phase. To the best of our knowledge, we synthesized and characterized, structurally and spectroscopically, the first crystalline isostructural actinyl(VI) (U, Np, Pu) complexes in an organic medium with di-t-butyl Salen. In addition, crystalline solids between novel water-soluble Salen-SO_3 and Saldien-SO_3 and uranium(VI) were also synthesized and characterized. Although the water-soluble ligands were successful in complexing Np(V) and Pu(VI), the redox stability of Np(VI) and Pu(V) proved to be more challenging. Information collected from these experiments increase the overall knowledge of the behavior in solution of the actinyl cations and allowed us to predict possible redox behavior during biphasic solvent extraction studies.

Thorough solvent extraction experiments were carried out between the organic soluble ligands and uranium(VI). Understanding as much as possible about the extraction system is important in order to analyze whether the process can be implemented on an industrial scale and to address potential shortcomings. The belief was that since the actinyl(VI) cations exhibit similar behavior in solution, results gathered from uranium(VI) studies could be extrapolated to

the other actinyl(VI) species. Solvent extraction studies allowed us to estimate the dependency of uranyl(VI) extraction on pH and ligand concentration. In addition, kinetic values and conditional thermodynamic parameters for the extraction of uranium(VI) were calculated. However, although the ligand was successful in complexing and stabilizing Np(VI) and Pu(VI), it was apparent that the complete stabilization would not translate to a biphasic solvent extraction system.

A more efficient option for the group separation of the actinyl cations could be through their sequestration in the aqueous phase. Biphasic competitive continuous extraction studies with the water-soluble ligands serving as holdback reagents against HDEHP as the extractant indicate their potential use as holdback reagents for group actinyl retention. Uranyl(VI) was successfully retained in the aqueous phase while trivalent lanthanides were extracted away. Although the ligand system reduces Np(VI) to Np(V), neptunium is also separated from trivalent lanthanides as the neptunyl cation is also retained in the aqueous phase. From complexation studies we understood that the water-soluble ligands stabilized plutonium in the hexavalent state, and the ligands also demonstrated the ability to also retain Pu(VI) in the aqueous phase. Studies with americium were brief, but the rapid reduction of Am(V) to Am(III) is believed to occur. Additional modification to the structure of the water-soluble ligands could improve on the redox stability of the actinyl cations and the ligands.

The work illustrates the difficulty in the successful closure of the nuclear fuel cycle, as the redox stability of the actinide pose a stark challenge. We believe that we have laid the foundation, framework and need for additional studies into the application of Schiff base ligands in a fuel cycle process. The use of water-soluble Schiff base ligands as holdback reagents for the actinyl cations has great potential and must be studied further. The field of actinide science in

general is exciting and there is much more to be uncovered. Exploring the reduction potential and redox properties of the ligand actinyl complexes can further illustrate details of actinyl behavior. It may also be worthwhile to carry out experiments with a nitrate or phosphate derived water-soluble Schiff base ligands to complement studies with the sulfate derivative. Modification of the lipophilic ligand system to include long chain hydrocarbons can possibly enhance solubility in organic diluents applicable for reprocessing. A more accurate depiction of radiolytic behavior demonstrated by the ligand system can be uncovered through biphasic radiolytic studies in a continuous flow loop system. The use of Schiff base ligands in nuclear fuel cycle applications is promising and provide an attractive alternative for the treatment of spent nuclear fuel not previously considered.

Bibliography

1. United Nations, D. o. E. a. S. A., Population Division, *World Population Prospects: The 2017 Revision, Key Findings and Advance Tables.* Working Paper No. ESA/P/WP/248. 2017.
2. Agency, I. E. *World Energy Outlook 2017*.
3. Agency, I. A. E., Nuclear Technology Review. Austria, 2017.
4. AGENCY, I. A. E., *Climate Change and Nuclear Power 2016*. INTERNATIONAL ATOMIC ENERGY AGENCY: Vienna, 2016.
5. Choppin, G.; Liljenzin, J.-O.; Rydberg, J.; Ekberg, C., Chapter 19 - Principles of Nuclear Power. In *Radiochemistry and Nuclear Chemistry (Fourth Edition)*, Academic Press: Oxford, 2013; pp 595-653.
6. Plompen, A. J. M., Minor Actinides, Major Challenges, the Needs for and Benefits of International Collaboration. *Nuclear Data Sheets* **2014,** *118*, 78-84.
7. Blue Ribbon Commission on America's Nuclear Future. Report to the Secretary of Energy. Washington DC, 2012.
8. Mathur, J. N.; Murali, M. S.; Nash, K. L., ACTINIDE PARTITIONING—A REVIEW. *Solvent Extraction and Ion Exchange* **2001,** *19* (3), 357-390.
9. Chwaszczewski, S.; Słowiński, B., Transmutation of radioactive waste. *Applied Energy* **2003,** *75* (1), 87-96.
10. Durst PC, M. E., B Boyer, I Therios, R Bean, A Dougan, and K Tolk, Advanced Safeguards Approaches for New TRU Fuel Fabrication Facilities. PNNL-17151, Pacific Northwest National Laboratory, Richland, WA, 2007.
11. Christiansen, B.; Apostolidis, C.; Carlos, R.; Courson, O.; Glatz, J. P.; Malmbeck, R.; Pagliosa, G.; Römer, K.; Serrano-Purroy, D., Advanced aqueous reprocessing in P&T strategies: Process demonstrations on genuine fuels and targets. In *Radiochimica Acta*, 2004; Vol. 92, p 475.
12. (a) Cotton, S., Introduction to the Lanthanides. In *Lanthanide and Actinide Chemistry*, John Wiley & Sons, Ltd: 2006; pp 1-7; (b) Cotton, S., Introduction to the Actinides. In *Lanthanide and Actinide Chemistry*, John Wiley & Sons, Ltd: 2006; pp 145-153.
13. Nash, K. L.; Lumetta, G. J., Advanced Separation Techniques for Nuclear Fuel Reprocessing and Radioactive Waste Treatment. Woodhead Publishing.
14. MAGILL Joseph, B. V., HAAS D., GALY J., SCHENKEL Roland, WIESE H.W., HEUSENER G., TOMMASI J., YOUINOU G., Impact Limits of Partitioning and Transmutation Scenarios on Radiotoxicity of Actinides in Radioactive Waste. *Nuclear Energy* **2003,** *42* (5).
15. W. B. Lanham, T. C. R., PUREX Process for Plutonium and Uraniun Recovery. Report ORNL-479, Oak Ridge National Laboratory. **1949**.
16. Schulz, W. W.; Bender, K. P.; Burger, L. L.; Navratil, J. D., *Science and technology of tributyl phosphate*. Baca Raton, FL (United States); CRC Press, Inc.; None: 1990; p Medium: X; Size: Pages: (260 p).
17. Rydberg, J., Solvent Extraction Principles and Practice, Revised and Expanded.
18. Nilsson, M.; Nash, K. L., Review Article: A Review of the Development and Operational Characteristics of the TALSPEAK Process. *Solvent Extraction and Ion Exchange* **2007,** *25* (6), 665-701.
19. Lumetta, G. J.; Gelis, A. V.; Braley, J. C.; Carter, J. C.; Pittman, J. W.; Warner, M. G.; Vandegrift, G. F., The TRUSPEAK Concept: Combining CMPO and HDEHP for Separating

Trivalent Lanthanides from the Transuranic Elements. *Solvent Extraction and Ion Exchange* **2013,** *31* (3), 223-236.
20. Magnusson, D.; Christiansen, B.; Foreman, M. R. S.; Geist, A.; Glatz, J. P.; Malmbeck, R.; Modolo, G.; Serrano-Purroy, D.; Sorel, C., Demonstration of a SANEX Process in Centrifugal Contactors using the CyMe4-BTBP Molecule on a Genuine Fuel Solution. *Solvent Extraction and Ion Exchange* **2009,** *27* (2), 97-106.
21. Aneheim, E.; Ekberg, C.; Fermvik, A.; Foreman, M.; Retegan, T.; Skarnemark, G., *A TBP/BTBP-based GANEX separation process. Part 1: Feasibility*. 2010; Vol. 28, p 437-458.
22. Danesi, P. R.; Chiarizia, R.; Scibona, G., The meaning of slope analysis in solvent extraction chemistry: The case of zinc extraction by trilaurylammonium chloride. *Journal of Inorganic and Nuclear Chemistry* **1970,** *32* (7), 2349-2355.
23. Moyer, B. A.; McDowell, W. J.; Baes, C. F.; Case, G. N.; Case, F. I., LIQUID-LIQUID EQUILIBRIUM ANALYSIS IN PERSPECTIVE.PART 1. SLOPE ANALYSIS OF THE EXTRACTION OF URANYL NITRATE FROM NITRIC ACID BY DI-2-ETHYLHEXYLSULFOXIDE. *Solvent Extraction and Ion Exchange* **1991,** *9* (5), 833-864.
24. Pearson, R. G., Hard and soft acids and bases, HSAB, part 1: Fundamental principles. *Journal of Chemical Education* **1968,** *45* (9), 581.
25. Choppin, G. R.; Morgenstern, A., THERMODYNAMICS OF SOLVENT EXTRACTION. *Solvent Extraction and Ion Exchange* **2000,** *18* (6), 1029-1049.
26. Miguirditchian, M.; Guillaneux, D.; Guillaumont, D.; Moisy, P.; Madic, C.; Jensen, M. P.; Nash, K. L., Thermodynamic Study of the Complexation of Trivalent Actinide and Lanthanide Cations by ADPTZ, a Tridentate N-Donor Ligand. *Inorganic Chemistry* **2005,** *44* (5), 1404-1412.
27. Ionova, G.; Ionov, S.; Rabbe, C.; Hill, C.; Madic, C.; Guillaumont, R.; Modolo, G.; Krupa, J. C., Mechanism of trivalent actinide/lanthanide separation using synergistic mixtures of di(chlorophenyl)dithiophosphinic acid and neutral O-bearing co-extractants. *New Journal of Chemistry* **2001,** *25* (3), 491-501.
28. Katz, J. J.; Morss, L. R.; Edelstein, N. M.; Fuger, J., Introduction. In *The Chemistry of the Actinide and Transactinide Elements*, Morss, L. R.; Edelstein, N. M.; Fuger, J., Eds. Springer Netherlands: Dordrecht, 2011; pp 1-17.
29. Denning, R. G., Electronic structure and bonding in actinyl ions. In *Complexes, Clusters and Crystal Chemistry*, Springer Berlin Heidelberg: Berlin, Heidelberg, 1992; pp 215-276.
30. Yoshida, Z.; Johnson, S. G.; Kimura, T.; Krsul, J. R., Neptunium. In *The Chemistry of the Actinide and Transactinide Elements*, Morss, L. R.; Edelstein, N. M.; Fuger, J., Eds. Springer Netherlands: Dordrecht, 2011; pp 699-812.
31. Clark, D. L.; Hecker, S. S.; Jarvinen, G. D.; Neu, M. P., Plutonium. In *The Chemistry of the Actinide and Transactinide Elements*, Morss, L. R.; Edelstein, N. M.; Fuger, J., Eds. Springer Netherlands: Dordrecht, 2011; pp 813-1264.
32. Mincher, B. J.; Martin, L. R.; Schmitt, N. C., Tributylphosphate Extraction Behavior of Bismuthate-Oxidized Americium. *Inorganic Chemistry* **2008,** *47* (15), 6984-6989.
33. Nash, K. L.; Madic, C.; Mathur, J. N.; Lacquement, J., Actinide Separation Science and Technology. In *The Chemistry of the Actinide and Transactinide Elements*, Morss, L. R.; Edelstein, N. M.; Fuger, J., Eds. Springer Netherlands: Dordrecht, 2011; pp 2622-2798.
34. Herbst, R. S.; Baron, P.; Nilsson, M., 6 - Standard and advanced separation: PUREX processes for nuclear fuel reprocessing. In *Advanced Separation Techniques for Nuclear Fuel Reprocessing and Radioactive Waste Treatment*, Woodhead Publishing: 2011; pp 141-175.

35. F. Vandegrift, G.; C. Regalbuto, M.; Aase, S.; Arafat, H.; Bakel, A.; L. Bowers, D.; P. Byrnes, J.; A. Clark, M.; W. Emery, J.; R. Falkenberg, J.; Gelis, A.; D. Hafenrichter, L., *LAB-SCALE DEMONSTRATION OF THE UREX+ PROCESS*. 2004.
36. Weaver, B. K., F. A, TALSPEAK: A NEW METHOD OF SEPARATING AMERICIUM AND CURIUM FROM THE LANTHANIDES BY EXTRACTION FROM AN AQUEOUS SOLUTION OF AN AMINOPOLYACETIC ACID COMPLEX WITH A MONOACIDIC ORGANOPHOSPHATE OR PHOSPHONATE, report, August 1, 1964; Tennessee.
37. Peppard, D. F.; Mason, G. W.; Maier, J. L.; Driscoll, W. J., Fractional extraction of the lanthanides as their di-alkyl orthophosphates. *Journal of Inorganic and Nuclear Chemistry* **1957,** *4* (5), 334-343.
38. Musikas, C.; Le Marois, G.; Fitoussi, R.; Cuillerdier, C., Properties and Uses of Nitrogen and Sulfur Donors Ligands in Actinide Separations. In *Actinide Separations*, AMERICAN CHEMICAL SOCIETY: 1980; Vol. 117, pp 131-145.
39. Musikas, C. V., P.; Pattite, D. , Progress in Trivalent Actinide-Lanthanide Group Separation. Proceedings of the International Solvent Extraction Conference (ISEC 1983), Denver, Colorado. **1983**.
40. Hudson, M. J.; Harwood, L. M.; Laventine, D. M.; Lewis, F. W., Use of Soft Heterocyclic N-Donor Ligands To Separate Actinides and Lanthanides. *Inorganic Chemistry* **2013,** *52* (7), 3414-3428.
41. Horeglad, P.; Nocton, G.; Filinchuk, Y.; Pecaut, J.; Mazzanti, M., Pentavalent uranyl stabilized by a dianionic bulky tetradentate ligand. *Chemical Communications* **2009,** (14), 1843-1845.
42. Takao, K.; Kato, M.; Takao, S.; Nagasawa, A.; Bernhard, G.; Hennig, C.; Ikeda, Y., Molecular Structure and Electrochemical Behavior of Uranyl(VI) Complex with Pentadentate Schiff Base Ligand: Prevention of Uranyl(V) Cation−Cation Interaction by Fully Chelating Equatorial Coordination Sites. *Inorganic Chemistry* **2010,** *49* (5), 2349-2359.
43. Ekstrom, A., Kinetics and mechanism of the disproportionation of uranium(V). *Inorganic Chemistry* **1974,** *13* (9), 2237-2241.
44. Copping, R.; Mougel, V.; Petit, S.; Auwer, C. D.; Moisy, P.; Mazzanti, M., A versatile precursor for non-aqueous neptunyl(v) chemistry. *Chemical Communications* **2011,** *47* (19), 5497-5499.
45. Berthon, C.; Boubals, N.; Charushnikova, I. A.; Collison, D.; Cornet, S. M.; Den Auwer, C.; Gaunt, A. J.; Kaltsoyannis, N.; May, I.; Petit, S.; Redmond, M. P.; Reilly, S. D.; Scott, B. L., *Inorg. Chem.* **2010,** *49*, 9554.
46. Grenthe, I.; Drożdżyński, J.; Fujino, T.; Buck, E. C.; Albrecht-Schmitt, T. E.; Wolf, S. F., Uranium*. In *The Chemistry of the Actinide and Transactinide Elements*, Morss, L. R.; Edelstein, N. M.; Fuger, J., Eds. Springer Netherlands: Dordrecht, 2011; pp 253-698.
47. Takao, K.; Tsushima, S.; Takao, S.; Scheinost, A. C.; Bernhard, G.; Ikeda, Y.; Hennig, C., X-ray Absorption Fine Structures of Uranyl(V) Complexes in a Nonaqueous Solution. *Inorganic Chemistry* **2009,** *48* (20), 9602-9604.
48. Mikael Nilsson, I. M., Proposal: Separation of High Valency Actinides from Used Nuclear Fuel. University of California, Irvine.
49. Cozzi, P. G., Metal-Salen Schiff base complexes in catalysis: practical aspects. *Chemical Society Reviews* **2004,** *33* (7), 410-421.

50. Gupta, K. C.; Sutar, A. K., Catalytic activities of Schiff base transition metal complexes. *Coordination Chemistry Reviews* **2008,** *252* (12), 1420-1450.
51. Zhou, L.; Cai, P.; Feng, Y.; Cheng, J.; Xiang, H.; Liu, J.; Wu, D.; Zhou, X., Synthesis and photophysical properties of water-soluble sulfonato-Salen-type Schiff bases and their applications of fluorescence sensors for Cu2+ in water and living cells. *Analytica Chimica Acta* **2012,** *735*, 96-106.
52. Al Zoubi, W., Solvent extraction of metal ions by use of Schiff bases. *Journal of Coordination Chemistry* **2013,** *66* (13), 2264-2289.
53. Panda, C. R.; Chakravortty, V.; Dash, K. C., A quadridentate Schiff base as an extractant for thorium/IV/, uranium/VI/ and zirconium/IV. *Journal of Radioanalytical and Nuclear Chemistry* **1987,** *108* (2), 65-75.
54. Bharara, M. S.; Strawbridge, K.; Vilsek, J. Z.; Bray, T. H.; Gorden, A. E. V., Novel Dinuclear Uranyl Complexes with Asymmetric Schiff Base Ligands: Synthesis, Structural Characterization, Reactivity, and Extraction Studies. *Inorganic Chemistry* **2007,** *46* (20), 8309-8315.
55. Sahu, S.; Chakravortty, V., Extraction of uranium(VI) with binary mixtures of a quadridentate Schiff base and various neutral donors. *Journal of Radioanalytical and Nuclear Chemistry* **1998,** *227* (1-2), 163-165.
56. Henglein, A., J. W. T. Spinks. R. J. Woods: An Introduction to Radiation Chemistry, Third Edition, John-Wiley and Sons, Inc., New York, Toronto 1990. ISBN 0-471-61403-3. 574 Seiten, Preis: DM 91, 45. *Berichte der Bunsengesellschaft für physikalische Chemie* **1991,** *95* (3), 451-451.
57. J. Mincher, B.; Mezyk, S., *Radiation chemical effects on radiochemistry: A review of examples important to nuclear power*. 2009; Vol. 97, p 519-534.
58. Nilsson, M.; Andersson, S.; Ekberg, C.; Foreman, M. R. S.; Hudson, M. J.; Skarnemark, G., Inhibiting radiolysis of BTP molecules by addition of nitrobenzene. In *Radiochimica Acta*, 2006; Vol. 94, p 103.
59. Pikaev, A. K.; Kabakchi, S. A.; Egorov, G. F., Some radiation chemical aspects of nuclear engineering. *International Journal of Radiation Applications and Instrumentation. Part C. Radiation Physics and Chemistry* **1988,** *31* (4), 789-803.
60. *Organic radiation chemistry handbook / [edited by] V. K. Milinchuk, V. I. Tupikov*. Ellis Horwood: 1989.
61. Bellido A, V.; Rubenich M, N., Influence of the Diluent on the Radiolytic Degradation of TBP in TBP, 30% (v/v)-Diluent- HNO3 Systems. In *Radiochimica Acta*, 1984; Vol. 36, p 61.
62. Sugo, Y.; Izumi, Y.; Yoshida, Y.; Nishijima, S.; Sasaki, Y.; Kimura, T.; Sekine, T.; Kudo, H., Influence of diluent on radiolysis of amides in organic solution. *Radiation Physics and Chemistry* **2007,** *76* (5), 794-800.
63. Reilly, S. D.; Runde, W.; Neu, M. P., Solubility of plutonium(VI) carbonate in saline solutions. *Geochimica et Cosmochimica Acta* **2007,** *71* (11), 2672-2679.
64. Weigel, F., Book Review: Plutonium Handbook – A Guide to the Technology. Edited by O. J. Wick with the cooperation of several associates. Preface by G. T. Seaborg. *Angewandte Chemie International Edition in English* **1969,** *8* (2), 155-156.
65. Sales, P. S., Electrodeposition Apparatus For Samples Preparation of Actinide Elements By Alpha Spectroscopy. Roswell, Ga.
66. (a) Handley, T. H.; Cooper, J. H., Quantitative electrodeposition of actinides from dimethylsulfoxide. *Analytical Chemistry* **1969,** *41* (2), 381-382; (b) Talvitie, N. A.,

Electrodeposition of actinides for .alpha. spectrometric determination. *Analytical Chemistry* **1972,** *44* (2), 280-283.
67. Hara, M.; Suzuki, S., Oxidation of americium(III) with sodium bismuthate. *Journal of Radioanalytical Chemistry* **1977,** *36* (1), 95-104.
68. Choppin, G.; Liljenzin, J.-O.; Rydberg, J.; Ekberg, C., Chapter 8 - Radiation Effects on Matter. In *Radiochemistry and Nuclear Chemistry (Fourth Edition)*, Academic Press: Oxford, 2013; pp 209-237.
69. (a) Gaunt, A. J.; Reilly, S. D.; Hayton, T. W.; Scott, B. L.; Neu, M. P., An entry route into non-aqueous plutonyl coordination chemistry. *Chemical Communications* **2007,** (16), 1659-1661; (b) Giesting, P. A.; Burns, P. C., Uranyl-organic complexes: structure symbols, classification of carboxylates, and uranyl polyhedral geometries. *Crystallography Reviews* **2006,** *12* (3), 205-255.
70. Kim, S. Y.; Takao, K.; Haga, Y.; Yamamoto, E.; Kawata, Y.; Morita, Y.; Nishimura, K.; Ikeda, Y., *Cryst. Growth Des.* **2010,** *10*, 2033.
71. Charushnikova, I. A.; Krot, N. N.; Starikova, Z. A., Variation of the An-O bond lengths in NaAnO2(OOCCH3)3 and (NH4)4AnO2(CO3)3, An = U(VI), Np(VI), and Pu(VI). *Radiochemistry* **2007,** *49* (6), 565-570.
72. Bandoli, G.; Clemente, D. A.; Croatto, U.; Vidali, M.; Vigato, P. A., Crystal and molecular structure of [NN[prime or minute]-ethylenebis(salicylideneiminato)](methanol)dioxouranium. *Journal of the Chemical Society, Dalton Transactions* **1973,** (21), 2331-2335.
73. Chuguryan, D. G.; Dzyubenko, V. I.; Grigor'ev, M. S.; Yanovskii, A. I.; Struchkov, Y. T., Crystal and molecular structure of uranium (VI) and neptunium (VI) complexes with N,N/prime/-bis(salicylidene)ethylenediamine. *Sov. Radiochem. (Engl. Transl.); (United States)* **1988**, Medium: X; Size: Pages: 39-44.
74. Gaunt, A. J.; May, I.; Neu, M. P.; Reilly, S. D.; Scott, B. L., Structural and Spectroscopic Characterization of Plutonyl(VI) Nitrate under Acidic Conditions. *Inorganic Chemistry* **2011,** *50* (10), 4244-4246.
75. Hawkins, C. A.; Bustillos, C. G.; Copping, R.; Scott, B. L.; May, I.; Nilsson, M., Challenging conventional f-element separation chemistry - reversing uranyl(vi)/lanthanide(iii) solvent extraction selectivity. *Chemical Communications* **2014,** *50* (63), 8670-8673.
76. Hawkins, C. A.; Bustillos, C. G.; May, I.; Copping, R.; Nilsson, M., Water-soluble Schiff base-actinyl complexes and their effect on the solvent extraction of f-elements. *Dalton Transactions* **2016,** *45* (39), 15415-15426.
77. Ebrahimi, H. P.; Hadi, J. S.; Abdulnabi, Z. A.; Bolandnazar, Z., Spectroscopic, thermal analysis and DFT computational studies of salen-type Schiff base complexes. *Spectrochimica Acta Part A: Molecular and Biomolecular Spectroscopy* **2014,** *117*, 485-492.
78. (a) Sjoblom, R.; Hindman, J. C., Spectrophotometry of Neptunium in Perchloric Acid Solutions1. *Journal of the American Chemical Society* **1951,** *73* (4), 1744-1751; (b) Hagan, P. G.; Cleveland, J. M., The absorption spectra of neptunium ions in perchloric acid solution. *Journal of Inorganic and Nuclear Chemistry* **1966,** *28* (12), 2905-2909.
79. (a) Ikeda-Ohno, A.; Hennig, C.; Rossberg, A.; Funke, H.; Scheinost, A. C.; Bernhard, G.; Yaita, T., Electrochemical and Complexation Behavior of Neptunium in Aqueous Perchlorate and Nitrate Solutions. *Inorganic Chemistry* **2008,** *47* (18), 8294-8305; (b) Takao, K.; Takao, S.; Scheinost, A. C.; Bernhard, G.; Hennig, C., Complex Formation and Molecular Structure of Neptunyl(VI) and -(V) Acetates. *Inorganic Chemistry* **2009,** *48* (18), 8803-8810; (c) Berg, J. M.;

Gaunt, A. J.; May, I.; Pugmire, A. L.; Reilly, S. D.; Scott, B. L.; Wilkerson, M. P., Unexpected Actinyl Cation-Directed Structural Variation in Neptunyl(VI) A-Type Tri-lacunary Heteropolyoxotungstate Complexes. *Inorganic Chemistry* **2015,** *54* (9), 4192-4199.
80. Pratopo, M. I.; Moriyama, H.; Higashi, K., Carbonate Complexation of Np(VI) in Near-Neutral Solutions. *Journal of Nuclear Science and Technology* **1993,** *30* (10), 1024-1029.
81. Cornet, S. M.; Haller, L. J. L.; Sarsfield, M. J.; Collison, D.; Helliwell, M.; May, I.; Kaltsoyannis, N., Neptunium(vi) chain and neptunium(vi/v) mixed valence cluster complexes. *Chemical Communications* **2009,** (8), 917-919.
82. Cohen, D., The absorption spectra of plutonium ions in perchloric acid solutions. *Journal of Inorganic and Nuclear Chemistry* **1961,** *18*, 211-218.
83. (a) Runde, W.; Reilly, S. D.; Neu, M. P., Spectroscopic investigation of the formation of PuO2Cl+ and PuO2Cl2 in NaCl solutions and application for natural brine solutions. *Geochimica et Cosmochimica Acta* **1999,** *63* (19), 3443-3449; (b) Lee, M. H.; Park, Y. J.; Kim, W. H., Absorption spectroscopic properties for Pu(III, IV and VI) in nitric and hydrochloric acid media. *Journal of Radioanalytical and Nuclear Chemistry* **2007,** *273* (2), 375-382.
84. Stobbe, B. C.; Powell, D. R.; Thomson, R. K., Schiff base thorium(iv) and uranium(iv) chloro complexes: synthesis, substitution and oxidation chemistry. *Dalton Transactions* **2017,** *46* (15), 4888-4892.
85. Jr., J. J. H.; Calvin, M., Paramagnetic Susceptibilities and Electronic Structures of Aqueous Cations of Elements 92 to 95. *The Journal of Chemical Physics* **1950,** *18* (3), 239-243.
86. Bertini, I.; Luchinat, C.; Parigi, G.; Ravera, E., Chapter 1 - Introduction. In *NMR of Paramagnetic Molecules (Second Edition)*, Elsevier: Boston, 2017; pp 1-24.
87. Sarsfield, M. J.; May, I.; Cornet, S. M.; Helliwell, M., Preference for Nitrogen versus Oxygen Donor Coordination in Uranyl- and Neptunyl(VI) Complexes. *Inorganic Chemistry* **2005,** *44* (21), 7310-7312.
88. Boghaei, D. M.; Mohebi, S., Non-symmetrical tetradentate vanadyl Schiff base complexes derived from 1,2-phenylene diamine and 1,3-naphthalene diamine as catalysts for the oxidation of cyclohexene. *Tetrahedron* **2002,** *58* (26), 5357-5366.
89. Akbari, A.; Fasihizad, A.; Ahmadi, M.; Machura, B., A uranium(VI) complex with a tetradentate N1,N4-disalicyliden-S-ethylisothiosemicarbazone ligand. *Polyhedron* **2017,** *128*, 188-197.
90. Bullock, J. I., Raman and infrared spectroscopic studies of the uranyl ion: the symmetric stretching frequency, force constants, and bond lengths. *Journal of the Chemical Society A: Inorganic, Physical, Theoretical* **1969,** (0), 781-784.
91. Hardwick, H. C.; Royal, D. S.; Helliwell, M.; Pope, S. J. A.; Ashton, L.; Goodacre, R.; Sharrad, C. A., Structural, spectroscopic and redox properties of uranyl complexes with a maleonitrile containing ligand. *Dalton Transactions* **2011,** *40* (22), 5939-5952.
92. Connick, R. E., Mechanism of the Disproportionation of Plutonium (V). *Journal of the American Chemical Society* **1949,** *71* (5), 1528-1533.
93. Infante, I.; Gomes, A. S. P.; Visscher, L., On the performance of the intermediate Hamiltonian Fock-space coupled-cluster method on linear triatomic molecules: The electronic spectra of NpO2+, NpO22+, and PuO22+. *The Journal of Chemical Physics* **2006,** *125* (7), 074301.
94. Matsika, S.; Pitzer, R. M.; Reed, D. T., Intensities in the Spectra of Actinyl Ions. *The Journal of Physical Chemistry A* **2000,** *104* (51), 11983-11992.

95. Copping, R.; Gaunt, A. J.; May, I.; Sharrad, C. A.; Collison, D.; Helliwell, M.; Fox, O. D.; Jones, C. J., Oxoneptunium(v) as part of the framework of a polyoxometalate. *Chemical Communications* **2006,** (36), 3788-3790.
96. Copping, R.; Mougel, V.; Den Auwer, C.; Berthon, C.; Moisy, P.; Mazzanti, M., A tetrameric neptunyl(v) cluster supported by a Schiff base ligand. *Dalton Transactions* **2012,** *41* (36), 10900-10902.
97. Hennig, C.; Ikeda-Ohno, A.; Tsushima, S.; Scheinost, A. C., The Sulfate Coordination of Np(IV), Np(V), and Np(VI) in Aqueous Solution. *Inorganic Chemistry* **2009,** *48* (12), 5350-5360.
98. Rabideau, S. W., The kinetics of the disproportionation of plutonium (V). *Journal of the American Chemical Society* **1957,** *79* (24), 6350-6353.
99. Casellato, U.; Guerriero, P.; Tamburini, S.; Vigato, P. A.; Graziani, R., Synthesis, properties, and crystal structures of new mono- and homo-binuclear uranyl(VI) complexes with compartmental Schiff bases. *Journal of the Chemical Society, Dalton Transactions* **1990,** (5), 1533-1541.
100. Karplus, M., Vicinal Proton Coupling in Nuclear Magnetic Resonance. *Journal of the American Chemical Society* **1963,** *85* (18), 2870-2871.
101. (a) Nguyen Trung, C.; Begun, G. M.; Palmer, D. A., Aqueous uranium complexes. 2. Raman spectroscopic study of the complex formation of the dioxouranium(VI) ion with a variety of inorganic and organic ligands. *Inorganic Chemistry* **1992,** *31* (25), 5280-5287; (b) Nguyen-Trung, C.; Palmer, D. A.; Begun, G. M.; Peiffert, C.; Mesmer, R. E., Aqueous Uranyl Complexes 1. Raman Spectroscopic Study of the Hydrolysis of Uranyl(VI) in Solutions of Trifluoromethanesulfonic Acid and/or Tetramethylammonium Hydroxide at 25°C and 0.1 MPa. *Journal of Solution Chemistry* **2000,** *29* (2), 101-129; (c) Vallet, V.; Wahlgren, U.; Grenthe, I., Probing the Nature of Chemical Bonding in Uranyl(VI) Complexes with Quantum Chemical Methods. *The Journal of Physical Chemistry A* **2012,** *116* (50), 12373-12380.
102. Cattalini, L.; Degetto, S.; Vidali, M.; Vigato, P. A., Uranyl complexes containing polydentate schiff bases. *Inorganica Chimica Acta* **1972,** *6* (Supplement C), 173-176.
103. Baroncelli, F.; Scibona, G.; Zifferero, M., The effect of additives and stabilizers on the extraction behaviour of U(VI) and Pu(IV) nitrates with tertiary amines. *Journal of Inorganic and Nuclear Chemistry* **1963,** *25* (2), 205-213.
104. Choppin Gregory, R.; Rao Lin, F., Complexation of Pentavalent and Hexavalent Actinides by Fluoride. In *Radiochimica Acta*, 1984; Vol. 37, p 143.
105. McCann, K.; Mincher, B. J.; Schmitt, N. C.; Braley, J. C., Hexavalent Actinide Extraction Using N,N-Dialkyl Amides. *Industrial & Engineering Chemistry Research* **2017,** *56* (22), 6515-6519.
106. Sasaki, Y.; Sugo, Y.; Suzuki, S.; Tachimori, S., THE NOVEL EXTRACTANTS, DIGLYCOLAMIDES, FOR THE EXTRACTION OF LANTHANIDES AND ACTINIDES IN HNO3–n-DODECANE SYSTEM. *Solvent Extraction and Ion Exchange* **2001,** *19* (1), 91-103.
107. Sasaki, Y.; Tsubata, Y.; Kitatsuji, Y.; Sugo, Y.; Shirasu, N.; Morita, Y.; Kimura, T., Extraction Behavior of Metal Ions by TODGA, DOODA, MIDOA, and NTAamide Extractants from HNO3 to n-Dodecane. *Solvent Extraction and Ion Exchange* **2013,** *31* (4), 401-415.
108. Pathak, P. N.; Ansari, S. A.; Kumar, S.; Tomar, B. S.; Manchanda, V. K., Dynamic light scattering study on the aggregation behaviour of N,N,N′,N′-tetraoctyl diglycolamide (TODGA) and its correlation with the extraction behaviour of metal ions. *Journal of Colloid and Interface Science* **2010,** *342* (1), 114-118.

109. Takao, K.; Ikeda, Y., Structural Characterization and Reactivity of UO2(salophen)L and [UO2(salophen)]2: Dimerization of UO2(salophen) Fragments in Noncoordinating Solvents (salophen = N,N‘-Disalicylidene-o-phenylenediaminate, L = N,N-Dimethylformamide, Dimethyl Sulfoxide). *Inorganic Chemistry* **2007,** *46* (5), 1550-1562.
110. Retegan, T.; Drew, M.; Ekberg, C.; Engdahl, E. L.; Hudson, M. J.; Fermvik, A.; Foreman, M. R. S.; Modolo, G.; Geist, A., Synthesis and Screening of t-Bu-CyMe4-BTBP, and Comparison with CyMe4-BTBP. *Solvent Extraction and Ion Exchange* **2014,** *32* (7), 720-736.
111. (a) Sekine, T.; Koike, Y.; Komatsu, Y., Kinetic Studies of the Solvent Extraction of Metal Complexes. I. The Extraction of the Beryllium(II)-TTA Chelate from Aqueous Perchlorate Media into Carbon Tetrachloride and Methyl Isobutyl Ketone. *Bulletin of the Chemical Society of Japan* **1971,** *44* (11), 2903-2911; (b) Sekine, T.; Yumikura, J.-i.; Komatsu, Y., Kinetic Studies of the Solvent Extraction of Metal Complexes. II. The Rate of the Extraction of Iron(III) with Thenoyltrifluoroacetone into Carbon Tetrachloride. *Bulletin of the Chemical Society of Japan* **1973,** *46* (8), 2356-2360.
112. Nilsson, M.; Nash, K. L., Trans-Lanthanide Extraction Studies in the TALSPEAK System: Investigating the Effect of Acidity and Temperature. *Solvent Extraction and Ion Exchange* **2009,** *27* (3), 354-377.
113. Ouyang, J.-M., SOLVENT EXTRACTION OF PALLADIUM(II) WITH A SCHIFF BASE AND SEPARATION OF PALLADIUM FROM Pd(II)-Pt(VI) MIXTURE. *Solvent Extraction and Ion Exchange* **1999,** *17* (5), 1255-1270.
114. Nash, K. L., *Studies of the thermodynamics of extraction f-elements*. ; Argonne National Lab., IL (US): 1998; p Medium: P; Size: 9 pages.
115. Kalina, D. G.; Mason, G. W.; Philip Horwitz, E., The thermodynamics of extraction of U(VI) and Th(IV) from nitric acid by neutral phosphorus-based organic compounds. *Journal of Inorganic and Nuclear Chemistry* **1981,** *43* (1), 159-163.
116. Nash, K. L.; Lavallette, C.; Borkowski, M.; Paine, R. T.; Gan, X., Features of the Thermodynamics of Two-Phase Distribution Reactions of Americium(III) and Europium(III) Nitrates into Solutions of 2,6-Bis[(bis(2-ethylhexyl)phosphino)methyl]pyridine N,P,P ‘-Trioxide. *Inorganic Chemistry* **2002,** *41* (22), 5849-5858.
117. Kandil, A. T.; Farah, K., Thermodynamic studies of TOPO adducts of europium and terbium tris-TTA chelates. *Journal of Inorganic and Nuclear Chemistry* **1980,** *42* (10), 1491-1494.
118. Bhatti, M. S., Temperature effect on the synergic extraction of europium by thenoyltrifluoroacetone in the presence of heterocyclic bidentate amines from acetate buffer solutions. *Journal of Radioanalytical Chemistry* **1980,** *57* (1), 69-78.
119. (a) Hughes, M. A.; Preston, J. S.; Whewell, R. J., The kinetics of the solvent extraction of copper(II) with LIX 64N reagents—II: Activation energies. *Journal of Inorganic and Nuclear Chemistry* **1976,** *38* (11), 2067-2069; (b) Roberto Danesi, P.; Chiarizia, R.; Coleman, C. F., The Kinetics of Metal Solvent Extraction. *C R C Critical Reviews in Analytical Chemistry* **1980,** *10* (1), 1-126; (c) El-Hefny, N. E., Kinetics and mechanism of extraction and stripping of neodymium using a Lewis cell. *Chemical Engineering and Processing: Process Intensification* **2007,** *46* (7), 623-629.
120. Bharara, M. S.; Heflin, K.; Tonks, S.; Strawbridge, K. L.; Gorden, A. E. V., Hydroxy- and alkoxy-bridged dinuclear uranyl-Schiff base complexes: hydrolysis, transamination and extraction studies. *Dalton Transactions* **2008,** (22), 2966-2973.

121. Elliot, A. J., A pulse radiolysis study of the temperature dependence of reactions involving H, OH and e-aq in aqueous solutions. *International Journal of Radiation Applications and Instrumentation. Part C. Radiation Physics and Chemistry* **1989,** *34* (5), 753-758.
122. Mincher, B. J.; Modolo, G.; Mezyk, S. P., Review Article: The Effects of Radiation Chemistry on Solvent Extraction 3: A Review of Actinide and Lanthanide Extraction. *Solvent Extraction and Ion Exchange* **2009,** *27* (5-6), 579-606.
123. Fermvik, A.; Berthon, L.; Ekberg, C.; Englund, S.; Retegan, T.; Zorz, N., Radiolysis of solvents containing C5-BTBP: identification of degradation products and their dependence on absorbed dose and dose rate. *Dalton Transactions* **2009,** (32), 6421-6430.
124. Farhataziz; Rodgers, M. A. J., *Radiation chemistry: principles and applications*. VCH Publishers,New York, NY: United States, 1987.
125. Mezyk, S. P.; Mincher, B. J.; Ekberg, C.; Skarnemark, G., Alpha and gamma radiolysis of nuclear solvent extraction ligands used for An(III) and Ln(III) separations. *Journal of Radioanalytical and Nuclear Chemistry* **2013,** *296* (2), 711-715.
126. Wilden, A.; Modolo, G.; Hupert, M.; Santiago-Schübel, B.; Löfström-Engdahl, E.; Halleröd, J.; Ekberg, C.; Mincher, B. J.; Mezyk, S. P., Gamma-Radiolytic Stability of Solvents Containing C5-BPP (2,6-Bis(5-(2,2-dimethylpropyl)-1H-pyrazol-3-yl)pyridine) for Actinide(III)/Lanthanide(III) Separation. *Solvent Extraction and Ion Exchange* **2016,** *34* (1), 1-12.